Spin-orbit coupling mediated electrical control of semiconductor spin qubits: from donor atoms to quantum dots

Abhikbrata Sarkar

A thesis in fulfilment of the requirements for the degree of

Doctor of Philosophy

UNSW
SYDNEY

School of Physics

Faculty of Science

The University of New South Wales

May 27, 2025

Thesis submission for the degree of Doctor of Philosophy

Thesis Title and Abstract | **Declarations** | Inclusion of Publications Statement | Corrected Thesis and Responses

ORIGINALITY STATEMENT

☑ I hereby declare that this submission is my own work and to the best of my knowledge it contains no materials previously published or written by another person, or substantial proportions of material which have been accepted for the award of any other degree or diploma at UNSW or any other educational institution, except where due acknowledgement is made in the thesis. Any contribution made to the research by others, with whom I have worked at UNSW or elsewhere, is explicitly acknowledged in the thesis. I also declare that the intellectual content of this thesis is the product of my own work, except to the extent that assistance from others in the project's design and conception or in style, presentation and linguistic expression is acknowledged.

COPYRIGHT STATEMENT

☑ I hereby grant the University of New South Wales or its agents a non-exclusive licence to archive and to make available (including to members of the public) my thesis or dissertation in whole or part in the University libraries in all forms of media, now or here after known. I acknowledge that I retain all intellectual property rights which subsist in my thesis or dissertation, such as copyright and patent rights, subject to applicable law. I also retain the right to use all or part of my thesis or dissertation in future works (such as articles or books).

For any substantial portions of copyright material used in this thesis, written permission for use has been obtained, or the copyright material is removed from the final public version of the thesis.

AUTHENTICITY STATEMENT

☑ I certify that the Library deposit digital copy is a direct equivalent of the final officially approved version of my thesis.

Thesis submission for the degree of Doctor of Philosophy

Thesis Title and Abstract | Declarations | **Inclusion of Publications Statement** | Corrected Thesis and Responses

UNSW is supportive of candidates publishing their research results during their candidature as detailed in the UNSW Thesis Examination Procedure.

Publications can be used in the candidate's thesis in lieu of a Chapter provided:

- The candidate contributed **greater than 50%** of the content in the publication and are the "primary author", i.e. they were responsible primarily for the planning, execution and preparation of the work for publication.
- The candidate has obtained approval to include the publication in their thesis in lieu of a Chapter from their Supervisor and Postgraduate Coordinator.
- The publication is not subject to any obligations or contractual agreements with a third party that would constrain its inclusion in the thesis.

☑ The candidate has declared that **their thesis has publications - either published or submitted for publication - incorporated into it in lieu of a Chapter/s. Details of these publications are provided below.**.

Publication Details #1

Full Title:	Optimisation of electron spin qubits in electrically driven multi-donor quantum dots
Authors:	Abhikbrata Sarkar, Joel Hochstetter, Allen Kha, Xuedong Hu, Michelle Y Simmons, Rajib Rahman, Dimitrie Culcer
Journal or Book Name:	npj Quantum Information
Volume/Page Numbers:	volume 8, page 127
Date Accepted/Published:	4 November 2022
Status:	published
The Candidate's Contribution to the Work:	I carried out the analytic calculations in the project, and strategically developed the results presented in the paper. I wrote the paper incorporating recommendations and rectifications suggested by the experimental collaborators. I am the first author of the published manuscript.
Location of the work in the thesis and/or how the work is incorporated in the thesis:	The published version of this work forms Chapter 2 of the thesis, with a brief overview of its key results and their relevance to the central theme presented at the beginning of the chapter.

Publication Details #2

Full Title:	Electrical operation of planar Ge hole spin qubits in an in-plane magnetic field
Authors:	Abhikbrata Sarkar, Zhanning Wang, Matthew Rendell, Nico W Hendrickx, Menno Veldhorst, Giordano Scappucci, Mohammad Khalifa, Joe Salfi, Andre Saraiva, AS Dzurak, AR Hamilton, Dimitrie Culcer
Journal or Book Name:	Physical Review B
Volume/Page Numbers:	volume 108, page 245301
Date Accepted/Published:	15 December 2023
Status:	published
The Candidate's Contribution to the Work:	I carried out the analytic calculations in the project, and strategically developed the results presented in the paper. I wrote the paper incorporating recommendations and rectifications suggested by the experimental collaborators. I am the first author of the published manuscript.
Location of the work in the thesis and/or how the work is incorporated in the thesis:	The published version of this work forms Chapter 3 of the thesis, with a brief overview of its key results and their relevance to the central theme presented at the beginning of the chapter.

Publication Details #3

Full Title:	Effect of disorder and strain on the operation of planar Ge hole spin qubits
Authors:	Abhikbrata Sarkar, Pratik Chowdhury, Xuedong Hu, Andre Saraiva, A. S. Dzurak, A. R. Hamilton, Rajib Rahman, S. Das Sarma, Dimitrie Culcer
Journal or Book Name:	Physical Review B
Volume/Page Numbers:	
Date Accepted/Published:	
Status:	submitted

The Candidate's Contribution to the Work:	I carried out the analytic calculations in the project, and strategically developed the results presented in the paper. I wrote the paper incorporating recommendations and rectifications suggested by the experimental collaborators. I am the first author of the published manuscript. The paper is live on arXiv as arXiv preprint 2502.06949.
Location of the work in the thesis and/or how the work is incorporated in the thesis:	The submitted version of this work forms Chapter 4 of the thesis, with a brief overview of its key results and their relevance to the central theme presented at the beginning of the chapter.

Candidate's Declaration

I confirm that where I have used a publication in lieu of a chapter, the listed publication(s) above meet(s) the requirements to be included in the thesis. I also declare that I have complied with the Thesis Examination Procedure.

Contents

List of Figures

List of Tables

Abstract

Semiconductors have brought about the modern age of information, enabling the innovation of transistors, microprocessors, and integrated circuits. Over time, the dimension of transistors have reduced, exponentially increasing the computation abilities of memory chips (Moore's law). The semiconductor foundry uses silicon and germanium as 'standard cMOS' semiconductor platforms, and has adopted the 'more-than-Moore' route in recent times via hybridization of chips and sensors. But the individual size of transistors is approaching the limit of the validity of classical physics. Quantum computation has emerged as the solution to the above problem, with additional advantages in terms of encryption, entanglement, and exponential speedup.

The spin angular momentum of an electron (or hole, nucleus) can constitute the basis of a quantum computer owing to its quantized nature and insensitivity to electric fields. This thesis focuses on spin qubit systems fabricated in semiconductors, particularly in group-IV semiconductors e.g. Si and Ge. Semiconductor spin qubits can be coherently controlled via microelectronics in atomistic length scales, and the material platform offers a direct route towards scaling up. During the past two decades, semiconductor spin qubit technology have burgeoned rapidly; leveraging single-shot readout, electrically driven spin resonance, error-correction techniques and multi-qubit control.

In this work, the theoretical investigation of phosphorus multidonor qubit in silicon has been carried out in view of the multi-valley effective mass approach. We show that such electron multidonor spin qubits can exhibit fast and coherent electrical control due to the difference in hyperfine interaction in neighboring dots. The collective interest in full electrical control of spin qubits have given rise to significant interest in hole spin qubits, where the large intrinsic spin-orbit interaction enables optimization of certain experimental parameters. Here we model a single hole spin qubit in planar $Ge/Si_{1-x}Ge_x$ heterostructure using the k.p formalism. We study nontrivial spin-orbit interaction enabled features of spin-3/2 hole qubits, contrasting to spin-1/2 electrons. Finally, we calculate the effects on hole qubits due to random alloy disorder and thermal contraction of metallic gatestack atop the planar germanium heterostructure. Our work builds the foundation for theoretical modelling of electron and hole spin qubits in planar group-IV semiconductors.

Acknowledgement

The journey of completing this PhD has been both challenging and deeply rewarding. I am immensely grateful to those who have supported and inspired me throughout this process. Their encouragement and guidance have been instrumental in making this thesis possible.

First and foremost, I extend my deepest gratitude to my Guru and primary supervisor, Dimitrie Culcer, whose guidance and teachings have been invaluable. His unwavering support, both professionally and personally, has shaped my academic growth. I am profoundly grateful for his mentorship, which provided me with exceptional opportunities and helped me navigate the many challenges of my PhD journey. I would also like to thank my joint primary supervisor Andrew Dzurak, my secondary supervisor Rajib Rahman, and Andre Saraiva for letting me learn from and collaborate with them throughout my PhD. Their discerning expertise in experimental techniques and computational analyses has significantly enhanced my comprehension and expanded the intellectual scope of this thesis. I am thankful to Michelle Simmons, Xuedong Hu, Joe Salfi, Jukka Vayrynen, Tetsuo Kodera and Sankar Das Sarma for invaluable discussions. I am indebted to Alex Hamilton for numerous intriguing interactions about physics and more.

This thesis would not have been possible without the amazing support of my colleagues and friends. I am incredibly fortunate to have had the support of my fellow group members Sina Gholizadeh, Zhanning Wang, James H. Cullen, and Rhonald Burgos Atencia. Their enthusiasm, camaraderie, and encouragement have been invaluable throughout my PhD. I deeply appreciate the collaboration and insights shared by Joel Hochstetter, Pratik Chowdhury, Allen Kha, Mathew Rendell, Mohammad Khalifa, Nico Hendrickx, Giordano Scappucci, and Menno Veldhorst, whose expertise greatly contributed to this work. I am deeply grateful to Marcus Goffage, Aaquib Shamin, Ajit Dash, Scott Liles, Serajum Monir, Krittika Kumar, Yoni Ashlea Alava, Jack Engdahl, Upendar Singh, Jesús Cifuentes, Isaac Vorreiter, Yu-ling Hsueh, Yik Kheng Lee and Jonathan Huang. I would also like to thank Nan Lee, Alexandar Hahn, Ronakraj Gosalia, Kira Platt-Behrens, Hassaan Sadat, Shefali Bharadwaj, Satish Verma, Nathan K. Long, Abhay Gupta, Abhirup Bhadra, Anjali Dhiman, Sattvik Narayan, Ridhhi Ghosh, Anirban Dey, Benjamin Wilhelm, Melanie Allgäuer, Keshavi Charde, Sangeet Kumar, Tristin Rice, Aman Khalid and Deepa Singh for their kindness and acquaintanceship that amounted to a lot of my personal growth. I am eternally grateful to Shagun Aggarwal for her love and support during this journey.

ACKNOWLEDGEMENT

I acknowledge UNSW and the School of Physics for their generous support, including scholarships, travel grants, computational resources, and administrative assistance. I would like to thank the ARC center of excellence Future low Energy Electronics and Technologies (FLEET) and its people for providing an incredibly collaborative platform. I sincerely appreciate the Sydney Quantum Academy (SQA) for awarding me an extension scholarship and for fostering a vibrant quantum research community in Sydney. I would like to thank my fellow SQA student committee members Adesh Kushwaha, Karl Lin, Jasleen Kaur, Zsolt Szabó and Rose Graham for providing me the opportunity to learn a few important management skills. I will always be sincerely thankful to the first year teaching community of UNSW School of Physics, especially Thomas Dixon, Kate Jackson and Jonathan Rebolledo Moya.

This PhD journey has been as incredible as the journey leading to it, sprinkled with indispensable interactions with all of my teachers at Katiahat BKAP Institution and later at IIT Kharagpur. I am grateful to my teacher Satyajit Sarkar for for sparking my enthusiasm for physics at an early stage and my Masters thesis supervisor Shailendra K. Varshney for his guidance and mentorship. I am sincerely grateful to Garnett Bryant for offering me a crucial early research opportunity that laid the foundation for my academic journey. A heartfelt thank you to my dear friends Omprakash Chandra, Subhadip Bouri, Judhajeet Basu, Diganta Sarkar, Neelakash Biswas, Satyabrata Baidya, Laboni Sarkar, Sohana Parvin, and Soumya Mondal, whose support and friendship have been a source of strength and joy throughout this journey.

Above all, I dedicate this thesis to my parents, whose unconditional love, sacrifices, and belief in me have made this journey possible. This achievement is as much theirs as it is mine.

تو در تمام جهان هستی و تمام جهان در توست
"You are in the entire universe,
and the entire universe is within you"
-Rumi

Publications and Presentations

List of Publications

- **Optimisation of electron spin qubits in electrically driven multi-donor quantum dots.** *npj Quantum Information volume 8, Article number: 127 (2022)*

  - **Abhikbrata Sarkar**, Joel Hochstetter, Allen Kha, Xuedong Hu, Michelle Y. Simmons, Rajib Rahman & Dimitrie Culcer.

- **Electrical operation of planar Ge hole spin qubits in an in-plane magnetic field** *Physical Review B 108, 245301 (2023)*

  - **Abhikbrata Sarkar**, Zhanning Wang, Matthew Rendell, Nico W. Hendrickx, Menno Veldhorst, Giordano Scappucci, Mohammad Khalifa, Joe Salfi, Andre Saraiva, A. S. Dzurak, A. R. Hamilton & Dimitrie Culcer.

- **Electrical operation of hole spin qubits in planar MOS silicon quantum dots** *Physical Review B 109, 075427 (2024)*

  - Zhanning Wang, **Abhikbrata Sarkar**, SD Liles, Andre Saraiva, A. S. Dzurak, A. R. Hamilton & Dimitrie Culcer.

- **Effect of disorder and strain on the operation of planar Ge hole spin qubits** *arXiv preprint 2502.06949 (2025)*

  - **Abhikbrata Sarkar**, Pratik Chowdhury, Xuedong Hu, Andre Saraiva, A. S. Dzurak, A. R. Hamilton, Rajib Rahman, S. Das Sarma & Dimitrie Culcer.

List of Presentations

Oral presentations:

- **Optimisation of electron spin qubits in electrically driven multi-donor quantum dots**

  American Physical Society (APS) March Meeting
  March 5 - March 10, 2023, Las Vegas, USA

- **Hole qubits: quantum computing with unfilled valence band states in semiconductors**

  Sydney Quantum Academy (SiQEW) student seminar
  June 29, 2023, Sydney, Australia

- **Electrical operation of planar hole qubits: Silicon vs. Germanium**

  Silicon Quantum Electronics Workshop (SiQEW)
  October 31 - November 2, 2023, Kyoto, Japan

- **Electrical operation of planar Ge hole spin qubits in an in-plane magnetic field**

  Australian and New Zealand Conference on Optics and Photonics and Australian Institute of Physics (ANZCOP-AIP) Summer Meeting
  December 3 - December 8, 2023, Canberra, Australia

Poster presentations:

- **Optimisation of electron spin qubits in electrically driven multi-donor quantum dots**
  Australian Institute of Physics (AIP) Congress
  December 11 - December 16, 2022, Adelaide, Australia

- **Effect of roughness in planar Ge hole spin qubit**
  Silicon Quantum Electronics Workshop (SiQEW)
  September 4 - September 6, 2024, Davos, Switzerland

Abbreviations

BIA	Bulk Inversion Asymmetry
CB	Conduction Band
CMOS	Complimentary Metal Oxide Semiconductor
EDSR	Electron Dipole Spin Resonance/ Electrically Driven Spin Resonance
EFA	Envelope Function Approximation
EMA	Effective Mass Approximation
ESR	Electron Spin Resonance
FID	Free Induction Decay
FinFET	Fin Field Effect Transistor
IIA	Interface Inversion Asymmetry
MOSFET	Metal Oxide Semiconductor Field Effect Transistor
QD	Quantum Dot
QW	Quantum Well
RTN	Random Telegraph Noise
SIA	Structural Inversion Asymmetry
SOC	Spin-Orbit Coupling
TBA	Tight Binding Approximation
VB	Valence Band

Preface

> "I can believe, that a girl alone might be walking on a narrow trail somewhere in the Rockies and might lose her step, and, rolling down to the precipice, manage to grab a tiny pine at the brink and so save herself from inevitable death. I can also imagine that, just at that time, a handsome cowboy might be riding the same trail, and, noticing the accident, tie his lasso to his horse's saddle and descend into the precipice to save the girl. But it looks to me extremely improbable that at the same time a cameraman would be present to record this exciting event on film!"
>
> -Niels Bohr.

George Gamow's book 'Thirty years that shook physics' mentions Bohr's above comment on the impossibility of knowing precisely both position and momentum of a particle, one of the ramifications of the probabilistic nature of quantum physics. Emerging from the besieging paradoxes of the statistical models of light absorption and emission, quantum mechanics soon became the key to understanding elementary electronic structures. Remarkably, the 'peculiarities' of quantum mechanics have amalgamated into quantum computing, the latest emissary of modern science and technology with a fundamental capability to outperform classical computation. Quantum computing necessitates the engineering of elementary systems (e.g. single electrons or holes confined in a quantum dot) in various material platforms, where the governing physics of the energetically or topologically protected quantum 'bits' often stems from condensed matter theory. In a broad sense, condensed matter theory describes the microscopic origin of the tangible properties in materials. In this study, semiconductor quantum dots in the few electron/hole regime will be theoretically modeled, constituting the building blocks of a feasible quantum computer. Condensed matter theory will be extensively applied not only to optimize the material induced phenomena; but also to approximate the microscopic laws of quantum physics in view of the mesoscopic energy hierarchy or symmetries, wherever appropriate.

At the dawn of the 20^{th} century Planck's theory of *'light quanta'*, a formalism that mitigates ultaviolet catastrophe of radiation by treating electromagnetic radiation as discrete packets of energies proportional to the wavelength ($E = h\nu$), would set modern physics in motion. Over the next three decades, the consequences of the quantum theory such as light-matter interaction (photo-electric effect, Compton scattering), wave-particle duality (de Broglie matter wave, Davisson-Germer electron diffraction), probability interpretation and superposition principle (uncertainty relation, Schrödinger wave equation) became imperative in understanding microscopic systems. Quantum mechanical description of electronic structure introduced the concept of **spin** angular momentum, an intrinsic property

of particles with no classical counterpart which was experimentally demonstrated in 1922 by Otto Stern and Walther Garlach. The Stern-Garlach apparatus is depicted in the figure

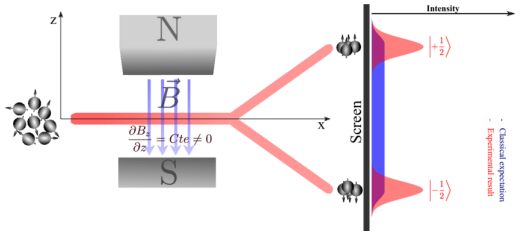

above, where a beam of silver atoms are passed through an inhomogeneous magnetic field. The magnetic moment proportional to the electron 'spin' ($\mu \propto \mathbf{S}$) would cause the silver atoms to deviate due to the magnetic force $\mathbf{F}_B \propto \mu \cdot \mathbf{B}$. Since the silver atoms are randomly oriented, classically the magnetic moment would acquire all values in the range $-\mu$ to μ, and a continuous mark would be seen when the atoms collide with a screen. Instead, two distinct spots are observed, signifying quantization of the spin angular momentum of the electron to create a two-level spin $\frac{1}{2}$ system.

Subsequently, quantum measurement was realized to have the distinct property that probabilistic microscopic systems collapses into a definitive state upon measuring, and in a sequence of measurements only the information of the final one prevails. The effect of quantum measurement on causality led to another peculiar property, entanglement. In 1935, Einstein-Podolsky-Rosen (EPR) paradox stated that the principle of locality in Schrödinfer's wave equation must be preserved via 'hidden variables'. This postulate was proved to be inconsistent by J.S. Bell in 1964. Furthermore, Bell inequalities asserted an upper limit of correlation for systems obeying local realism, and specially prepared microscopic systems would violate the upper limit of Bell inequalities by virtue of quantum entanglement. Parallel to the revolution in information technology through transistors over the next two decades, quantum information was conceptualized by the likes of Wiesner, Bennett and Feynman. The motivation was two-fold: synthesizing elementary quantum systems to study the fundamental principles of quantum mechanics, and using properties of quantum bits or qubits to gain advantage over classical computation. While the latter route saw the emergence of quantum algorithms (Shor, Deutsch-Jozsa, Grover) and quantum cyptography (BB84), the former laid the groundwork to develop novel architectures for qubit engineering. The key requirements for a suitable platform for quantum computation are given by the DiVincenzo criteria:

- "A scalable physical system with well characterized qubits": the quantum analog of binary bits, denoted by orthogonal basis states $|0\rangle$ and $|1\rangle$. A well characterised qubit implies precise knowledge of the Hamiltonian, and minimal coupling to higher energy states.
- "The ability to initialize the state of the qubits to a simple fiducial state, such as $|000..\rangle$": a necessary requirement for efficient quantum error correction.
- "Long relevant decoherence times, much longer than the gate operation time": decoherence is key to emergence of classical behaviour. Detrimental to quantum com-

puting, dephasing should be slower by a factor of $10^3 - 10^5$ with respect to the 'clock time' of the fault-tolerant quantum computer.

- "A 'universal' set of quantum gates": single- and two-qubit gates have to be synthesized, preferably by controlling physical interactions in the system, e.g. exchange.
- "A qubit-specific measurement capability": majority of the quantum register can be read out after the computation with high fidelity.

Semiconductor spin qubits enable fault-tolerant quantum computing in view of the DiVincenzo criteria, thanks to their potential scalability and compatibility with classical electronics for coherent control and readout. Condensed matter theory has provided crucial cognizance of semiconductor quantum computing during its evolution. While Dirac equation (1928) explained relativistic origin of the interplay between spin- and orbital-degrees of freedom, known as the spin-orbit coupling (SOC); Bloch wave formalism (1928) and band structure theory interpreted electronic structure with lattice periodicity and distinguished metals, semiconductors and insulators. The invention of transistors in 1947 unfolded a widespread investigation of semiconductor physics. By the 1980s, the concepts of symmetry and topology had rendered condensed matter theory a sophisticated field concerning various novel phenomena in semiconductors, superconductors and topological phases; and theory of invariants had significant implication in spintronics. Superconducting and topological quantum computation have since burgeoned, while semiconductor qubits have managed to harness the fabrication supremacy of high quality *on-chip* integration, especially in silicon.

Quantum computation with spin can be traced back to the mathematics of the spin-$\frac{1}{2}$ system, where a qubit can be designated as a probabilistic superposition of spin-up and spin-down states: $|\psi\rangle = \alpha\,|0\rangle + \beta\,|1\rangle$, with respective probabilities given by $|\alpha|^2$ and $|\beta|^2$. External conditions can alter the nature of the superposition, essentially 'rotating' the spin in the Bloch sphere. These operations form the irreducible representation $\mathcal{D}_{1/2}$ of the full rotation group with the following matrices:

$$\mathbb{I} = \begin{pmatrix} 1 & 0 \\ 0 & 1 \end{pmatrix};\ \sigma_x = \begin{pmatrix} 0 & 1 \\ 1 & 0 \end{pmatrix};\ \sigma_y = \begin{pmatrix} 0 & -i \\ i & 0 \end{pmatrix};\ \sigma_z = \begin{pmatrix} 1 & 0 \\ 0 & -1 \end{pmatrix} \tag{1}$$

Single qubit gates for various of these rotations can be implemented via microwave pulses. For two spins, the representation becomes $\mathcal{D}_{1/2} \otimes \mathcal{D}_{1/2} = \mathcal{D}_0 \oplus \mathcal{D}_1$, allowing two-qubit gates e.g. CNOT (panel 1) which enables quantum entanglement (panel 2). Physically, such two-qubit gates in spin qubits can be employed via exchange interaction between two spins, an example pulse sequence of which is shown below (panel 3-4).

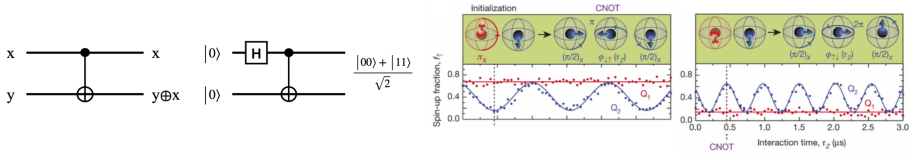

The advantage of quantum computing originates from the fact that a quantum state preserves its probabilistic composition unless 'looked at'. Along with spin, the orbital structure of the particle and the corresponding symmetry also play a role, paving the way for spin-orbit coupling mediated gate control. In a nutshell, to describe a single spin qubit operation in a semiconductor quantum dot (QD), one requires to know the dispersion of the energy levels in the QD, and the effect of external fields on the spin and orbital energies. This is summarized as the qubit Hamiltonian $H_{\rm QD}{=}H_{\mathbf{k}} + V_{\rm QD} + g^*\mu_B\sigma\cdot\mathbf{B} + e\mathbf{E}\cdot\mathbf{r} + H_{\rm SO}$, where the first two terms denote the kinetic and potential energies of the confined particle. The next two terms define the external electromagnetic environment, and the last term suggests the spin-orbit coupling which usually moderates single-qubit gates. For two qubits, exchange interaction couples the spins and orbital degrees of freedom, inducing terms such as $J\,\sigma_1\cdot\sigma_2$.

Spin of the extra electron of a phosphorus donors in silicon can make a highly coherent Kane qubit. With donors, the QD confinement potential for the conduction band electron comes for free, and coherent qubit control is possible via a nearby ESR channel. Moreover, silicon benefits from immense fabrication advancements, offering minimal disorder and potential scalability. More recently, gate-defined valence band hole spin qubits in high mobility germanium and silicon quantum dots have gained tremendous interest due to the large intrinsic spin-orbit couplings. A detailed theoretical study is imperative to harness the variability of spin qubit properties in these architectures. Despite the stark contrast in the nature of confinement, valley and band structure; both electron and hole spins in group-IV semiconductor quantum dots showcase full electrical and highly coherent qubit operation. The governing physics stems from the underlying symmetry, and its reduction due to the intrinsic and extrinsic interactions.

INSTITUT INTERNATIONAL DE PHYSIQUE SOLVAY

SEPTIÈME CONSEIL DE PHYSIQUE -- BRUXELLES. 22-29 OCTOBRE 1933

Photo Benjamin Couprie 26, avenue Louise, Bruxelles

H. A. KRAMERS N. F. MOTT G. GAMOW P. BLACKETT M. COSYNS Aug. PICCARD

E. STAHEL P. A. M. DIRAC J. ERRERA C. D. ELLIS E. O. LAWRENCE

E. HENRIOT F. JOLIOT W. HEISENBERG E. T. S. WALTON P. DEBYE B. CABRERA W. BOTHE Ed. BAUER J. E. VERSCHAFFELT J. D. COCKROFT L. ROSENFELD

F. PERRIN E. FERMI M. S. ROSENBLUM W. PAULI E. HERZEN R. PEIERLS

E. SCHRÖDINGER Mme I. JOLIOT N. BOHR A. JOFFÉ Mme CURIE O. W. RICHARDSON Lord RUTHERFORD M. de BROGLIE Mlle L. MEITNER J. CHADWICK

P. LANGEVIN Th. DE DONDER L. de BROGLIE

Absents : A. EINSTEIN et Ch.-Eug. GUYE

Chapter 1

Introduction

"In condensed matter physics, we can see quantum mechanics at work on a human scale."

- Anthony J. Leggett

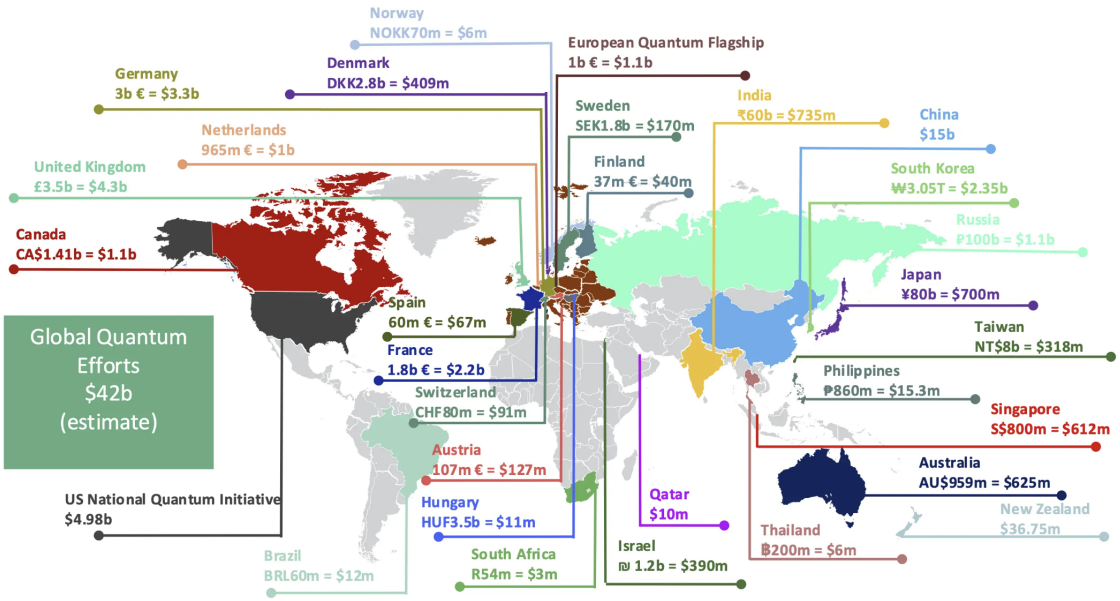

Figure 1.1: **Country-wise map of public sector investment in quantum computing.** The total public funding accounts for $42 billion, while private sector funding amounts to $8 billion (not shown).

$50+ Billion is the cumulative public and private investment in quantum computing over the past two decades (fig. 1.1).[1] With a projected economic value up to $2 Trillion by 2035 across chemical, life sciences, finance and mobility industries, quantum computing holds the key to the future of secure information processing. By virtue of the probabilistic superposition that constitutes the structure of quantum 'bits', or 'qubits', curated quantum algorithms offer exponential speedup over classical computing. The complexity of the classical computing chip, i.e. the number of transistors on the chip, was predicted to be doubled every 18 months by Gordon Moore.[1] For five decades, the exponential growth in silicon based chip optimization, along with wireless telecommunications, digital storage data capacity and latency, and supercomputing power have been well represented by the 'Moore's Law' (fig. 1.2). The original paper from 1965 comes with two incredible predictions, firstly,

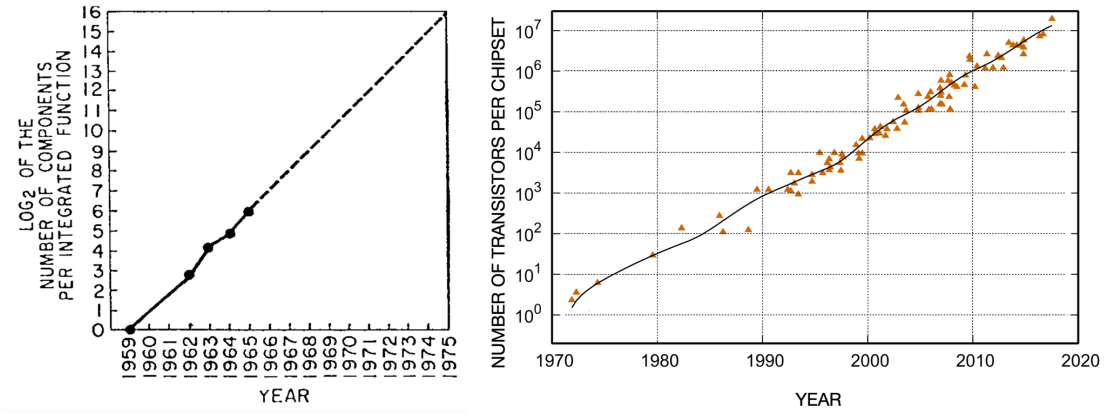

Figure 1.2: **Moore's Law.** (left) The original plot by Gordon Moore in 1965 predicting $2^{16} \approx 65000$ transistors on a single silicon chip by 1975.[1] (right) Moore's law remained valid for the next five decades (data from the *scipython* website).

"integrated circuits will lead to such wonders as home computers or at least terminals connected to a central computer, automatic controls for automobiles, and personal portable communications equipment" (fig. 1.3). Secondly, *"Silicon is likely to remain the basic material...silicon will predominate at lower frequencies because of the technology which has already evolved around it and its oxide, and because it is an abundant and relatively inexpensive starting material"*. Since 2015, the semiconductor industry has adopted the 'more than Moore' approach, which prioritizes hybridization of small chips as well as RF/optical

[1] figure from the QURECA website.

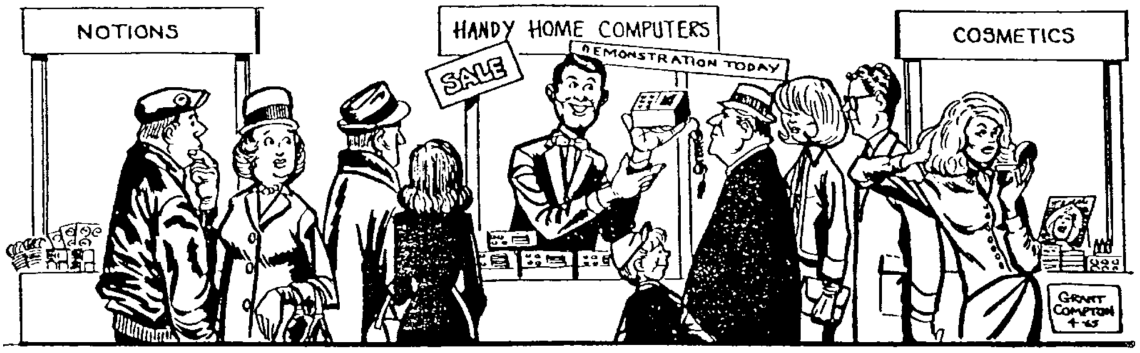

Figure 1.3: **Personal computers being sold as an everyday commodity,** as envisaged by Moore. The sketch is taken from his 1965 paper giving Moore's law.[1]

components and sensors. Today, the most powerful silicon based chip can accommodate a staggering 200 Billion transistors within 20"×30"×15" cubic inches. However, even with high quality chipset integration and FinFET technology, the size of the individual transistors within such integrated chips is pushing the limit of validity for the laws of classical physics. At atomic length scales, the electronic charge carrier would exhibit probabilistic behavior according to the laws of quantum mechanics. On one hand, the classical basis of computation is governed by the electronic current across a transistor turning 'on' above a threshold voltage and turned 'off' otherwise, constituting a binary 'bit' with 0 and 1 levels. Such a discrete two-level bit is possible to be constructed at the atomic length scale taking quantum mechanics into consideration, but, in contrast to the classical counterpart, a quantum bit, or 'qubit' is the probabilistic superposition of the quantum mechanical $|0\rangle$ and $|1\rangle$ states, commonly denoted as $|\psi\rangle = p\,|0\rangle + \sqrt{1-p^2}\,|1\rangle$. This produces the fundamental advantage of quantum computation while scaling up: for example, a two-qubit system $|\psi_1\psi_2\rangle = p_1p_2\,|00\rangle + p_1\sqrt{1-p_2^2}\,|01\rangle + p_2\sqrt{1-p_1^2}\,|10\rangle + \sqrt{(1-p_1^2)(1-p_2^2)}\,|11\rangle$ forms a 2^2=4 computational space. In general, n qubits produce a basis size of 2^n, while n classical bits lead to a basis size of n. This exponential speedup with quantum computing has been backed by extensive theoretical and experimental research, and novel qubit architectures have been engineered in microscopic systems across several material platforms. A functional quantum computer consisting of only a few hundred qubits would be required to handle the most complex tasks, although making them fault-tolerant via quantum error correction would eventually require 10^6 physical qubits. While the second quantum

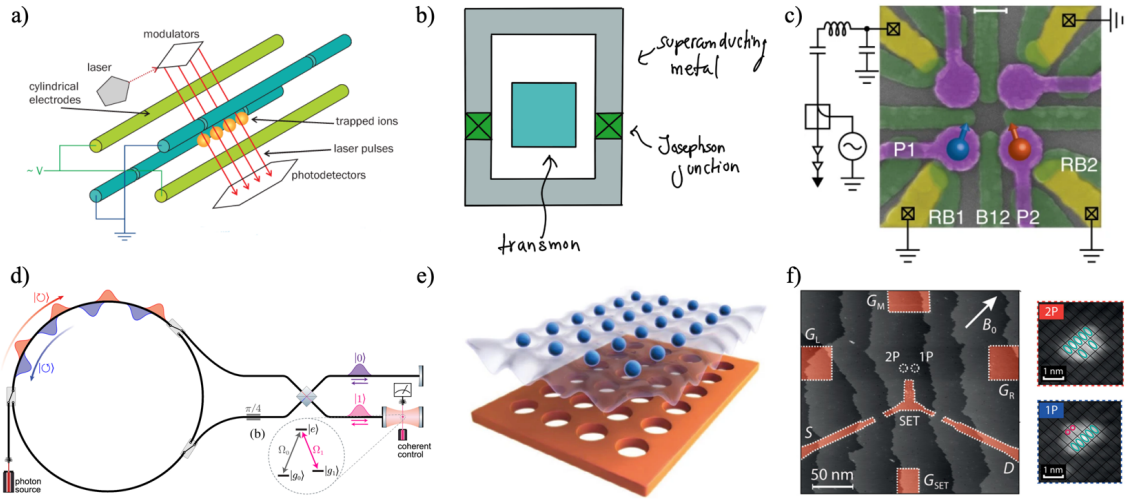

Figure 1.4: **Various feasible quantum computing architectures** in practice today: a) trapped ion qubit b) (superconducting qubit), c) solid state qubit in microscopic quantum dots defined via electrical confinements or gates,[2] d) optical qubit,[3] e) neutral atom,[4] f) impurity spin qubit, e.g. donor qubit[5].

revolution remains in the noisy intermediate-scale qubit (NISQ) era with the realization of $10^2 - 10^3$ physical qubits, quantum computing already hints at surpassing Moore's law in near future.[2]

While superconducting qubits and trapped-ion qubits have seen significant development, and optical qubits and neutral atom systems hold the key to quantum networking, the traditional semiconductor platforms show huge promise as a feasible host of quantum circuits. Because of advanced fabrication technology, group III-V (e.g. GaAs), or group IV (e.g. silicon, germanium) semiconductors can feature fault-tolerant qubits comprised of the spin and charge degrees of freedom of electrons or holes (fig. 1.4). In this study, the main focus will be on gate-defined and self-defined quantum dot spin qubits in group IV semiconductors. More specifically, coherent control of the multidot system with electron spin on deterministically doped phosphorus in silicon will be studied, where all-electrical qubit operation is enabled via engineered spin-orbit coupling. Hole spin qubits in gate-defined quantum dots will be inspected next, where the presence of intrinsic spin-orbit

[2]With error correction playing a huge role, quantum computation requires a different measure of its growth, e.g. Rose's Law.

coupling authorizes non-trivial electrical tuneability of qubit parameters.

1.1 Working principle of spin qubits

As delineated before, a qubit can be either in the 0 or the 1 state, or in a superposition of 0 and 1 state; hence, its state is denoted in the Dirac notation as $|\Psi\rangle = \alpha\,|0\rangle + \beta\,|1\rangle$, with the probabilities adding to unity: $|\alpha|^2 + |\beta|^2 = 1$. In other words, qubits can be interpreted as unit vectors in a two-dimensional complex vector space. In fact, the state of a qubit can be re-written as:

$$|\Psi\rangle = \cos\frac{\theta}{2}\,|0\rangle + e^{i\phi}\sin\frac{\theta}{2}\,|1\rangle \tag{1.1}$$

which enables representation of the qubit state as a point on a unit three-dimensional

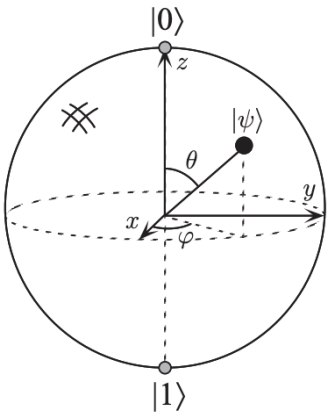

Figure 1.5: **The Bloch sphere** describes all single qubit rotations.[6] The $\theta = 0$ state signify the $|0\rangle$, or $|\uparrow\rangle$ spin state, and $\theta = \pi$ signify the $|1\rangle$, or $|\downarrow\rangle$ spin state. The equal superposition state $\frac{|\uparrow\rangle+|\downarrow\rangle}{\sqrt{2}}$ points along the x-axis ($\theta = \pi/2$, $\phi = 0$). Transition between the spin qubit levels $|\downarrow\rangle \rightleftharpoons |\uparrow\rangle$ would mean applying $R_x(\theta)$ or $R_y(\theta)$ rotations in the Bloch sphere (image is taken from Ref. [6]).

spherical surface, known as the Bloch sphere (fig. 1.5). Alterations in the qubit state are known as gate operations, some physical example of which could be altering the polarization of a photon or ionizing an electron from ground state to excited state. All such single-qubit gates can be described as rotations in the Bloch sphere. Spin qubits comprise of the spin-up $|\uparrow\rangle$ as $|0\rangle$ and spin-down $|\downarrow\rangle$ as $|1\rangle$ state, which are energetically differ-

entiated in an external magnetic field. An example of a gate operation on a spin qubit could be the electron spin resonance (ESR), where a magnetic pulse can rotate the spin $|\downarrow\rangle \leftrightarrow |\uparrow\rangle$ (known as the X gate), and depending on the duration of the pulse, can also induce a superposition such as $|+\rangle = (|\downarrow\rangle + |\uparrow\rangle)/\sqrt{2}$ (known as the H gate). Note that physical realization of spin qubits may involve the orbital degree of freedom as well, and the gate operations in that case are described in the 'dressed' qubit energy subspace which takes into account both spin and orbital angular momentum. Paradoxically, the superposition of qubit states does not translate to the classical act of measuring the qubit state, which would collapse into either $|\downarrow\rangle$ or $|\uparrow\rangle$ when observed. For example, measurement of $|+\rangle$ might give $\downarrow$, and the resultant qubit state after the measurement would be $|\downarrow\rangle$. The real implication of the superposition can be observed if 100 (ideally, infinite) identical $|+\rangle$ quantum states were measured; where the final state after measurement would be $|\downarrow\rangle$ approximately 50 times and $|\uparrow\rangle$ approximately other 50 times.

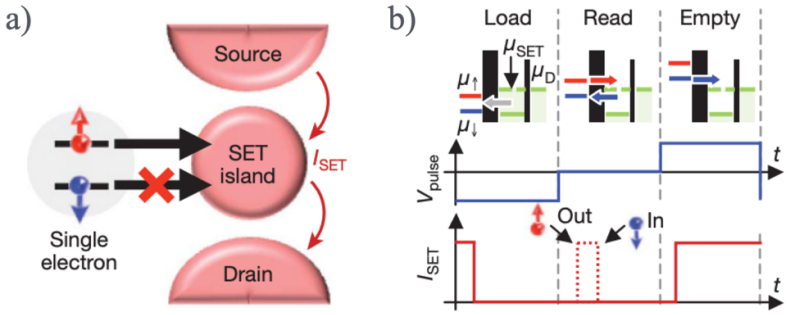

Figure 1.6: **The single-shot readout scheme** for deterministic initialization of spin qubits. a) The electrostatic and tunnel coupled SET island produces current peaks in I_{SET} based on the spin-state on the qubit site. b) This spin-to-charge conversion allows high-fidelity readout (images taken from Ref. 7).

How can a spin qubit be initialized in a known spin state and read out after gate operation(s), considering that any observation would destroy the probabilistic nature? This challenge is overcome by the single-shot readout technique (fig. 1.6), leveraging the concept of spin-to-charge conversion. A charge detector (generally single-electron transistors or single-hole transistors) can be electrostatically and tunnel coupled to the qubit as well as the source and drain electrodes. In presence of an external magnetic field $\mathbf{B}$, the spin-up and spin-down energy levels differ by the Zeeman splitting $\Delta E = g\mu_B B$, where g is

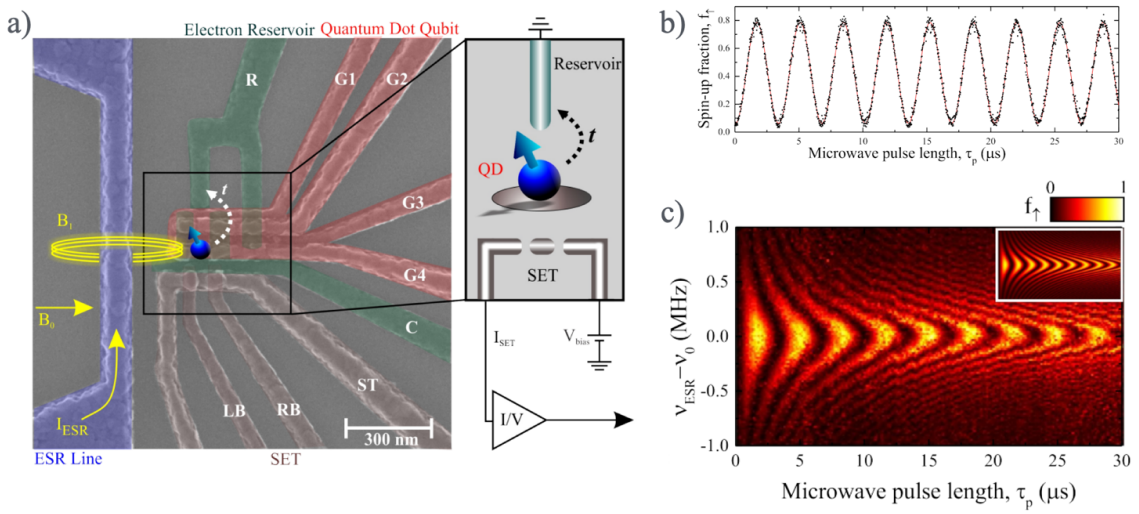

Figure 1.7: **Electron Spin Resonance experiment setup:** a) Gate-defined quantum dot electron spin qubit with on-cip transmission line for applying ESR pulses (images taken from Ref. 8). b) Electron spin-up fraction as a function of the microwave burst duration, exhibiting ESR Rabi oscillation. c) Electron spin-up fraction as a function of microwave frequency detuning from the resonance frequency and microwave burst duration, exhibiting the Rabi-Chevron fringes.

the gyromagnetic ratio and μ_B is the Bohr magneton. Loading or emptying the qubit site can change the chemical potential of the detector due to the strong tunnelling. Due to spin blockade, characteristic peaks in the source-drain current I_{SD} are observed only for allowed chemical potential values of the charge detector. Single-shot readout allows initialization of the qubit with a desired spin angular momentum without any actual measurement of the state. The ability to read out a single spin with high fidelity, combined with spin resonance experiments, constitutes the basic of coherent spin qubit control.

The primary spin rotation technique is the electron spin resonance (ESR), where an alternating magnetic field $\tilde{\mathbf{B}}_{ac}$ in resonance with the qubit Larmor frequency $f_L{=}g\mu_B B/\hbar$ rotates the spin, as shown in figure 1.7. A microwave pulse sequence with periodic π pulses is usually employed via an ESR channel near the qubit to generate $\tilde{\mathbf{B}}_{ac} \perp \mathbf{B}$; and at resonance, the characteristic Rabi-Chevron fringes are observed. However, in the presence of spin-orbit coupling (SOC), the electric component $\tilde{\mathbf{E}}_{ac}$ of the applied EM wave can also induce electric dipole spin resonance (EDSR), since SOC creates an effective mag-

netic field proportional to the momentum of the electron/hole constituting the qubit. The absorption rate of the microwave signal with frequency ω_{MW} is given by,

$$I(\omega_{MW}) = 2\ Re[\sigma(\omega_{MW})]\tilde{E}_0^2 + 2\omega_{MW} g^2 \mu_B^2\ Im[\chi(\omega_{MW})]\tilde{B}_0^2 \tag{1.2}$$

where $\tilde{E}_0$ and $\tilde{B}_0$ are the electric and magnetic component amplitudes of the EM wave, $\sigma(\omega_{MW})$ is the optical conductivity and $\chi(\omega_{MW})$ is the magnetic susceptibility. Comparing the relative strengths of the electric and magnetic dipole contributions, it is understood that the second term is much weaker in presence of the spin-orbit coupling. EDSR opens up the possibility of low-power, full-electrical control of spin qubits. However, there exists finite detuning of the resonant frequency in spin-rotation experiments, which causes the Rabi oscillations to eventually decay with characteristic timescale $T_{2,Rabi}$.

The quantification of spin qubits' interaction with their environment is carried out in the form of longitudinal (relaxation) and transverse (decoherence) process. In the language of quantum information theory, the former is also called a bit-flip error, which is mediated by the quasiparticle of the lattice vibration i.e. phonons. An energy exchange between the qubit and the phonon modes can cause the qubit to relax from $|\uparrow\rangle$ to $|\downarrow\rangle$. Experimentally, the relaxation timescale T_1 is measured by introducing certain wait time τ_w after the π pulse induced $|\downarrow\rangle \rightarrow |\uparrow\rangle$ rotation, and measuring the population $P_\uparrow$. The aggregate dephasing effect of the later process is denoted by the characteristic time T_2^*, which can be measured by the Ramsey experiment. Two $\pi/2$ pulses are applied to the qubit in spin-down state, with a wait time τ_w between the pulses. For really short τ_w, the Ramsey sequence flips the spin. But the Larmor precision causes more precision of the spin along the equator of the Bloch sphere for longer wait time after the first pulse, and for $t_w \sim (n/2f_L)$, the qubit returns to the spin-down state after the second pulse. As a result, an oscillation between the qubit states is observed. This oscillatory pattern shows a decay for longer t_w, attributed to the static inhomogeneities from the environment (e.g. charge traps) influencing the qubit which eventually just stays at the equator. Incidentally, some of this phase-flip error can be reduced by applying more curated pulse sequences (fig. 1.8). Examples of such dynamical refocusing techniques which extend the qubit coherence are Hahn echo and CPMG dynamical decoupling. Hahn echo, consisting of a $\pi/2$ pulse,

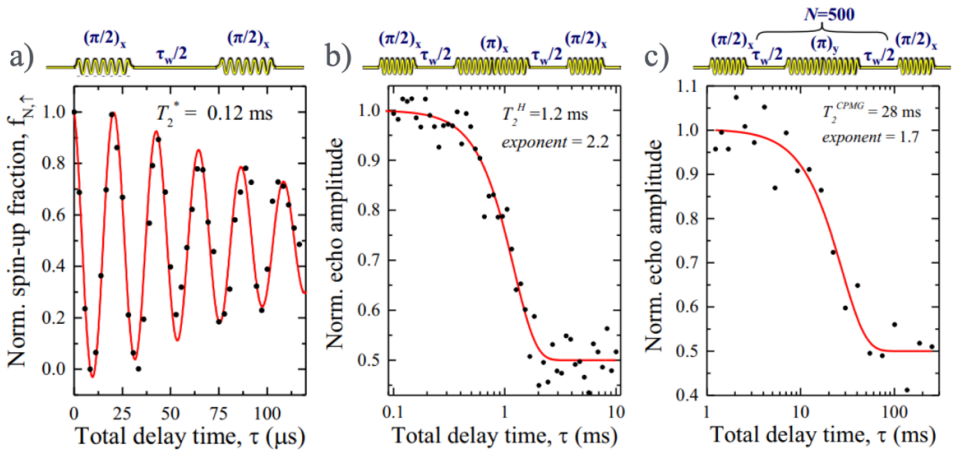

Figure 1.8: **Measurements of spin qubit decoherence:** a) Ramsey free induction decay experiment with a delay time τ_w between two $\pi/2$ pulses, b) Hahn echo measurement with an additional π pulse between the $\pi/2$ pulses, c) Carr-Purcell-Meiboom-Gill (CPMG) experiment with repeated π pulses in between (images taken from Ref. 8).

followed by a wait time of τ_w, a subsequent π pulse followed by another wait time of τ_w and a final $\pi/2$ pulse; counteracts the transverse 'fanning' of the qubit state along the equator. This measurement produces the improved decoherence timescale T_2, which can see further betterment via repetition of the π pulses as implemented in the Carr-Purcell-Meiboom-Gill (CPMG) pulse sequence. In fact, the aggregate dephasing is related to the transverse spin decay and static decay as follows:

$$\frac{1}{T_2^*} = \frac{1}{T_2} + \frac{1}{T_2'} \tag{1.3}$$

1.2 Experimental development of spin qubits in silicon and germanium

Spin qubits have been realized in various semiconductor material platforms, in self-defined as well as gate-defined quantum dots. Large variety is exhibited in the type of geometry (e.g. coupled planar quantum dots, nanowire etc.), type of primary carrier (e.g. electron or hole), and number of particles constituting one spin qubit (e.g. single spin, singlet-triplet etc.). The underlying universal control mechanism for many of these qubits largely

follows the two initial proposals outlined in fig. 1.9: the Loss-Divincenzo qubit,[9] and the Kane (donor) qubit.[10]

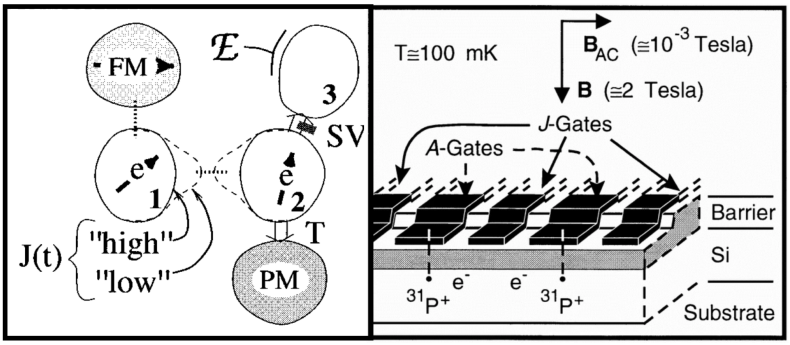

Figure 1.9: **Schematic of the Loss-Divincenzo qubit (LD qubit) and the Kane qubit.** In the Loss-divincenzo proposal, two quantum dot spin qubits, labeled 1 and 2, can be subjected to single qubit rotations via the ferromagnetic (FM) and the paramagnetic (PM) dots; and two-qubit gate operation can be performed by controlling the exchange interaction via the barrier between the dots (left).[9] The Kane proposal uses an one dimensional array of ^{31}P donors and electrons in Si separated by gate barriers. The resonance frequency of the nuclear spin qubits are controlled via the A gates, whereas the J gates control the electron-mediated interaction between neighboring qubits (right).[10]

The single-shot spin readout was originally demonstrated in planar GaAs/AlGaAs heterostructure QD, where the ferromagnetic island of the Loss-Divincenzo proposal was replaced with spin-to-charge conversion via reservoir coupling. In fact, III-V semiconductor platforms found initial success in initialization, control, and measurement of single- and two-electron spin qubits, but presence of nonzero nuclear magnetic moment (I$\neq$0) implied a short coherence time.[11–15] With 95% non-magnetic nuclei (I=0), natural silicon provides excellent qubit coherence with donor and gate-defined electron qubits, and isotopic purification leads to further improvement.[16] Deterministic doping and development of high-mobility quantum dot architecture posed significant challenges in Si platforms, but the highly sophisticated cMOS technology in Si constitutes a clear route towards scaling up beyond the NISQ era quantum computing. Additionally, group IV materials do not exhibit any piezo-electric phonon coupling. As discussed below, several architectures hosting spin qubits in group-IV semiconductors have satisfied ultra-fast, coherent and scalable

quantum computation.

1.2.1 Loss-Divincenzo qubits

The Loss-Divincenzo proposal theorized electrical one- and two-qubit gates via controlling the tunneling barrier gate voltage of coupled quantum dots hosting spin-1/2 single electrons (fig. 1.10). The LD qubit Hamiltonian in the Hubbard limit is given by: $H_{tot}=\frac{1}{4}J(t)\sigma_1 \cdot \sigma_2 + \frac{1}{2}g\mu_B \mathbf{B} \cdot \sigma_1$. In the LD proposal, lowering the tunnel barrier would

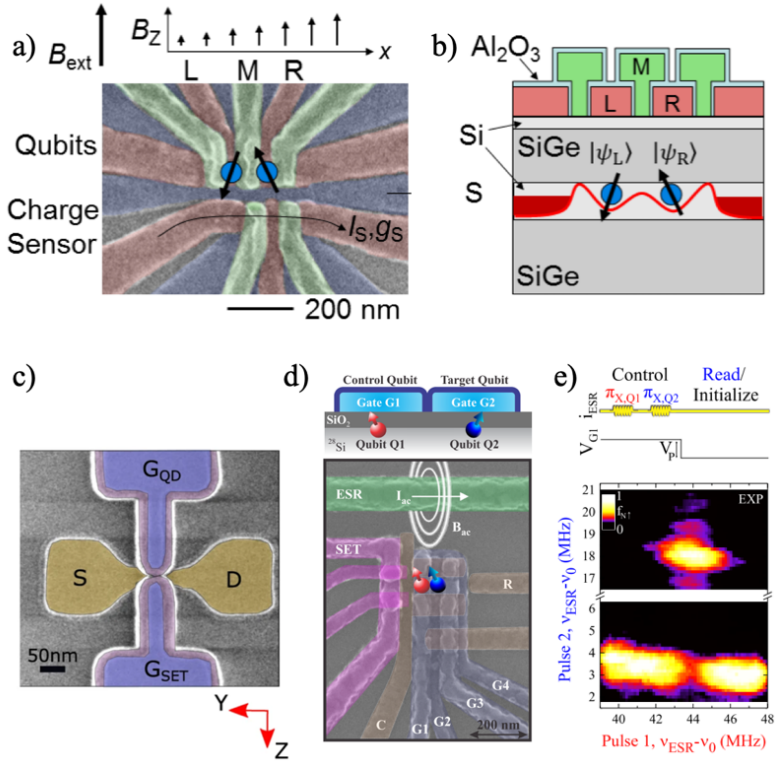

Figure 1.10: **Examples of Loss-Divincenzo qubits.** a-b) Coupled quantum dots in the silicon layer of Si/SiGe heterostructures with an attached micromagnet providing transverse coupling for fast qubit operation (images taken from Ref. 17). c) False-coloured scanning electron microscpy (SEM) image of electron spin qubit device in silicon CMOS with micromagnet and spin-valley coupling (image taken from Ref. 18). d-e) Gate-defined double quantum dot confining electron spins in natural silicon epilayer. A CNOT operation is realized by applying a π-pulse to Q1 before operation on Q2. Depending on Q1, Q2 rotates as the σ_z component controls the ESR resonance frequency of Q2 (images taken from Ref. 19).

result in a Heisenberg exchange coupling producing entanglement.[9] The spin manipulations were envisaged to be achieved via magnetic coupling to nearby ferromagnetic dot. Time dependent manipulation of **B** would constitute the single qubit operations, while a $\sqrt{\text{SWAP}}$ operation would be possible via $J(t)$ unitary evolution. High fidelity spin readout of LD qubit was first demonstrated for GaAs electrons by Elzermann et al,[11] but since been achieved in group-IV semiconductors as well, e.g. in $Si/Si_{0.7}Ge_{0.3}$ heterostructure hosting ^{28}Si quantum well.[20] In devices based on silicon CMOS technology, fast Rabi frequency of spin rotations ($f_R \sim 10$ MHz) via ESR mechanism were observed.[19, 21] However, the addressibility of individual qubits in an array became a huge question with the initial global control of ESR. Also the high power dissipation with ESR raised additional concerns about the qubit lifetime. The first issue could be overcome by novel means, e.g. using gate-tunability of the qubit g-factor [8]. But EDSR opened up the possibility of selective, as well as tunable qubit control, since it is a localizable, low-power mechanism. As outlined before, in the presence of spin-orbit coupling, EDSR becomes the primary spin rotation mechanism when the qubit is subjected to an ac microwave pulse. The early approaches of Nowack et al. [14] and Pioro-Ladriere et al. [22] saw electrical control of III-V semiconductor electron spin qubits to be achieved by leveraging either the intrinsic SOC, or the extrinsic SOC due to a micromagnet. More recently, Kawakami et al. have demonstrated EDSR in Si/SiGe device with micromagnet,[23] Croot et al. have shown EDSR spin rotation in Si/SiGe DQD via the flopping-mode mechanism,[24] and Klemt et al. have employed micromagnet based EDSR in Si CMOS device. [18] Two-qubit gates have been implemented via electrically controlled exchange interaction between two LD qubits in Si/SiGe heterostructures.[25] Subsequently, Veldhorst et al, [19] Watson et al, [26] Zazac et al, [17] Petit et al [27] have achieved coherent CNOT and CZ rotations of two qubits as well as high fidelity single qubit gates, hence demonstrating the full set of gates of an LD qubit.

1.2.2 Donor qubits

Kane proposed quantum computation in silicon using ^{31}P donor nuclear spin array with a gate-based sensing technique. In the Kane quantum computer, distant nuclear spins can couple via electron spin due to the hyperfine interaction, which can be enabled (disabled) via 'J'-gates by turning on (off) electron wavefunction overlap. Another set of gates, known as 'A'-gates, can electrically modify the electron wavefunction and in turn the resonance frequency of the nuclear spins, again by tuning the strength of the hyperfine interaction.[10] Scanning tunnelling microscope (STM) lithography and masked

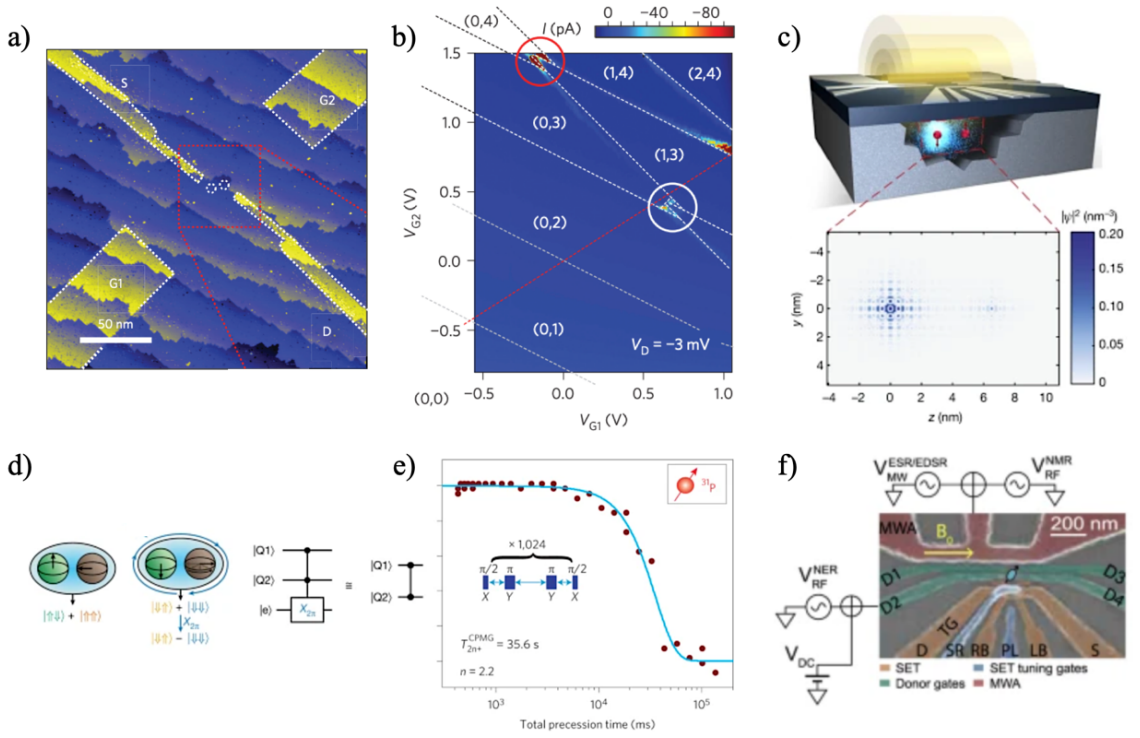

Figure 1.11: **Examples of Kane qubits with donor electron and nuclear spins.** a-b) STM image and charge stability diagram for demonstrating Pauli spin blockade in a double quantum dot with ^{31}P donor clusters in silicon (images taken from Ref. 28). c-d) Two qubit CZ gate with nuclear spin on two adjacent ^{31}P donors coupled to an electron spin shared by the donors (images taken from Ref. 29). e) Nuclear spin qubit coherence exceeding 30 seconds with CPMG pulse sequence on isotopically purified ^{28}Si sample (image taken from Ref. 30). f) ^{123}Sb qubit platform in silicon constituting a 16 dimensional Hilbert space (image taken from Ref. [31]).

ion-implantation methods have enabled incorporation of shallow ^{31}P donors in a silicon

substrate. Single P donor has 45 meV ionization energy and the spin of the nucleus and the extra electron of the P donor can constitute qubits in a naturally occurring quantum confinement with high degree of coherence. The nuclear gyromagnetic ratio is ∼2000 times smaller than the electron gyromagnetic ratio, so the nuclear spin qubit and the electron spin qubit can be addressed individually at different energy scales/ frequencies. Following the Kane proposal, gate-voltage control has been demonstrated (fig. 1.11), allowing high fidelity initialization and readout of single ^{31}P donor bound electron[7] and nuclear spins.[32] Betterment of electron readout in masked ion-implanated donor qubits has been enabled by the use of nearby cryogenic amplifiers.[33, 34] Same has been done for STM patterned donor qubits.[35, 36] Multi-donor dots have been synthesized as well, where the exchange interaction between the donor bound electrons can be controlled.[37] ESR spin rotation of donor bound electrons in natural silicon suffered fast damping due to the hyperfine interaction with the remnant nuclear spin in the sample.[38] Isotopic enrichment[30] demonstrated Rabi oscillation with long coherence time, with dynamical decoupling schemes protecting the qubits for seconds.[39, 40] EDSR via engineered spin-orbit coupling has been proposed in dot-donor or donor-donor systems,[41, 42] which may come from the hyperfine interaction, or an adjacent micro-magnet. In accordance with the original Kane proposal of using the donor nuclear spin as qubit, and using the electron for controlling the hyperfine interaction; high fidelity nuclear spin qubits[32, 39, 43] have exhibited really long coherence times $\sim$ 30 seconds.[30] Instead of phosphorus, higher magnetic moment nuclei such as antimony (Sb) with I=7/2 together with the electron spin can be used for producing 'qudits' with larger Hilbert space.[31, 44, 45] Two-qubit gates have been successfully employed for exchange coupled donor qubits,[28, 46–48] and via two nuclear spins hyperfine coupled to one electron based on geometric phases.[29] Interestingly for electrons in conduction band there exist multivalley interference, which induces atomic scale exchange oscillations for donor bound electron qubits.[49–52]

1.2.3 Hole qubits

More recently, holes in the valence band of group-IV semiconductors have emerged as a viable qubit candidate. Contrasting to electrons, holes exhibit *intrinsic* spin-orbit coupling due to the valence band having nonzero angular momentum (l=1). Hence a spin-$\frac{1}{2}$ hole has a total angular momentum of $j = \frac{3}{2}$ in the topmost valence band. Naturally, hole spin qubits have featured ultra-fast full electrical gate control in planar germanium (e.g. $Ge/Si_{1-x}Ge_x$ heterostructures) and silicon (e.g. c-MOS) quantum dot systems (fig. 1.12). The strong SOC inadvertently exposes hole qubits to noise, but at the same time, offers electrical tunability of the band structure and the qubit energy structure. This implies a possibility of a 'trade-off' between fast gate operation and coherent control of the hole spin. Besides, hole transport is majorly governed by the zone center (k=0), and hence devoid of valley degeneracy. The p-type valence band also implies vanishing contact hyperfine interaction with nuclear spins, limiting the decoherence mechanism to those of gate induced nature. Silicon MOS devices offer a great platform for hole quantum computing, but Ge enjoys a few state-of-the-art fabrication advantages in the 'More than Moore' race: namely, a very low effective mass of $0.05\,m_0$,[3] high mobility exceeding 10^6 $cm^2V^{-1}s^{-1}$ and compatibility with high-κ dielectrics.

Much theoretical predictions of hole spin quantum computation were made soon after the conception of electron spin qubits, motivated by long hole spin lifetime measured in InGaAs quantum dots. Significant experimental advances have taken place over the last decade or so. The motivation to develop high mobility p-channels led to the advent of $Ge/Si_{1-x}Ge_x$ heterostructures with strained Ge layer supporting two dimensional hole gas, and subsequently Ge/Si core-shell nanowire and Ge hut wire featuring one dimensional hole gas strongly confined in the Ge. Operation to the last hole, as well as singlet-triplet qubits have been featured in Ge, along with 4-qubit processor, 16-qubit crossbar Ge array. Harnessing the large intrinsic spin-orbit coupling of Ge, which has a spin-orbit energy gap of $\Delta_{SO} = 325$ meV, fast one- and two-qubit logic has been measured. The concept

[3] m_0=9.108×10^{-31} kg denotes the free electron mass. To quickly compare, Si electrons have longitudinal effective mass of $0.19\,m_0$ and a transverse effective mass of $0.91\,m_0$.

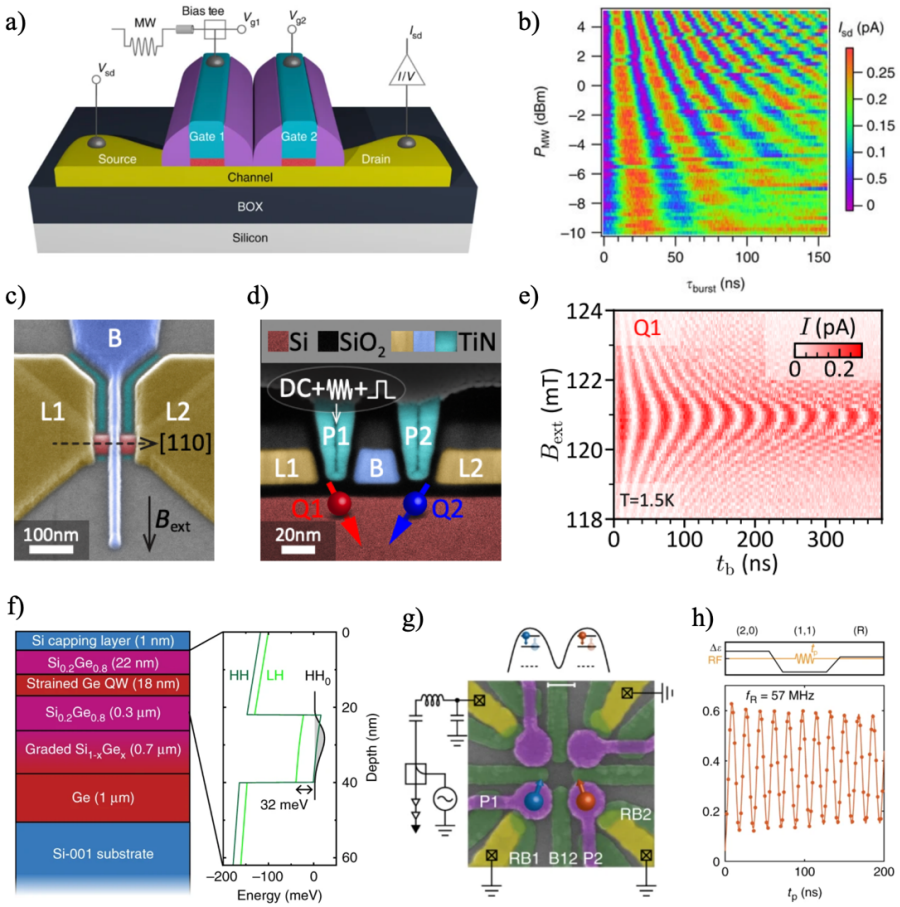

Figure 1.12: **Examples of hole qubits architectures.** a-b) Hole double quantum dot synthesized in a silicon-on-insulator nanowire field-effect transistor, exhibiting fast EDSR (images taken from Ref. 53). c-e) False-colour SEM and TEM images of a FinFET device in silicon showing coherent single hole spin qubit at 4 Kelvin, with the characteristic Rabi-chevron fringes (images taken from Ref. 54). f) Ge/SiGe heterostruture favoring the formation of strained Ge hole quantum well (QW) due to type-I band alignment (image taken from Ref. 55). g-h) Fast EDSR Rabi oscillation of a single hole qubit defined in a 2×2 planar germanium QD array (images taken from Ref. 2).

of operational *sweet spots* and *sweet lines* have emerged in Ge, where specific magnetic field orientation and potential profile enable the fast nanoseconds-scale hole spin EDSR rotation despite slow microseconds-scale decoherence. Silicon cMOS planar devices have demonstrated large tunability of spin qubit properties by electrical (gate) and mechanical (strain) means. Silicon has a smaller spin-orbit energy gap of $\Delta_{SO} = 44$ meV, leading to nontrivial mixing with the split-off band. Si hole is heavier (effective mass $0.2m_0$), which

results in smaller dot size. Si finFET devices[54, 56] have demonstrated hole spin qubit operation over 4 Kelvin. The large g-factor anisotropy for holes symbolizes the spin-orbit coupling mediated Zeeman interaction, and plays a huge role in one and two qubit logic (e.g. g-tensor modulation resonance, coherent Δg driven oscillation).

1.2.4 Singlet-triplet qubits

While the exchange interaction J between two spins in a double quantum dot system is crucial for constructing two-qubit gates, it can also be used for defining a singlet-triplet qubit. The detuning of the DQD levels offers control over the energy splitting $J(\epsilon)$ between the spin singlet state S and the T_0 spin triplet state, and the presence of tranverse coupling ΔB_z via the hyperfine / g factor difference between dots / micromagnet implies a ST_0 qubit operation. At a specific DQD detuning, the singlet S state exhibits

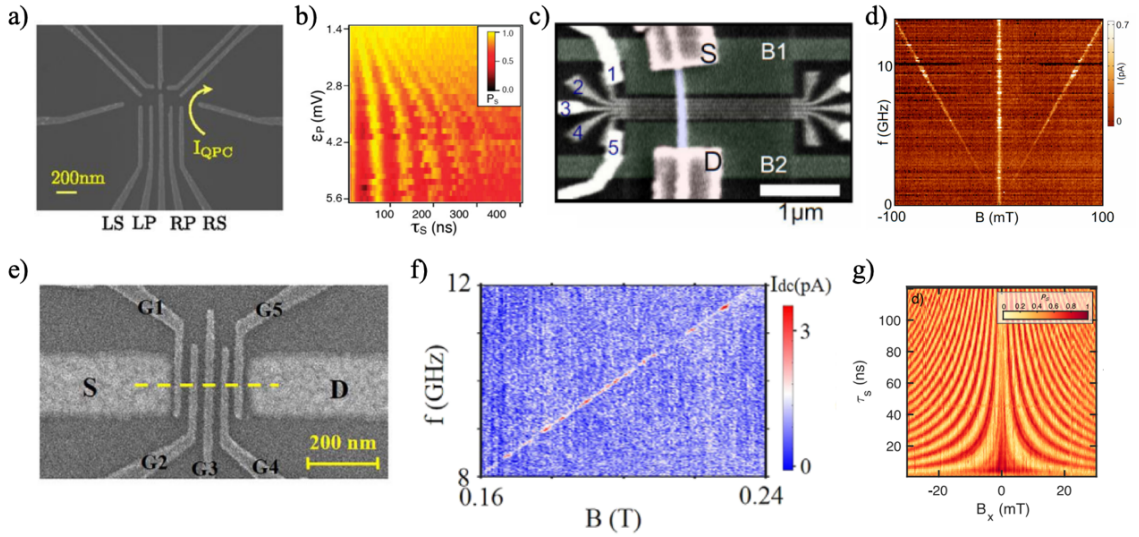

Figure 1.13: **Examples of singlet-triplet qubits** a-b) Micromagnet mediated Singlet-triplet qubit operation in Si/SiGe heterostructure, with characteristic rabi-Chevron oscillations (images taken from Ref. 57). c-d) InAs nanowire device showcasing a singlet-triplet qubit, showing EDSR V-shape when the Larmor frequency is mapped against the microwave drive frequency and magnetic field (images taken from Ref. 58). e-f) Germanium hut wire singlet-triplet qubit with holes, showing the characteristic EDSR line at resonance (images taken from Ref. 59). g) Δg driven oscillation of a singlet-triplet hole spin qubit in planar silicon cMOS device (image taken from Ref. [60]).

an energy anticrossing with the T_- triplet state, since $J(\epsilon)$ compensates for the triplet Zeeman splitting E_z. Around anticrossing, an ST_- qubit can be defined with $E_z - J(\epsilon)$ energy splitting. Again, the transverse coupling responsible for the anti-crossing gap Δ_{ST} can originate from various spin-orbit interactions. Pauli spin blockade (PSB) in the double quantum dot is employed for initialization and readout of singlet-triplet qubits.[25, 61, 62] Fast single-qubit gates are enabled via a large transverse effective field ΔB_z (fig. 1.13), although it might result in lower PSB fidelity due to the enhanced relaxation process. The Latched readout protocol has been introduced to counteract this problem.[63–65] Charge noise is the main source of decoherence for ST qubits in group-IV semiconductors, originating from the two-axis control's dependence on detuning and SOC. Two-qubit gates can be realized from the capacitive coupling of two nearby ST qubits, where the change in the exchange oscillation frequency of one qubit can effect the charge configuration of the other qubit.

1.2.5 Flopping-mode, hybrid architectures and more

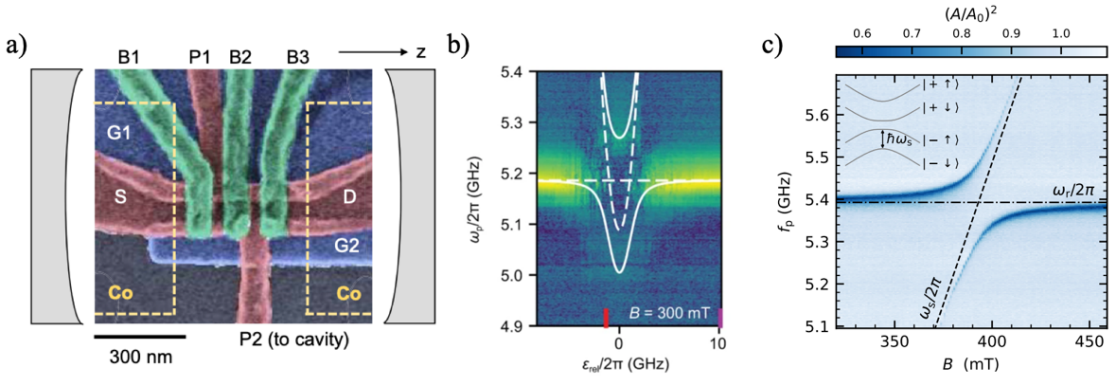

Figure 1.14: **Flopping-mode and hybrid semiconductor-superconductor qubit examples** a) SEM image of flopping-mode electron qubit in Si/SiGe double quantum dot leveraging the large dipole moment (image taken from Ref. 24). b) Signature of strong electron spin-photon coupling in InAs nanowire device, showing anti-crossing of the qubit and resonator when the resonator transmission is plotted against detuning and probe frequency (image taken from Ref. 66). c) Signature of strong hole spin-photon coupling in silicon nanowire double quantum dot-microwave resonator (DQD-MWR) hybrid device. The transmission amplitude anticrossing is observed when spin qubit transmission frequency matches bare resonator frequency (image taken from Ref. 67).

A few other spin-qubit architectures have seen significant development in group-IV semiconductor platforms, with the aim of improving the qubit quality factor Q (generally given by the number of spin-flips before the qubit dephases), or scaling up. A flopping mode qubit uses the large electric dipole of double quantum dot setup with a magnetic field gradient to achieve a fast, second order spin manipulation via the charge states. More recently, strong capacitive coupling between superconducting resonators and quantum dots have drawn attention to hybrid semiconductor-superconductor systems, which are ideal for reaching strong spin–photon, or charge-photon coupling; paving the way to long-range quantum circuit and scaling up quantum devices. Experiments in past years have observed double quantum dot in Si[68] and resonant exchange qubit in GaAs[69] exhibiting strong coupling between the spin and charge degrees of freedom of electron and microwave photon (fig. 1.14). The hybrid platforms have also been able to unlock new technological precedence, such as RF reflectometry via resonator response in gate-based dispersive sensing,[70] and in-situ tunnel barrier instead of conventional gate electrodes which simplifies the integration with superconducting circuits.[66, 71] Importantly, there are fundamental advantages for hole-photon systems due to the intrinsic spin-orbit interaction of holes offering fine tuning of hybrid quantum circuits.[67] Planar Ge hole QD with cubic Rashba favors Majorana bound states[72] and Andreev spin qubits.[73, 74] Also, hole singlet-triplet qubits can be operated at much lower fields, making on-chip integration with superconducting resonators more plausible. By and large, the study of semiconductor spin qubits beyond the two qubit regime remains juvenile. Coherent control of qubit arrays have seen significant effort, especially in 2D arrays with electron quantum dots, donors and hole quantum dots.

1.3 Theory of donor and hole spin qubits in silicon and germanium

Under quantum confinement, the wavefunction and energies of discrete levels of a particle are given by the Schödinger wave equation. For the simplest example of an hydrogen

atom, the single electron Schödinger equation is:

$$\hat{H}\Psi(r,\theta,\phi) = \left(-\frac{\hbar^2\nabla^2}{2\mu} - \frac{e^2}{4\pi\epsilon_0 r}\right)\Psi(r,\theta,\phi) = E\Psi(r,\theta,\phi) \tag{1.4}$$

The solution is well known:

$$\Psi_{nlm}((r,\theta,\phi)) = \sqrt{\left(\frac{2}{na_0^*}\right)^3 \frac{(n-l-1)!}{2n(n+l)!}} e^{-\frac{r}{na_0^*}} \left(\frac{r}{na_0^*}\right)^l L_{n-l-1}^{2l}(r/na_0^*)\, Y_l^m(\theta,\phi) \tag{1.5}$$

where $a_0^* = \frac{4\pi\epsilon_0\hbar^2}{\mu e^2}$ is the reduced Bohr radius, $\mu = \frac{m_e M}{M+m_e}$ is reduced mass of the free electron with mass m_e due to the nucleus of mass M, and n, l, m denote the principle, orbital and azimuthal quantum numbers, respectively. The energies are given by, $E_n = \frac{m_e e^4}{2(4\pi\epsilon_0)^2\hbar^2}\frac{1}{n^2}$. Scaling up the scenario to a crystal, where many nuclei contribute to the electronic Hamiltonian, the overlaps result in very small energy splittings, essentially forming continuum energy bands (fig. 1.15). The energy dispersion in these bands, known

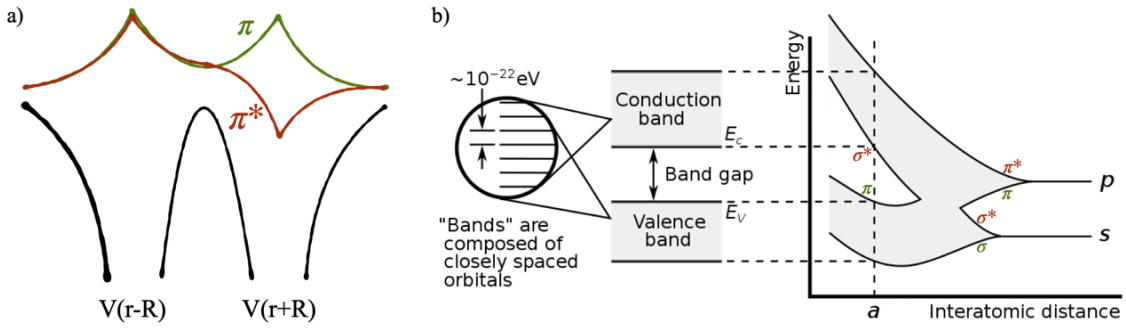

Figure 1.15: **Overlap of atomic orbitals leading to formation of energy bands.** a) The wavefunction of two adjacent Coulomb potentials centered at $-\mathbf{R}$ and $\mathbf{R}$ overlaps either symmetrically (π) or anti-symmetrically (π^*), with an energy gap between the π and π^* orbitals. b) The electronic structure in a lattice is a result of symmetric or antisymmetric overlap of the orbitals at lattice sites, where the energy gap between consecutive orbitals are very small ($\sim 10^{-27}$ eV), essentially forming a continuous 'band' of energy (image source: *wikipedia*).

as the 'band structure', determines how an electron or a hole moves in a crystal. Band structures also contains a lot of information about the effect of electric and magnetic fields on the electronic properties of various materials. Explicit calculation of band structures

would involve solving the many-body Hamiltonian:

$$\begin{aligned}\hat{H} &= \sum_i \frac{p_i^2}{2m_i} + \sum_j \frac{P_j^2}{2M_j} + \frac{1}{2}\sum_{j',j}{}' \frac{Z_j Z_{j'} e^2}{4\pi\epsilon_0 |\mathbf{R}_j - \mathbf{R}_{j'}|} \\ &\quad -\frac{1}{2}\sum_{j,i} \frac{Z_j e^2}{4\pi\epsilon_0 |\mathbf{r}_i - \mathbf{R}_j|} + \frac{1}{2}\sum_{i,i'}{}' \frac{e^2}{4\pi\epsilon_0 |\mathbf{r}_i - \mathbf{r}_{i'}|} \end{aligned} \tag{1.6}$$

Sophisticated *ab initio* methods such as density fucntional theory (DFT) and tight binding (TB) can be applied to solve band structures as well as equilibrium lattice spacings and vibrational frequencies of semiconductors. While group-IV semiconductors silicon and germanium have indirect bandgaps,[4] III-V semiconductor GaAs has a direct bandgap (fig. 1.16). Si and Ge are deemed as 'standard' CMOS materials, with Ge emerging as compatible with superconductivity due to ease of forming Ohmic contacts, as well as optical transition capabilities with strain rendering Ge a direct bandgap semiconductor.[75] Often

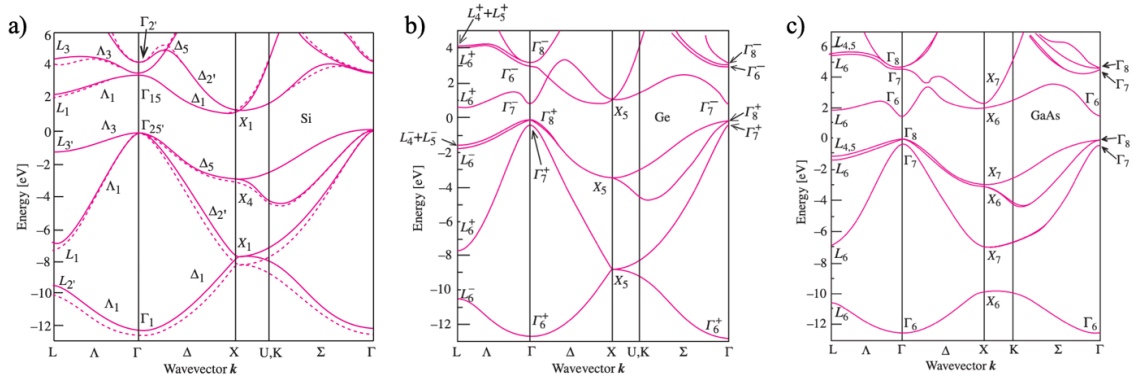

Figure 1.16: **Examples of electronic band structures**: a) silicon, b) germanium, c) gallium arsenide (Ref. 76). While Si and Ge have indirect bandgaps, GaAs has a direct bandgaps. The symmetry operation of the bands under point group O_h are denoted by the BSW notation for Si, and by the Koster notation for Ge and GaAs (See Subsection 1.3.5 for a detailed discussion). The three high symmetry directions in the Brillouin zone of the fcc lattice can be highlighted,- the [100] direction ($\Gamma - \Delta - X$), the [111] direction ($\Gamma - \Lambda - L$) and the [110] direction ($\Gamma - \Sigma - K$).

approximations from condensed matter theory can be implemented to study quantum mechanical properties of semiconductor crystals, which aids in bypassing the computational

[4]The conduction band minima of Si is near the X point with the band gap energy E_g^X=1.12 eV. On the other hand, the conduction band minima of Ge is at the L point, and the indirect bandgap is E_g^L=0.66 eV. However, the direct bandgap of Ge is only 0.14 eV higher at E_g^Γ=0.8 eV.

load of an accurate numerical description. Since this study focuses on semiconductor quantum dots, whose quantum confinement by and large renders only the physics around the band minima relevant, few such approximations can be made.

1.3.1 Effective mass approximation

The recipe of drawing an analogy between the mathematics of a two-level quantum system and spin states of an electron or hole in a crystal is provided by the effective mass approximation (EMA). EMA can incorporate lattice periodicity, external electric and magnetic fields, spin-orbit coupling, strain as long as the underlying crystal potential is buried in the bulk band structure parameters. For direct bandgap semiconductors and valence bands, the single particle Schrödinger equation[5] in a crystal lattice is:

$$[H_0 + U(\mathbf{r})]\Psi(\mathbf{r}) = \left[\frac{(-i\hbar\nabla)^2}{2m_0} + V_0(\mathbf{r}) + U(\mathbf{r})\right]\Psi(\mathbf{r}) = E\Psi(\mathbf{r}) \tag{1.7}$$

where $V_0(\mathbf{r})$ is the lattice periodic potential, and $U(\mathbf{r})$ is slowly varying confinement (responsible for forming quantum dot, nanowire etc). $U(\mathbf{r})$ can be treated as perturbation, and the solution can be expanded in Bloch states $\phi_{n\mathbf{k}}(\mathbf{r})$=$e^{i\mathbf{k}\cdot\mathbf{r}}u_{n\mathbf{k}}(\mathbf{r})$ with modulating coefficients $\psi_n(\mathbf{k})$ as follows,[6]

$$\Psi(\mathbf{r}) = \sum_{n,\mathbf{k}} \psi_n(\mathbf{k})\phi_{n\mathbf{k}}(\mathbf{r}) \tag{1.8}$$

Plugging eqn. 1.8 back into the Schrödinger equation and integrating over the real space after multiplying with $\phi^*_{n'\mathbf{k}'}(\mathbf{r})$,

$$\sum_{n,\mathbf{k}} \left[(E_n(\mathbf{k}) - E)\delta_{n\mathbf{k},n'\mathbf{k}'} + U_{n'\mathbf{k}',n\mathbf{k}}\right]\psi_n(\mathbf{k}) = 0 \tag{1.9}$$

$E_n(\mathbf{k})$ is the unperturbed dispersion which satisfies $H_0\Psi(\mathbf{r}) = E_n(\mathbf{k})\Psi(\mathbf{r})$ and $U_{n'\mathbf{k}',n\mathbf{k}}$= $\int d^3r\, \phi^*_{n'\mathbf{k}'}(\mathbf{r})\, U(\mathbf{r})\, \phi_{n\mathbf{k}}(\mathbf{r}) = \langle n\mathbf{k}|\, U(\mathbf{r})\, |n'\mathbf{k}'\rangle$ denotes the matrix element of the perturbating potential. Employing the Fourier transform of the potential $U(\mathbf{q})$= $\int d^3q e^{i\mathbf{q}\cdot\mathbf{r}}U(\mathbf{r})$, the

[5]Deducing 1.7 from 1.6 involves the valence electron approximation, the Born-Oppenheimer approximation, and the mean-field approximation.

[6]Bloch's theorem: solutions to the Schrödinger equation in a periodic potential can be expressed as plane waves modulated by periodic functions.

matrix element of perturbation becomes

$$\begin{aligned} U_{n'\mathbf{k}',n\mathbf{k}} &= \int d^3q U(\mathbf{q}) \left(\int d^3r \, e^{i(\mathbf{k}-\mathbf{k}'+\mathbf{q})} u^*_{n'\mathbf{k}'}(\mathbf{r}) u_{n\mathbf{k}}(\mathbf{r}) \right) \\ &= \sum_{\mathbf{K},\mathbf{K}'} \int d^3q U(\mathbf{q}) \left(\int_{BZ} d^3r \, e^{i(\mathbf{k}-\mathbf{k}'+\mathbf{q})\cdot\mathbf{r}} C^{n*}_{\mathbf{K}} C^{n'}_{\mathbf{K}'} e^{i(\mathbf{K}-\mathbf{K}')\cdot\mathbf{r}} \right) \end{aligned} \tag{1.10}$$

where $u_{n\mathbf{k}}(\mathbf{r}) = \sum_{\mathbf{K}} C^n_{\mathbf{K}} e^{i\mathbf{K}\cdot\mathbf{r}}$ is the periodic part of the Bloch functions, expanded in plane waves. The real-space integral in the parentheses is the Bloch integral, carrying out which results in,-

$$\sum_{n,\mathbf{k}} \left[(E_n(\mathbf{k}) - E)\delta_{n\mathbf{k},n'\mathbf{k}'} + \sum_{\mathbf{K},\mathbf{K}'} C^{n*}_{\mathbf{K}} C^{n'}_{\mathbf{K}'} U(\mathbf{k}' - \mathbf{k} - (\mathbf{K} - \mathbf{K}')) \right] \psi_n(\mathbf{k}) = 0 \tag{1.11}$$

The Bloch integral for different bands can be approximated to not contribute,-

$$\sum_{\mathbf{k}} \left[(E_n(\mathbf{k}) - E)\delta_{\mathbf{k},\mathbf{k}'} + \sum_{\mathbf{K},\mathbf{K}'} C^*_{\mathbf{K}} C_{\mathbf{K}'} U(\mathbf{k}' - \mathbf{k} - (\mathbf{K} - \mathbf{K}')) \right] \psi_n(\mathbf{k}) = 0 \tag{1.12}$$

Considering screened hydrogenic profile for $U(\mathbf{r})$, further assumptions can be made considering the simple case where the band minima is situated at $\mathbf{k}$=0:

1. Only states close to $\mathbf{k}$=0 contribute to the matrix element of U, which implies $|\mathbf{k}'-\mathbf{k}|$ is small. In fact, $|\mathbf{k}' - \mathbf{k}| \ll |\mathbf{K} - \mathbf{K}'|$.

2. Terms for $\mathbf{K} \neq \mathbf{K}'$ are neglected, since $|U(\mathbf{k}' - \mathbf{k} - (\mathbf{K} - \mathbf{K}'))| \ll |U(\mathbf{k}' - \mathbf{k})|$.

3. The coefficients of the plane wave expansion of the periodic part of the Bloch functions now follow $C^*_{\mathbf{K}} C_{\mathbf{K}'} \equiv |C_{\mathbf{K}}|^2 = 1$, due to orthogonality of the Bloch functions.

4. The Bloch integral in Eqn. 1.10 limits $\mathbf{k}$ and $\mathbf{k}'$ in the first Brillouin zone. This limitation is now removed, and the sum over $\mathbf{k}$ in Eqn. 1.12 can be carried out over the entire k-space.

5. In the vicinity of the band minima, the dispersion is parabolic, $E_n(\mathbf{k}) = E_n(\mathbf{0}) + \frac{\hbar^2 k^2}{2m^*_n}$.

Applying assumptions 1-4, Eqn. 1.9 can now be simplified to.

$$\sum_{\mathbf{k}} \left[(E_n(\mathbf{k}) - E)\delta_{\mathbf{k},\mathbf{k}'} + U(\mathbf{k}' - \mathbf{k}) \right] \psi_n(\mathbf{k}) = 0 \tag{1.13}$$

Now, applying convolution theorem to the second term of eqn. 1.13, and expanding $E_{n\sigma}(\mathbf{k})$ in the vicinity of the band minima as per the assumption 5, the effective mass equation of the n-th band is derived,-

$$\left[\frac{\hbar^2 k^2}{2m_n^*} + U(\mathbf{r})\right]\psi_n(\mathbf{r}) = (E - E_n(0))\psi_n(\mathbf{r}) \tag{1.14}$$

In presence of external magnetic field, the unperturbed dispersion is rather given by $E_{n\sigma}(\mathbf{k})$, σ signifying the spin of the particle. Alternative to Eqn. 1.14, $E_{n\sigma}(\mathbf{k})$ can be expanded in the vicinity of the band minima according to the $\mathbf{k}\cdot\mathbf{p}$ theory, where the following equation transpires:

$$\left[E_n(0) + U(\mathbf{r}) + \frac{(-i\hbar\nabla + e\mathbf{A})^2}{2m_0} + \sum_{n',\sigma'}\frac{1}{m_0}(-i\hbar\nabla + e\mathbf{A})\cdot\mathbf{P}_{n\sigma,n'\sigma'} + \sum_{n',\sigma'}\Delta_{n\sigma,n'\sigma'} + g\mu_B\mathbf{B}\cdot\sigma\right]\psi_{n\sigma}(\mathbf{r}) = E\psi_{n\sigma}(\mathbf{r}) \tag{1.15}$$

with $\mathbf{P}_{n\sigma,n'\sigma'} \approx \langle n\sigma|\,\mathbf{p}\,|n'\sigma'\rangle$ is the canonical momentum matrix element, and $\Delta_{n\sigma,n'\sigma'} = \frac{\hbar}{4m_0^2c^2}\langle n\sigma|\,\mathbf{p}\cdot\sigma\times(\nabla V_0)\,|n'\sigma'\rangle$ is the matrix element of the spin-orbit coupling. One can search for the correlation between Eqns. 1.14 and 1.15, and it can be envisaged that the emergence of the effective mass is the result of the perturbation due to the canonical momentum matrix element. This is discussed in more detail in the next section.

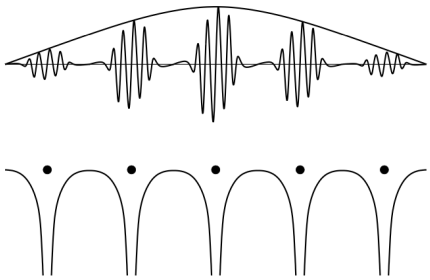

Figure 1.17: **The envelope function approximation.** The orbitals due to the periodic lattice potential are described by the Bloch functions, whereas the envelope function due to the slowly varying potential slowly modulates the Bloch functions (image taken from Ref. [77]).

The EMA equation 1.15 is also known as the multiband envelope function approximation (EFA) Hamiltonian, because at small $\mathbf{k}$, the 'envelope' function $\psi_{n\sigma}(\mathbf{r})$ is long-range. In

fact, it slowly modulates the fast oscillating Bloch functions in the crystal (fig. 1.17). The total wavefunction in real space can be calculated as $\Psi(\mathbf{r}) = \sum_{n,\mathbf{k},\sigma} \psi_{n\sigma}(\mathbf{k}) e^{i\mathbf{k}\cdot\mathbf{r}} u_{n\mathbf{k}}(\mathbf{r}) \approx \sum_n u_{n\mathbf{0}}(\mathbf{r}) \psi_{n\sigma}(\mathbf{r})$, where the Bloch function expansion has been approximated to the band-edge $u_{n\mathbf{k}}(\mathbf{r}) \approx u_{n\mathbf{0}}(\mathbf{r})$, and $\psi_{n\sigma}(\mathbf{r}) = \sum_{\mathbf{k}} e^{i\mathbf{k}\cdot\mathbf{r}} \psi_{n\sigma}(\mathbf{k})$.

1.3.1.1 Multivalley physics and donors

The wavefunction of a single electron confined in a Phosphorus donor potential in silicon can be deduced using EFA, since the donor atom potential essentially form a quantum dot with wavefunction localized around the Si conduction band minima. As an indirect band-gap semiconductor, Si conduction band minima is located at

$$\{\mathbf{k}_\xi^{(0)}\}_{\xi\in[1,6]} = \frac{2\pi}{a_{\mathrm{Si}}}\{(0,0,\pm 0.85),(0,\pm 0.85,0),(\pm 0.85,0,0)\} \tag{1.16}$$

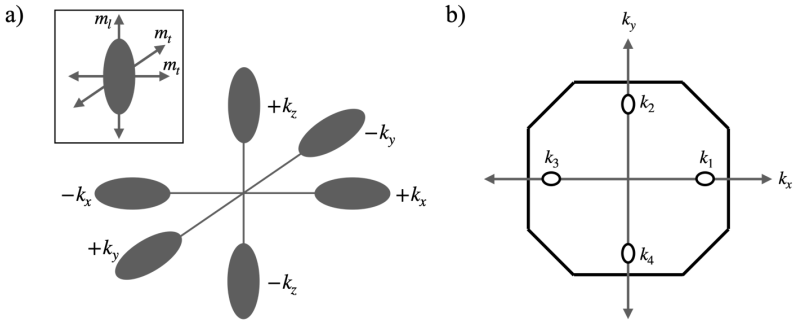

Figure 1.18: **The six degenerate valleys of Si conduction band in the reciprocal space.** a) The six valleys of the Si conduction band at the wave vectors $\{\mathbf{k}_\xi^{(0)}\}_{\xi\in[1,6]}$. The resultant wavefunction has anisotropic Bohr radius due to the anisotropy in the CB effective mass. b) The $k_x - k_y$ plane cut with the valleys shown with respect to the Brillouin zone of Si.

These local extrema in the reciprocal space are known as *valleys* (fig. 1.18). Since Si conduction band exhibits no orbital angular momentum (l=0), the spin-orbit coupling term $\Delta_{n\sigma,n'\sigma'}$ in the multiband equation vanishes. The rest of eqn. 1.15 can be transformed to the multivalley effective mass problem:

$$\left[E_c(\mathbf{k}_\xi^{(0)}) - \frac{\hbar^2}{2m_\parallel^*}\frac{\partial^2}{\partial z_\xi^2} - \frac{\hbar^2}{2m_\perp^*}\left(\frac{\partial^2}{\partial x_\xi^2} + \frac{\partial^2}{\partial y_\xi^2}\right) + U_D(\mathbf{r})\right] F_\xi(\mathbf{r}) = E F_\xi(\mathbf{r});\ \ \xi \in [1,6] \tag{1.17}$$

where z_ξ is the direction parallel to the vector $\mathbf{k}_\xi^{(0)}$, in which the electron effective mass is $m_\parallel^*$=0.916 m_0. The transverse directions evince electron effective mass of $m_\perp^*$=0.191 m_0. The perturbation $U_D(\mathbf{r})$ is due to replacing Si atom with the P donor atom. The spin d.o.f. related terms have not been included so far in writing eqn. 1.17. Noticeably, the effective mass eqn. 1.17 has a six-fold degenerate solution, which constitute the basis for the representation of the tetrahedral symmetry group T_d about the donor atom. In reality, this degeneracy is lifted, and the lowest states are a singlet with an experimentally measured 45.5 meV ionization energy, followed by a triplet (57.35 meV) and a doublet state (58.77 meV). Correct linear combination of the valley envelope functions F_ξ to form the lowest energy states $\psi_i = \sum_{\xi=1}^{6} \alpha_i^{(\xi)} F_\xi(\mathbf{r})$ are predicted from the group theory;

$$\begin{aligned}
\alpha_1^{(\xi)} &= \frac{1}{\sqrt{6}}(1,1,1,1,1,1);\ (A_1) \qquad \alpha_2^{(\xi)} = \left.\begin{array}{c} \frac{1}{2}(1,1,-1,-1,0,0) \\ \frac{1}{\sqrt{12}}(-1,-1,-1,-1,2,2) \end{array}\right\};\ (E) \\
\alpha_3^{(\xi)} &= \left.\begin{array}{c} \frac{1}{\sqrt{2}}(1,-1,0,0,0,0) \\ \frac{1}{\sqrt{2}}(0,0,1,-1,0,0) \\ \frac{1}{\sqrt{2}}(0,0,0,0,1,-1) \end{array}\right\};\ (T_1)
\end{aligned} \tag{1.18}$$

with α_1 coefficients constituting the lowest energy solution. The effective mass anisotropy leads to an anisotropic Bohr radius of the electron wavefunction, captured by the variational form. For example,

$$F_z(\mathbf{r}) = \frac{1}{\sqrt{\pi a^2 b}} \mathrm{Exp}\left[\left(\frac{z^2}{b^2} + \frac{x^2+y^2}{a^2}\right)^{\frac{1}{2}}\right] \tag{1.19}$$

The variational Bohr radius a and b can be calculated by minimizing the energy E. The full ground state wavefunction on a single P donor is $\Psi(\mathbf{r}) = \frac{1}{\sqrt{6}} \sum_{\xi=1}^{6} F_\xi(\mathbf{r})\, \phi_{\mathbf{k}_\xi^{(0)}}(\mathbf{r})$. The variational formalism can be extended to calculate the ground state wavefunction of multi-donor dots as well. For example, ground state wavefunction of an electron on 2P dot will be given by, $\Psi_{2D}(\mathbf{r}) = \frac{1}{\sqrt{\sum_\xi w_\xi^2}} \sum_\xi w_\xi S_\xi$, where w_ξ represents the valley weights. S_ξ signifies the symmetric combination of ξ-th valley wavefunction. For example, $S_{+x} = N_{+x}\left(F_{+x}(\mathbf{r}-\mathbf{R})\phi_{\mathbf{k}_\xi^{(0)}}(\mathbf{r}-\mathbf{R}) + F_{+x}(\mathbf{r}+\mathbf{R})\phi_{\mathbf{k}_\xi^{(0)}}(\mathbf{r}+\mathbf{R})\right)$, where the two P donors are situated at $-\mathbf{R}$ and $\mathbf{R}$, and N_{+x} is the normalization factor. This is discussed in detail in chapter 2.

1.3.1.2 $\mathbf{k}\cdot\mathbf{p}$ formalism and holes

A concise yet flexible approach within the general EFA framework of eqn. 1.15 is the $\mathbf{k}\cdot\mathbf{p}$ formalism. Again starting from the unperturbed Schrödinger equation for the Bloch states, albeit neglecting the effect of external electric and magnetic fields,

$$\left[\frac{p^2}{2m_0}+V_0(\mathbf{r})\right]e^{i\mathbf{k}\cdot\mathbf{r}}u_{n\mathbf{k}}(\mathbf{r})=E_n(\mathbf{k})e^{i\mathbf{k}\cdot\mathbf{r}}u_{n\mathbf{k}}(\mathbf{r}) \tag{1.20}$$

The kinetic operator can act on the plane wave to produce the Schrödinger equation for the lattice periodic part:

$$\left[\frac{p^2}{2m_0}+V_0(\mathbf{r})+\frac{\hbar^2k^2}{2m_0}+\frac{\hbar}{m_0}\mathbf{k}\cdot\mathbf{p}\right]u_{n\mathbf{k}}(\mathbf{r})=E_n(\mathbf{k})u_{n\mathbf{k}}(\mathbf{r}) \tag{1.21}$$

Importantly for any wave vector $\mathbf{k}_0$, $\{u_{n\mathbf{k_0}}\}$ constitutes a complete orthogonal basis. In the case of the band minima being at $\mathbf{k}=0$, the band structure including spin degrees of freedom is given in terms of the band-edge Bloch functions: $|n\mathbf{k}\rangle=\sum_{n',\sigma'}c_{nn'\sigma'}\,|u_{n'\mathbf{0}}(\mathbf{r})\rangle\otimes|\sigma'\rangle$. In presence of SOC, the eigenvalue equation for the dispersion $E_n(\mathbf{k})$ becomes

$$\left(E_n(\mathbf{0})+\frac{\hbar^2k^2}{2m_0}\right)c_{nn\sigma}(\mathbf{k})+\sum_{n',\sigma'}\left(\frac{\hbar}{m_0}\mathbf{k}\cdot\mathbf{P}_{n\sigma,n'\sigma'}+\Delta_{n\sigma,n'\sigma'}\right)c_{nn'\sigma'}(\mathbf{k})=E_n(\mathbf{k})c_{nn\sigma}(\mathbf{k}) \tag{1.22}$$

where $\mathbf{P}_{n\sigma,n'\sigma'}$, $\Delta_{n\sigma,n'\sigma'}$ are the same band-structure parameters as described in EFA. Momentarily ignoring the SOC term, $E_n(\mathbf{k})$ can be evaluated treating the $\mathbf{k}\cdot\mathbf{p}$ term in eqn. 1.22 as perturbation. In a direct bandgap semiconductor conduction band for example, up to second order $E_n(\mathbf{k})$=$E_n(\mathbf{0})+\frac{\hbar^2k^2}{2m_n^*}$ denotes the n-th band energy dispersion, where

$$\frac{1}{m_n^*}\approx\frac{1}{m_0}+\frac{2}{m_0^2}\sum_{n'}\frac{\langle n|\,\mathbf{p}\,|n'\rangle^2}{E_n(\mathbf{0})-E_{n'}(\mathbf{0})} \tag{1.23}$$

describes the *effective mass approximation* of the particle in the n-th band.

Contrasting to the electrons in the lowest conduction band (CB), the holes in the topmost valence band (VB) has nonzero angular momentum $l=1$, resulting in p-type orbital. The VB minima of group-IV semiconductors are situated at $\mathbf{k}=0$, so valley degeneracy vanishes. However, the nonzero l leads to intrinsic spin-orbit coupling, lifting the degeneracy

of the topmost VB at all k. The origin of the intrinsic SOC lies in relativity,[7] in view of which a particle moving in an electric field with velocity $\mathbf{v}$ 'feels' a magnetic field in its frame of reference according to Lorentz transformation: $\mathbf{B}' \propto \frac{\mathbf{v} \times \nabla V_0}{c^2}$, where the electric field originates due to gradient of the microscopic lattice periodic potential V_0. The resultant magnetic interaction would have to be

$$-m_0 \lambda_{SO} \mathbf{S} \cdot \mathbf{v} \times \left(\frac{dV_0}{dr} \frac{\mathbf{r}}{r} \right) = \lambda_{SO} \mathbf{S} \cdot \mathbf{r} \times \mathbf{p} = \lambda_{SO} \mathbf{S} \cdot \mathbf{L}; \quad \left(\lambda_{SO} = \frac{1}{2m_0^2 c^2} \frac{1}{r} \frac{dV_0}{dr} \right) \tag{1.24}$$

The lattice potential is assumed to be a central potential $V_0(\mathbf{r})$ for calculating λ_{SO}.

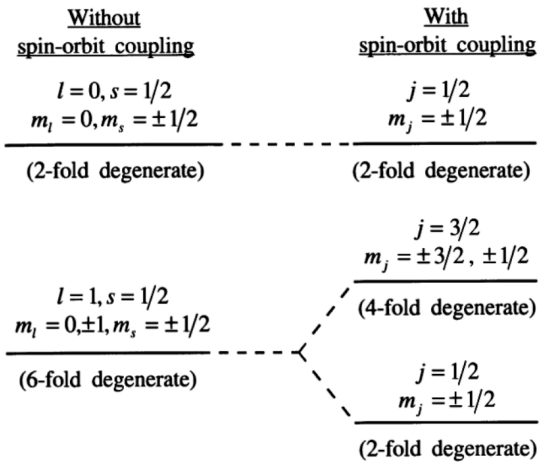

Figure 1.19: **The total angular momentum eigenstates in presence of SOC.** The lowest conduction band is s-type with zero orbital angular momentum; and the valence band is p-type with $l = 1$. In presence of spin-orbit coupling, the bands are eigenstates of the total angular momentum $\mathbf{J} = \mathbf{L} + \mathbf{S}$ with modified energy levels from $j = l - s$ to $j = l + s$ (illustration taken from Ref. [78]).

Without any external magnetic field, the degeneracy at $\mathbf{k}$=0 (three fold orbital, six-fold with spin) of the topmost VB is lifted, since the p-orbitals with spin angular momentum becomes eigenstates of the total angular momentum $\mathbf{J} = \mathbf{L} + \mathbf{S}$ (fig. 1.19). Linear combinations of p-orbitals and spin-1/2 states constitute the resultant $|l\, s; j\, m_j\rangle$ bands (from group theory, $(1) \oplus \left(\frac{1}{2}\right) = \left(\frac{3}{2}\right)$) according to the Clebsch–Gordan coefficients $\langle l\, s; m_j\, m_s | l\, s; j\, m_j \rangle$ (Tab. 1.1). The hole quantum dot dimensions are typically in the order of 10 nm, which

[7]The relativistic *Dirac equation* produces a generic emergence of spin-orbit coupling in form of the Pauli-Schrödinger equation. The Lorenz transformation argument presented here is rather simplistic, and neglects the contribution of the atomic core to SOC.

$\langle l,\, m_s \vert$ \ $\vert j,\, m_j\rangle$	$\left\vert \frac{3}{2},\, \frac{3}{2}\right\rangle$	$\left\vert \frac{3}{2},\, \frac{1}{2}\right\rangle$	$\left\vert \frac{3}{2},\, -\frac{1}{2}\right\rangle$	$\left\vert \frac{3}{2},\, -\frac{3}{2}\right\rangle$	$\left\vert \frac{1}{2},\, \frac{1}{2}\right\rangle$	$\left\vert \frac{1}{2},\, -\frac{1}{2}\right\rangle$
$\left\langle 1,\, \frac{1}{2}\right\vert$	1	0	0	0	0	0
$\left\langle 1,\, -\frac{1}{2}\right\vert$	0	$-\sqrt{\frac{1}{3}}$	0	0	$\sqrt{\frac{2}{3}}$	0
$\left\langle 0,\, \frac{1}{2}\right\vert$	0	$\sqrt{\frac{2}{3}}$	0	0	$\sqrt{\frac{1}{3}}$	0
$\left\langle 0,\, -\frac{1}{2}\right\vert$	0	0	$\sqrt{\frac{2}{3}}$	0	0	$\sqrt{\frac{1}{3}}$
$\left\langle -1,\, \frac{1}{2}\right\vert$	0	0	$\sqrt{\frac{1}{3}}$	0	0	$-\sqrt{\frac{2}{3}}$
$\left\langle -1,\, -\frac{1}{2}\right\vert$	0	0	0	1	0	0

Table 1.1: **The Clebsch–Gordan coefficients for writing the $j = 3/2$ states** in terms of the $l = 1$ p-orbitals.

restricts the relevant band structure close to the Γ-point. First, without SOC, the $\mathbf{k}\cdot\mathbf{p}$ theory can be applied in the vicinity of $\mathbf{k} = 0$ to evaluate the multiband valence band version of eqn. 1.22:

$$\sum_{j,l=1}^{3}\left[\left(\left(E_n(\mathbf{0})+\frac{\hbar^2k^2}{2m_0}\right)\delta_{jl}+\frac{\hbar^2}{m_0^2}\sum_{m>3}\frac{\langle j|\,\mathbf{k}\cdot\mathbf{p}\,|m\rangle\langle m|\,\mathbf{k}\cdot\mathbf{p}\,|l\rangle}{E_n(\mathbf{0})-E_m(\mathbf{0})}\right)\otimes\mathbb{I}_{2\times2}\right]c_{nl\sigma}(\mathbf{k})=E_n(\mathbf{k})c_{nl\sigma}(\mathbf{k}) \tag{1.25}$$

where the n-th band is expressed as the expansion about band-edge l=1 states, i.e. $|n\mathbf{k}\rangle = \sum_l c_{nl}\,|u_l(\mathbf{0})\rangle\otimes|\sigma\rangle$, and the spin degeneracy without the spin-orbit coupling is reflected in the 2×2 identity matrix. Finally including SOC, the LHS 6×6 matrix of eqn. 1.25 undergoes a basis transformation, and the resultant hole dispersion is given by the Luttinger-Kohn Hamiltonian:

$$\begin{aligned}
H_{LK} &= \begin{pmatrix}
P+Q & 0 & -S & R & -\frac{1}{\sqrt{2}}S & \sqrt{2}R \\
0 & P+Q & R^* & S^* & -\sqrt{2}R^* & -\frac{1}{\sqrt{2}}S^* \\
-S^* & R & P-Q & 0 & -\sqrt{2}Q & \sqrt{\frac{3}{2}}S \\
R^* & S & 0 & P-Q & \sqrt{\frac{3}{2}}S^* & \sqrt{2}Q \\
-\frac{1}{\sqrt{2}}S^* & -\sqrt{2}R & -\sqrt{2}Q^* & \sqrt{\frac{3}{2}}S & P+\Delta_{SO} & 0 \\
\sqrt{2}R^* & -\frac{1}{\sqrt{2}}S & \sqrt{\frac{3}{2}}S^* & \sqrt{2}Q^* & 0 & P+\Delta_{SO}
\end{pmatrix} \\
P &= \frac{\hbar^2}{2m_0}\gamma_1\left(k_x^2+k_y^2+k_z^2\right);\;\; Q=-\frac{\hbar^2}{2m_0}\gamma_2\left(2k_z^2-k_x^2-k_y^2\right) \\
R &= \frac{\sqrt{3}\hbar^2}{2m_0}\left[-\gamma_2\left(k_x^2-k_y^2\right)+2i\gamma_3k_xk_y\right];\;\; S=\frac{\sqrt{3}\hbar^2}{m_0}\gamma_3\left(k_x-ik_y\right)k_z
\end{aligned} \tag{1.26}$$

Δ_{SO} signifies the spin-orbit gap, separating the j=3/2 and j=1/2 VB states. The band

structure parameters γ_1, γ_2, γ_3 are determined by considering quasi-degenerate perturbation methods (e.g. Löwdin partitioning) due to excited conduction and valence bands. Notably, to describe a hole quantum dot, the QD confinement have to be added to the

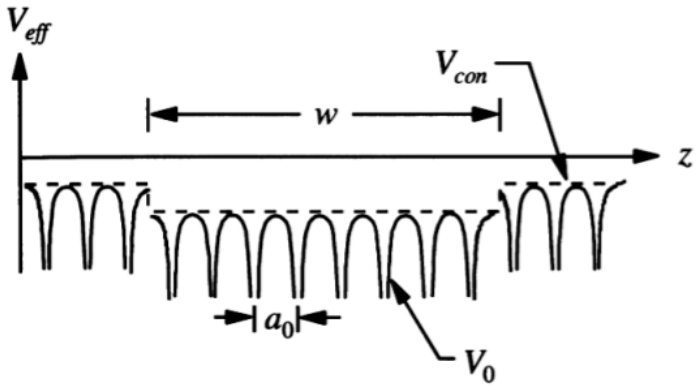

Figure 1.20: **The two different length scales of confinement in quantum dots.** The effective potential V_{eff} is a result of the co-existance of the lattice periodic potential V_0 which has a length scale of the order of the lattice spacing a_0, and the quantum dot confinement V_{con} coming from the gates (image taken from Ref. [78]).

Luttinger-Kohn Hamiltonian; and a possible theoretical model of the hole QD to deduce a formula similar to eqn. 1.19 would have to take into the account the nature of the confinement (fig. 1.20). This is in stark contrast with modeling a donor system where the quantum dot confinement is of 'self-defined' nature, since it originates from replacing silicon atoms with P donors. We return to this discussion in chapter 3 and 4.

1.3.2 Spin resonance mechanism

Effective mass approximations, along with the knowledge of the confinement, provide the spin qubit energy levels, effectively described in the Bloch sphere as:

$$\hat{H}_{QD} = E_0\mathbb{I} + g\mu_B\mathbf{B}_0 \cdot \sigma \tag{1.27}$$

The subscription 'QD' stands for quantum dot, since we would mostly concern ourselves with spin qubits formulated in QD systems. It is convenient to discuss the spin resonance operation with respect to the E_0 orbital level. An alternating magnetic field introduces a

time dependent term in the qubit Hamiltonian:

$$\hat{H}_{QD} = g\mu_B \mathbf{B}_0 \cdot \sigma + g\mu_B \mathbf{B}_{ac} \cos(\omega t + \phi) \cdot \sigma \tag{1.28}$$

Considering the simple case of $\mathbf{B}_0 = B_0\hat{\mathbf{z}}$, and $\mathbf{B}_{ac} = B_{ac}\hat{\mathbf{x}}$,

$$\hat{H}_{QD} = g\mu_B B_0 \sigma_z + g\mu_B B_{ac} \cos(\omega t + \phi)\sigma_x \tag{1.29}$$

Similar to classical mechanics, the Hamiltonian is the generator of time evolution in quantum mechanics, $\hat{H}_{QD}\Psi = i\hbar\frac{\partial}{\partial t}\Psi$. For convenience, the wavefunction can be transformed in the rotating frame of the Larmor precession with frequency ω as follows: $\psi = R_z(-\omega t)\Psi$, where $R_i(\theta)$'s denote the rotation in the Bloch sphere about the i-th axis,

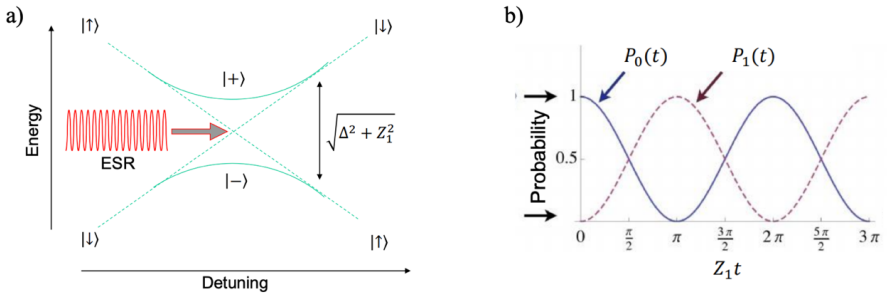

Figure 1.21: **Rabi oscillation of spin qubit under microwave pulse in resonance with the qubit Zeeman splitting.** a) The qubit eigenenergies as a function of detuning from the resonance frequency, b) The probability of the spin-up fraction oscillating with time due to ESR (images taken from 'Contemporary Physics A: Quantum Matter and Information' (PHYS6183) course lecture notes, convened by Prof. Michelle Simmons, UNSW).

$$R_i(\theta) = e^{-i\theta\sigma_i/2} = \cos\left(\frac{\theta}{2}\right)\mathbb{I} - i\sin\left(\frac{\theta}{2}\right)\sigma_i \tag{1.30}$$

The time evolution equation can now be transformed as follows:

$$\begin{aligned}
i\hbar\frac{\partial}{\partial t}\psi &= i\hbar\frac{\partial}{\partial t}R_z(-\omega t)\Psi \\
&= i\hbar R_z(-\omega t)\frac{\partial}{\partial t}\Psi + i\hbar\Psi\frac{\partial}{\partial t}R_z(-\omega t) \\
&= R_z(-\omega t)\hat{H}_{QD}\Psi - \frac{\omega\sigma_z}{2}\hbar R_z(-\omega t)\Psi \\
&= R_z(-\omega t)\hat{H}_{QD}R_z(-\omega t)^\dagger\psi - \frac{\omega\sigma_z}{2}\hbar R_z(-\omega t)R_z(-\omega t)^\dagger\psi \\
&= \left(-\frac{\omega\sigma_z}{2}\hbar + R_z(-\omega t)\hat{H}_{QD}R_z(-\omega t)^\dagger\right)\psi = \hat{H}^R_{QD}\,\psi
\end{aligned} \tag{1.31}$$

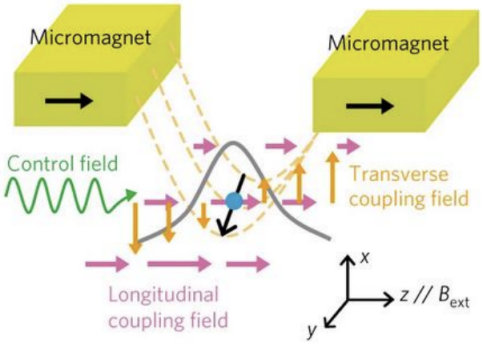

Figure 1.22: **Electrically driven spin resonance (EDSR) mechanism under micromagnet induced SOC.** The magnetic field gradient provided by the micromagnet, together with the longitudinal coupling ac electric field acts as an effective ac magnetic field, flipping the qubit spin when in resonance with the qubit Zeeman splitting (image source: PHYS6183 course lecture notes, UNSW).

The rotating Hamiltonian $\hat{H}^R_{QD}$ can be simplified,-

$$\begin{aligned}
\hat{H}^R_{QD} &= \left(-\frac{\omega\sigma_z}{2}\hbar + R_z(-\omega t)\hat{H}_{QD}R_z(-\omega t)^\dagger\right) \\
&= -\frac{\hbar\omega}{2}\sigma_z + R_z(-\omega t)\left(g\mu_B B_0\sigma_z + g\mu_B B_{ac}\cos(\omega t+\phi)\sigma_x\right)R_z(-\omega t)^\dagger \\
&= \left(g\mu_B B_0 - \frac{\hbar\omega}{2}\right)\sigma_z + g\mu_B B_{ac}\frac{(e^{i(\omega t i+\phi)} + e^{-i(\omega t+\phi)})}{2}R_z(-\omega t)\sigma_x R_z(-\omega t)^\dagger \\
&= \frac{\Delta}{2}\sigma_z + \frac{Z_1}{2}(e^{-i\phi}\sigma_+ + e^{i\phi}\sigma_-) + \frac{Z_1}{2}(e^{2i\omega t+\phi}\sigma_+ + e^{-(2i\omega t+\phi)}\sigma_-)
\end{aligned} \tag{1.32}$$

where $\Delta = (2g\mu_B B_0 - \hbar\omega)$ is the detuning from the resonance frequency, and $Z_1 = g\mu_B B_{ac}/2$. Applying the rotating wave approximation, the rapidly oscillating third term can be neglected, and the qubit Hamiltonian in the rotating frame has the final form:

$$\hat{H}^R_{QD} = \frac{\Delta}{2}\sigma_z + \frac{Z_1}{2}(\cos(\phi)\,\sigma_x + \sin(\phi)\,\sigma_y) \tag{1.33}$$

Equation 1.33 describes electron spin resonance. At zero detuning, and when the microwave pulse has a phase $\phi = 0$, a qubit initialized in $|\uparrow\rangle$ state would exhibit the following time evolution: $\Psi(t) = e^{-i\sigma_x\frac{Z_1}{2\hbar}t}\,|\uparrow\rangle$, resulting in Rabi oscillation (fig. 1.21).

In contrast, the basic mechanism of electrically driven spin resonance or EDSR relies on an alternating electric field, coupled with an engineered spin-orbit field, e.g. a micromagnet

(fig. 1.22). For a micromagnet producing spatially varying magnetic field $B_m(z)$ parallel to the static $B_0\hat{\mathbf{z}}$, the EDSR driving Hamiltonian at zero detuning and zero phase would be $\hat{H}^R_{QD} = \frac{g\mu_B}{4} A(E_{ac}) \frac{\partial B_m(z)}{\partial z} \sigma_x$. Here A denotes the amplitude of the qubit wavefunction displacement under the electric field, i.e. the dipole length.

1.3.3 Spin relaxation mechanism

Importantly, deriving the electronic band structure involves the Born-Oppenheimer approximation, which entails an adiabatic interaction between the valence electrons and the core electrons attached to the nucleus. In other words, the core electrons move rigidly with the nucleus, and the resultant ionic motion is decoupled from the motion of the valence electrons. Phenomenologically, the equation of motion for the ions can be obtained by expanding the Hamiltonian of the ions as a function of their displacements $\delta\mathbf{R}_j$ from their equilibrium positions $\mathbf{R}_{j0}$: $H_{ion} = H_0(\mathbf{R}_{j0}) + H'(\delta\mathbf{R}_j)$. This displacement can be caused by the direct Coulomb repulsion between ions, or passive ion-ion interaction via the valence electrons, where motion of an ion impacts the valence electron distribution which in turn displaces another ion. In the harmonic approximation, the effect of lattice vibration is then described by:

$$H'(\mathbf{u}_{kl}) = \frac{1}{2} M_k \left(\frac{d\mathbf{u}_{kl}}{dt} \right)^2 + \frac{1}{2} \sum_{k',l'} \mathbf{u}_{kl} \cdot \Phi(kl, k'l') \cdot \mathbf{u}_{k'l'} \tag{1.34}$$

where $\mathbf{u}_{kl}$ denotes the displacement of the k-th ion in the l-th unit cell, and $\Phi(kl, k'l')$ are known as the force constants. The force constants have translational symmetry, which means that the displacement vectors can be written as a Bloch wave:

$$\mathbf{u}_{kl}(\mathbf{q}, \omega) = \mathbf{u}_{k0} \exp\left[i(\mathbf{q} \cdot \mathbf{R}_l - \omega t)\right] \tag{1.35}$$

Substituting this into the ion Hamiltonian, the following matrix equation emerges,-

$$\sum_{k'} [D_{kk'}(\mathbf{q}) - \omega^2 \delta_{kk'}] \mathbf{u}_{k'0} = 0 \tag{1.36}$$

where the dynamical matrix $D_{kk'}(\mathbf{q})$ is the mass-modified Fourier transform of the force constant $\Phi(kl, k'0)$. The vibrational frequency eigenvalues of Eqn. 1.36 correspond to

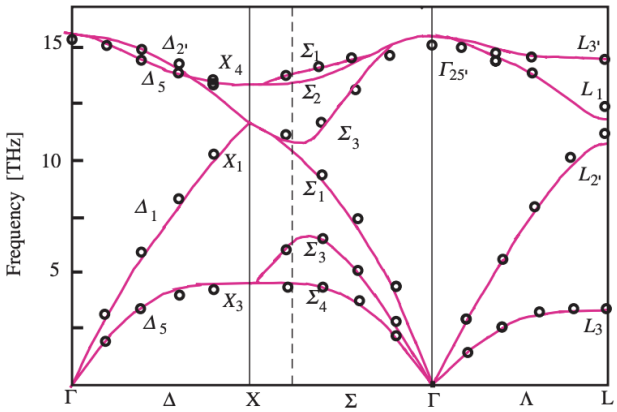

Figure 1.23: **The phonon dispersion of Si** along the high symmetry directions of the Brillouin zone. Near the Γ point, the acoustic phonon modes belong to the Γ_{15} (Γ_4^-) irreducible representation of O_h, while the optical phonon modes transform as Γ'_{25} (Γ_5^+).[76]

quantized levels with $(n+1/2)\hbar\omega$ energies. The creation and annihilation of a 'quantum of vibration', or phonon, is described in terms of the eigenvectors of Eqn. 1.36 which are the vibrational amplitudes $\mathbf{u}_{k0}$. The resultant $\mathbf{q}-\omega$ relationship is known as the phonon dispersion curve (fig. 1.23).

The interaction between the valence electronic motion and the rigid ion motion is called the electron-phonon interaction. For spin qubits, this is eventually the interaction between the spin levels and the lower energy, long wavelength ($k \sim \Gamma$) acoustic phonon modes. The electron-phonon Hamiltonian can be written as a Taylor series expansion of the electronic band structure: $\hat{H}_{e-ph} = \frac{\partial \hat{H}_e}{\partial \mathbf{R}_j}\Big|_{\mathbf{R}_{j0}} \cdot \delta\mathbf{R}_j \approx \frac{\partial E_{nk}}{\partial \mathbf{R}_j}\Big|_{\mathbf{R}_{j0}} \cdot \delta\mathbf{R}_j$, If all $\delta\mathbf{R}_j$ are identical, the lattice sees an overall translation, which leaves the electronic band structure invariant. Hence, the gradient of displacement, $\frac{\partial \delta\mathbf{R}_i}{\partial \mathbf{R}_j}$, changes the band structure. The symmetrized tensor[8] of this gradient is the strain tensor $\varepsilon_{i,j}$:

$$\varepsilon^{\alpha}_{i,j}(\mathbf{R}) = \frac{1}{2}\left(\frac{\partial(\delta\mathbf{R}_i)^{\alpha}}{\partial \mathbf{R}_j} + \frac{\partial(\delta\mathbf{R}_j)^{\alpha}}{\partial \mathbf{R}_i}\right) = \frac{q}{2}(\hat{q}_i u^{\alpha}_j + \hat{q}_j u^{\alpha}_i), \quad i,j \in \{x,y,z\} \tag{1.37}$$

The electron-phonon Hamiltonian in terms of the strain tensor as: $\hat{H}_{e-ph} = \partial E_{nk}|_{i,j}\ \varepsilon^{\alpha}_{i,j}$. The change in the electronic band structure ∂E_{nk} is parametrized by the deformation potentials $\mathcal{D}$. The phonon polarization is indexed with α, which could be longitudinal or

[8]The anti-symmetrized tensor $f^{\alpha}_{i,j} = \frac{1}{2}\left(\frac{\partial\delta\mathbf{R}_i)}{\partial \mathbf{R}_j} - \frac{\partial\delta\mathbf{R}_j}{\partial \mathbf{R}_i}\right)$ rotates the crystal, and therefore does not affect the electronic states.

transverse, depending on whether the displacement $\delta\mathbf{R}$ is parallel or perpendicular to the phonon wave vector $\mathbf{q}$. Using second quantization on Eqn. 1.35, the displacement is given by, $\mathbf{u}^{\alpha} = i\sqrt{\frac{\hbar}{2V_c\rho\omega_{\mathbf{q},\alpha}}}\left(a^{\dagger}_{\mathbf{q},\alpha} - a_{\mathbf{q},\alpha}\right)\exp\left[i(\mathbf{q}\cdot\mathbf{R} - \omega_{\mathbf{q},\alpha}t)\right]\hat{c}^{\alpha}_{j}$, where $\hat{c}$ is the polarisation unit vector. The strain tensor can now be written as,

$$\varepsilon^{\alpha}_{i,j}(\mathbf{R}) = \frac{i}{2}\sqrt{\frac{\hbar}{2V_c\rho\omega_{\mathbf{q},\alpha}}}q(\hat{c}^{\alpha}_{i}\hat{q}_j + \hat{c}^{\alpha}_{j}\hat{q}_i)(e^{-i\mathbf{q}\cdot\mathbf{R}}a_{\mathbf{q},\alpha} + e^{i\mathbf{q}\cdot\mathbf{R}}a^{\dagger}_{\mathbf{q},\alpha})e^{-i\omega_{\mathbf{q},\alpha}t} \tag{1.38}$$

The coordinate systems for the three polarizations are understood as $l : (r, \theta, \phi)$; $t : (r, \theta + \frac{\pi}{2}, \phi)$; $w : (r, \frac{\pi}{2}, \phi + \frac{\pi}{2})$. Using $\omega_{\mathbf{q},\alpha} = v_{\alpha}q$,

$$\varepsilon^{\alpha}_{i,j}(\mathbf{R}) = i\sqrt{\frac{\hbar}{2V_c\rho v_{\alpha}}}\sqrt{q}\mathcal{A}^{\alpha}_{\varepsilon,ij}e^{i\mathbf{q}\cdot\mathbf{R}}(a_{-\mathbf{q},\alpha} + a^{\dagger}_{\mathbf{q},\alpha})e^{-i\omega_{\mathbf{q},\alpha}t} \tag{1.39}$$

where v_{α} are the acoustic phonon velocities, and we assumed $\frac{1}{2}(\hat{c}^{\alpha}_{i}\hat{q}_j + \hat{c}^{\alpha}_{j}\hat{q}_i) = \mathcal{A}^{\alpha}_{\varepsilon,ij}$. The electron-phonon Hamiltonian is given by:

$$H_{e-ph} = i\sqrt{\frac{\hbar}{2V_c\rho v_{\alpha}}}\sqrt{q}\mathcal{D}_{ij}\mathcal{A}^{\alpha}_{\varepsilon,ij}e^{i\mathbf{q}\cdot\mathbf{R}}(a_{-\mathbf{q},\alpha} + a^{\dagger}_{\mathbf{q},\alpha})e^{-i\omega_{\mathbf{q},\alpha}t} \tag{1.40}$$

The matrix elements of $\mathcal{A}^{\alpha}_{\varepsilon,ij}$ are sketched out below:

$$\mathcal{A}^{\alpha}_{\varepsilon} = \frac{1}{2}\begin{pmatrix} 2\hat{c}^{\alpha}_{x}\hat{q}_x & \hat{c}^{\alpha}_{x}\hat{q}_y + \hat{c}^{\alpha}_{y}\hat{q}_x & \hat{c}^{\alpha}_{x}\hat{q}_z + \hat{c}^{\alpha}_{z}\hat{q}_x \\ \hat{c}^{\alpha}_{y}\hat{q}_x + \hat{c}^{\alpha}_{x}\hat{q}_y & 2\hat{c}^{\alpha}_{y}\hat{q}_y & \hat{c}^{\alpha}_{y}\hat{q}_z + \hat{c}^{\alpha}_{z}\hat{q}_y \\ \hat{c}^{\alpha}_{z}\hat{q}_x + \hat{c}^{\alpha}_{x}\hat{q}_z & \hat{c}^{\alpha}_{z}\hat{q}_y + \hat{c}^{\alpha}_{y}\hat{q}_z & 2\hat{c}^{\alpha}_{z}\hat{q}_z \end{pmatrix} \tag{1.41}$$

The phonon wave vector has the components $\overrightarrow{q} \rightarrow \{q\sin\theta\cos\phi, q\sin\theta\,\sin\phi, q\cos\theta\}$; so the unit vectors for $\mathbf{q}$ are given by: $\hat{q} \rightarrow \{\sin\theta\cos\phi,\, \sin\theta\,\sin\phi,\, \cos\theta\}$. The polarization wave vectors are as follows:

- $\hat{c}^{l} \rightarrow q^{-1}\{q_x, q_y, q_z\} = \{\sin\theta\cos\phi,\, \sin\theta\cos\phi,\, \cos\theta\}$
- $\hat{c}^{t} \rightarrow q^{-1}(q_x^2 + q_y^2)^{-\frac{1}{2}}\{q_xq_z, q_yq_z, -(q_x^2 + q_y^2)\} = \{\cos\theta\cos\phi,\, \cos\theta\sin\phi, -\sin\theta\}$
- $\hat{c}^{w} \rightarrow (q_x^2 + q_y^2)^{-\frac{1}{2}}\{q_y, -q_x, 0\} = \{-\sin\phi,\, \cos\phi,\, 0\}$

Using the decompositions above, the matrix elements of $\mathcal{A}^{\alpha}_{\varepsilon,ij}$ for the three polarizations can be written as follows:

$$\mathcal{A}^{l}_{\varepsilon} = \frac{1}{2}\begin{pmatrix} 2\frac{q_x^2}{q^2} & 2\frac{q_xq_y}{q^2} & 2\frac{q_xq_z}{q^2} \\ 2\frac{q_yq_x}{q^2} & 2\frac{q_y^2}{q^2} & 2\frac{2q_yq_z}{q^2} \\ 2\frac{q_zq_x}{q^2} & 2\frac{q_zq_y}{q^2} & 2\frac{q_z^2}{q^2} \end{pmatrix} = \frac{1}{q^2}\begin{pmatrix} q_x^2 & q_xq_y & q_xq_z \\ q_yq_x & q_y^2 & q_yq_z \\ q_zq_x & q_zq_y & q_z^2 \end{pmatrix}$$

$$\mathcal{A}^t_\varepsilon = \frac{1}{2}\begin{pmatrix} 2\frac{q_z}{q}\frac{q_x}{\sqrt{q_x^2+q_y^2}}\frac{q_x}{q} & 2\frac{q_z}{q}\frac{q_x}{\sqrt{q_x^2+q_y^2}}\frac{q_y}{q} & \frac{q_xq_z}{q\sqrt{q_x^2+q_y^2}}\frac{q_z}{q} - \frac{\sqrt{q_x^2+q_y^2}}{q}\frac{q_x}{q} \\ 2\frac{q_z}{q}\frac{q_x}{\sqrt{q_x^2+q_y^2}}\frac{q_y}{q} & 2\frac{q_z}{q}\frac{q_y}{\sqrt{q_x^2+q_y^2}}\frac{q_y}{q} & \frac{q_yq_z}{q\sqrt{q_x^2+q_y^2}}\frac{q_z}{q} - \frac{\sqrt{q_x^2+q_y^2}}{q}\frac{q_y}{q} \\ \frac{q_xq_z}{q\sqrt{q_x^2+q_y^2}}\frac{q_z}{q} - \frac{\sqrt{q_x^2+q_y^2}}{q}\frac{q_x}{q} & \frac{q_z^2q_y-q_x^2q_y-q_y^3}{q^2\sqrt{q_x^2+q_y^2}} & -2\frac{q_z}{q}\frac{\sqrt{q_x^2+q_y^2}}{q} \end{pmatrix}$$

$$\mathcal{A}^w_\varepsilon = \frac{1}{2}\begin{pmatrix} -2\frac{q_y}{\sqrt{q_x^2+q_y^2}}\frac{q_x}{q} & -\frac{q_y}{\sqrt{q_x^2+q_y^2}}\frac{q_y}{q} + \frac{q_x}{\sqrt{q_x^2+q_y^2}}\frac{q_x}{q} & -\frac{q_y}{\sqrt{q_x^2+q_y^2}}\frac{q_z}{q} \\ \frac{q_x^2-q_y^2}{q\sqrt{q_x^2+q_y^2}} & 2\frac{q_xq_y}{q\sqrt{q_x^2+q_y^2}} & \frac{q_xq_z}{q\sqrt{q_x^2+q_y^2}} \\ -\frac{q_yq_z}{q\sqrt{q_x^2+q_y^2}} & \frac{q_xq_z}{q\sqrt{q_x^2+q_y^2}} & 0 \end{pmatrix} \tag{1.42}$$

Alternatively, the matrices can be written in terms of θ and ϕ:

$$\mathcal{A}^l_\varepsilon = \begin{pmatrix} \sin^2\theta\cos^2\phi & \sin^2\theta\sin\phi\cos\phi & \sin\theta\cos\theta\cos\phi \\ \sin^2\theta\sin\phi\cos\phi & \sin^2\theta\sin^2\phi & \sin\theta\cos\theta\sin\phi \\ \sin\theta\cos\theta\cos\phi & \sin\theta\cos\theta\sin\phi & \cos^2\theta \end{pmatrix}$$

$$\mathcal{A}^t_\varepsilon = \begin{pmatrix} \frac{1}{2}\sin 2\theta\cos^2\phi & \frac{1}{4}\sin 2\theta\sin 2\phi & \frac{1}{2}\cos 2\theta\cos\phi \\ \frac{1}{4}\sin 2\theta\sin 2\phi & \frac{1}{2}\sin 2\theta\sin^2\phi & \frac{1}{2}\cos 2\theta\sin\phi \\ \frac{1}{2}\cos 2\theta\cos\phi & \frac{1}{2}\cos 2\theta\sin\phi & -\frac{1}{2}\sin 2\theta \end{pmatrix}$$

$$\mathcal{A}^w_\varepsilon = \frac{1}{2}\begin{pmatrix} -\sin 2\phi\sin\theta & \cos 2\phi\sin\theta & -\sin\phi\cos\theta \\ \cos 2\phi\sin\theta & \sin 2\phi\sin\theta & \cos\phi\cos\theta \\ -\sin\phi\cos\theta & \cos\phi\cos\theta & 0 \end{pmatrix} \tag{1.43}$$

The longitudinal[9] process of spin relaxation occurs via the electron-phonon Hamiltonian, which causes the following spin qubit transition $|\uparrow\rangle \rightleftharpoons |\downarrow\rangle$ state, creating or annihilating a phonon in the process. The relaxation rate Γ_1 is given by the Fermi's golden rule:

$$\Gamma_1 = \frac{1}{T_1} = \sum_\alpha \left(\frac{2\pi}{\hbar} \sum_{\mathbf{q}} \left| \langle\uparrow| H_{e-ph} |\downarrow\rangle_\alpha \right|^2 \delta\left(g\mu_B B_0 - \hbar\omega_{\alpha,\mathbf{q}} \right) \right) \tag{1.44}$$

[9]Here, relaxation and decoherence has been often labeled as longitudinal and transverse processes, which refers to the spin precession along the meridian and equator of the Bloch sphere due to the interaction between the qubit and its environment.

1.3.4 Spin decoherence mechanism

As discussed before, the transverse processes of spin qubits interacting with their environment are quantified as spin decoherence. Several experimental tactics could measure decoherence, e.g. the Ramsey experiment, where a $\pi/2$ pulse rotates the qubit initialized in the $|\downarrow\rangle$ state: $|\psi(t=0)\rangle = R_x(\pi/2)\,|\downarrow\rangle$. The spin would Larmor precess along the equator due to the global Zeeman field $\mathbf{B}_0$, but the presence of noise would introduce a fluctuating magnetic field $\mathbf{V}(t)$ as perturbation to the qubit Hamiltonian:

$$\hat{H} = \hat{H}_Q + \hat{V}(t) = g\mu_B \sigma \cdot \mathbf{B}_0 + \frac{1}{2}\sigma \cdot \mathbf{V}(t) \tag{1.45}$$

A statistical study of the Ramsey experiment can be carried out assuming the time evo-

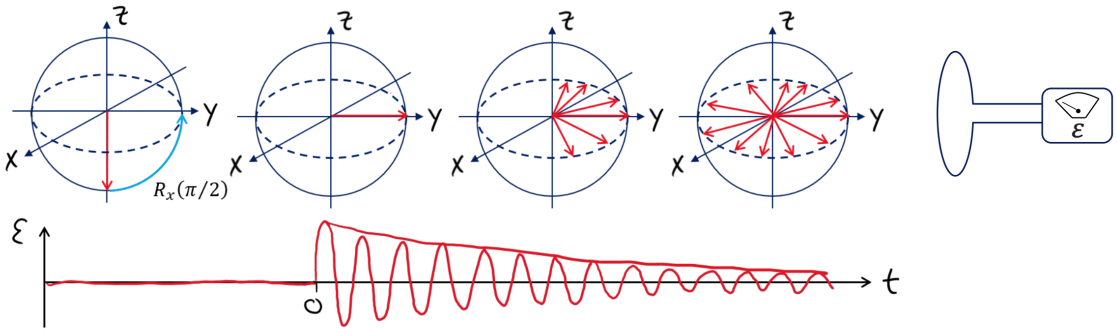

Figure 1.24: **Free induction decay (FID)** of spin in the Ramsey protocol. A pick-up coil is aligned along the y-axis to measure the resultant e.m.f. from the time varying magnetic flux of the rotating spins. At $t = 0$, the e.m.f. is the highest, but due to the qubit dephasing, the net magnetization decreases at finite t, and the e.m.f. gradually drops to zero (image source: 'Quantum Devices and Computers' (ELEC4605) lecture notes, course convened by A/Prof. Jarryd Pla, UNSW).

lution of an ensemble of spins exposed to noise, but the results are equally applicable for repeated measurement of a single spin. It can be shown that the effect of noise imparts a time-dependent phase shift $\phi(t)$ on the qubit. At $t = 0$, all spins in the ensemble (or all measurements of the single spin) experience $\phi(t) = 0$, hence the e.m.f. due to Larmor precession induced time-varying magnetic flux is maximum. Since each spin experiences slightly different $\phi(t)$, at finite t coherence is destroyed as the spins point in several directions along the equator, and the net e.m.f. decays to zero,- known as the free induction decay or FID (fig. 1.24).

Theoretical modelling of spin qubit dephasing depends on the specific type of noise. Noise could originate from other spins in the vicinity, as well as nearby charge traps, or the clock noise of the microwave drive, or Johnson-Nyquist noise on $\mathbf{B}_0$. For a single charge defect, the noise term can be modeled as follows,- $\sigma \cdot \mathbf{V}(t)$=$V\sigma_z(-1)^{N(t)}$, where $V = \delta\epsilon_z$ denotes the fluctuation in the qubit Zeeman splitting, and the Poisson variable $N(t) = 0, 1$ denotes the random switching with switching time τ. The choice above is motivated by the fact that in microscopic devices the alternating capture and emission of carriers at (tunnelling in and out of) an individual defect site produces discrete switching in the device resistance, known as the random telegraph signal or RTS (e.g. fig. 1.25). The time-dependent phase

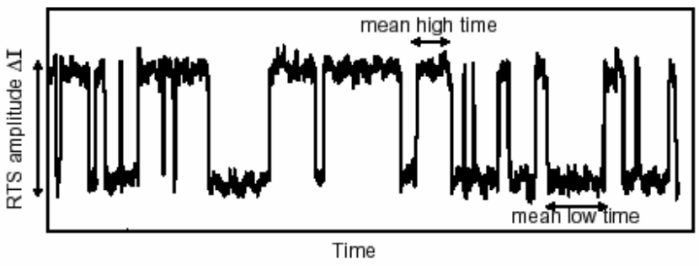

Figure 1.25: **An example of random telegraph signal** in the time-domain trace of the drain current of a MOSFET device.[79]

can be defined as

$$\phi(t) = \frac{V}{\hbar}\int_0^{t'}(-1)^{N(t')}dt' \tag{1.46}$$

In the rotating frame of reference of the precessing spin, the time evolution of the density matrix is given by

$$\rho(t) = e^{-\frac{i}{\hbar}\int_0^t \hat{V}(t')dt'}\rho(t=0)e^{\frac{i}{\hbar}\int_0^t \hat{V}(t')dt'} \tag{1.47}$$

The initial density matrix can be written as

$$\rho(t=0) = |\psi(t=0)\rangle\langle\psi(t=0)| = R_x(\pi/2)\,|\downarrow\rangle\langle\downarrow|\,R_x(\pi/2)^\dagger = \frac{1}{2}(\mathbb{I}+\sigma_z) \tag{1.48}$$

Equations 1.46, 1.47 can be substituted into Eqn. 1.48 as follows,

$$\rho(t) \;=\; e^{-i\phi(t)\sigma_z}\frac{1}{2}(\mathbb{I}+\sigma_z)e^{i\phi(t)\sigma_z} = \frac{1}{2}\begin{pmatrix} 1 & -ie^{-i\phi(t)} \\ ie^{i\phi(t)} & 1 \end{pmatrix} \tag{1.49}$$

The off-diagonal terms signify the dephasing matrix element between the $|\downarrow\rangle$ and $|\uparrow\rangle$ states. The time evolution algebra of the Pauli matrices gives the time evolution of the initial spin pointing towards y,

$$S_y(t) = tr\,\sigma_y\,\rho(t) = S_{oy}\,tr\begin{pmatrix}0 & -i\\ i & 0\end{pmatrix}\frac{1}{2}\begin{pmatrix}1 & -ie^{-i\phi(t)}\\ ie^{i\phi(t)} & 1\end{pmatrix} = S_{oy}\cos\,\phi(t) \tag{1.50}$$

For repeated measurements, the expectation value $\langle\cos\,\phi(t)\rangle$ has to be calculated, which turns out to be $e^{-\chi(t)}$, with $\chi(t) = \langle\phi(t)^2\rangle/2$. The coherence decay function $\chi(t)$ can be calculated as follows:

$$\begin{aligned}\chi(t) &= \frac{\overline{V^2}}{2\hbar^2}\left\langle\int_0^{t_1}(-1)^{N(t_1)}dt_1\int_0^{t_2}(-1)^{N(t_2)}dt_2\right\rangle = \frac{\overline{V^2}}{2\hbar^2}\int_0^{t_1}\int_0^{t_2}\left\langle(-1)^{N(t_1)}(-1)^{N(t_2)}\right\rangle dt_1dt_2\\ &= \frac{\overline{V^2}}{2\hbar^2}\int_{-\infty}^{\infty}\int_{-\infty}^{\infty}g(t_1-t_2)f(t_1,t)f(t_2,t)dt_1dt_2\end{aligned} \tag{1.51}$$

where $g(t_1 - t_2)$ is the autocorrelation of the ergodic random telegraph noise (RTN),[10] whose statistics do not change over time, hence the expectation value has been replaced by a time average. The range of the integrals have been extended to infinity by introducing the 'hat' functions $f(t_1, t)$, $f(t_2, t)$. Equation. 1.51 can be rearranged using Fourier transformation to write the well known formula[80]:

$$\chi(t) = \frac{\overline{V^2}}{2\hbar^2}\frac{1}{\pi}\int_0^{\infty}S(\omega)|\mathcal{F}(\omega,t)|^2\,d\omega = \frac{\overline{V^2}}{2\hbar^2}\frac{1}{\pi}\int_0^{\infty}S(\omega)\frac{\sin^2(\omega t/2)}{(\omega/2)^2}\,d\omega \tag{1.52}$$

where $S(\omega)$ is the power spectral density of the noise, given by the Fourier transform of the autocorrelation,[11] and $\mathcal{F}(\omega, t)$ is the Fourier transform of the 'hat' functions. The decoherence time T_2^* is simply the $1/e$ decay period of $e^{-\chi(t)}$. Knowledge of the power spectral density of the noise would allow for decoherence time calculation. Comparing the two time scales of the problem: the switching time and the fluctuation in Zeeman energy, it can be assumed that RTN only contributes as long as $|V| < \frac{\hbar}{\tau}$. The appropriate formula for the coherence decay function in this regime is $\chi(t) = \frac{(\delta\epsilon_z)^2\tau}{2\hbar^2}t$, leading to $\frac{1}{T_2^*}\Big|_{FID} = \frac{(\delta\epsilon_z)^2\tau}{2\hbar^2}$ as the RTN decoherence time expression.[12]

[10] For RTN, the autocorrelation can be calculated as $g(t_1 - t_2) = e^{|t_2-t_1|/\tau}$.

[11] the power spectral density: $S(\omega) = \int_{-\infty}^{\infty}e^{-i\omega t}e^{-|t|/\tau} = \frac{2\tau}{1+\omega^2\tau^2}$.

[12] A couple more assumptions have been made here. Firstly, the switching time τ has been assumed to be same for the repeated measurements. Secondly, the energy fluctuation is assumed to be constant, hence $\overline{V^2} = (\delta\epsilon_z)^2$.

For a distribution of charge traps, the overall spectral power density is given by

$$S_V(\omega) = \int_0^\infty \rho(\tau)\, d\tau\, \frac{2\tau}{1+\omega^2\tau^2} = \int_0^\infty F(E,T)dE \frac{2\tau_0 e^{E/k_BT}}{1+\omega^2\tau_0^2 e^{2E/k_BT}} \tag{1.53}$$

In writing Eqn. 1.53, the switching time has been written as a function of temperature, $\tau = \tau_0 e^{E/k_BT}$, where $1/\tau_0$ is the attempt frequency to overcome the activation energy E. The distribution of the switching times has been mapped to the distribution of activation energies, $\rho(\tau)\, d\tau \rightarrow F(E,T)dE$. Simplifying $S_V(\omega)$ as follows:

$$\begin{aligned} S_V(\omega) &= \int_0^\infty \frac{2\tau_0 F(E,T)dE}{e^{-E/k_BT} + e^{2\ln\,\omega\tau_0} e^{E/k_BT}} = \int_0^\infty \frac{2\tau_0 e^{-\ln\,\omega\tau_0} F(E,T)dE}{e^{-\ln\,\omega\tau_0} e^{-E/k_BT} + e^{\ln\,\omega\tau_0} e^{E/k_BT}} \\ &= \frac{1}{\omega}\int_0^\infty \frac{F(E,T)dE}{\cosh\frac{E+k_BT\,\ln\,\omega\tau_0}{k_BT}} \approx \frac{k_BTF(E_\omega,T)}{2\pi\omega} = F(E_\omega,T)k_BT\,\frac{1}{f} \end{aligned} \tag{1.54}$$

where E_ω=$k_BT\,\ln\,\omega\tau_0$. Therefore, a distribution of charge defects gives a $1/f$ power spectrum, and the resultant coherence decay function is,-

$$\chi(t) = \frac{\overline{V^2}}{\hbar^2}\frac{F(E_\omega,T)k_BT}{\pi^2}\int_{\omega_0}^\infty \frac{\sin^2(\omega t/2)}{\omega^3}\, d\omega \approx \left(\frac{t}{T_2^*|_{1/f}}\right)^2 \ln\frac{1}{\omega_0 t} \tag{1.55}$$

where ω_0 is the low-frequency cut-off, typically given by the inverse of the measurement time, and $\frac{1}{T_2^*}\Big|_{1/f} = \delta\epsilon_z\sqrt{\frac{F(E_\omega,T)k_BT}{\pi^2\hbar^2}}$ is the $1/f$ dephasing rate. Similarly, the T_2 decoherence time for Hahn echo measurement can be calculated,

$$\chi(2\tau) = \frac{\overline{V^2}}{2\hbar^2}\frac{1}{\pi}\int_0^\infty S(\omega)\frac{\sin^4(\omega\tau/2)}{(\omega/4)^2}\, d\omega \approx \left(\frac{2\tau}{T_2}\right)^3 \tag{1.56}$$

1.3.5 (A)symmetries: a closer look at spin-orbit coupling

Knowledge of the underlying symmetries of group-IV semiconductors in the context of their band dispersion is rather useful. Not only does it circumvent the complication of analytical evaluation of the band structure, the effect of external conditions on the physical properties of semiconductor quantum dot systems can also be understood by starting from the highest symmetry, and realizing how the external perturbation gradually decreases the symmetry. Unit cells of Si and Ge lattices have face-centered cubic (fcc) diamond structure with two atoms per unit cell. In the reciprocal space, the Brillouin zone of the diamond structure is highly symmetrical, i.e. it remains unchanged under various

rotations about high-symmetry directions such as [100], [110] and [111]. These symmetry operations result in symmetrized wave functions of a particle moving in the said crystal. Another consequence is the identical energy structure of different wave vectors $\mathbf{k}$ and $\mathbf{k}'$ if they are related by symmetry.

irreducible representation \ group elements	E	C_2	S_4	σ_d	C_3	i	σ_h	C_4	C_2'	S_6
Γ_1 (Γ_1^+)	1	1	1	1	1	1	1	1	1	1
Γ_2 (Γ_2^+)	1	1	-1	-1	1	1	1	-1	-1	1
Γ_{12} (Γ_3^+)	2	2	0	0	-1	2	2	0	0	-1
Γ_{25} (Γ_5^-)	3	-1	1	-1	0	-3	1	-1	1	0
Γ_{15} (Γ_4^-)	3	-1	-1	1	0	-3	1	1	-1	0
Γ_1' (Γ_1^-)	1	1	-1	-1	1	-1	-1	1	1	1
Γ_2' (Γ_2^-)	1	1	1	1	1	-1	-1	-1	-1	-1
Γ_{12}' (Γ_3^-)	2	2	0	0	-1	-2	-2	0	0	1
Γ_{25}' (Γ_5^+)	3	-1	-1	1	0	3	-1	-1	1	0
Γ_{15}' (Γ_4^+)	3	-1	1	-1	0	3	-1	1	-1	0

Table 1.2: **The character table of the space group O_h.** The 'classes', signified by the column headers, define differnt symmetry operations. The irreducible representations, or the row headers, are named after the notation introduced by Bouckaert, Smoluchowski and Wigner (BSW notation); and the Koster notation is given in brackets.

From group theory, the symmetry operations of the diamond crystal form the point group $O_h = T_d \otimes C_i$ (or $Fd3m$), where T_d is the tetrahedral symmetry point group, and C_i group consists of identity and inversion symmetry. The group is summarized by the character table of its classes and irreducible representations. Classes are defined as sets of group elements T satisfying $aT{=}Ta$ for any element a of the group, e.g. for O_h group $\{i\}$ signifying inversion, $\{3\sigma_h\}$ denoting reflection on each of the three equivalent (100) planes, and so on. Representations are matrices of specific symmetry transformations, and a large matrix can be formed to signify all the operations in the group for a representation. This large matrix can be decomposed into block-diagonal matrices, which are known as irreducible representations. The wavefunction of a particle at the Γ point in different bands can be mapped to eigenfunctions of various irreducible representations, generally denoted

by Γ_μ^ν. Finally, traces of the irreducible representation matrices are called characters, which take up the same value for all elements of a class.

The above discussion of symmetry constitutes the basic idea behind the theory of invariants, which dictates that the Hamiltonian must be invariant under all the symmetry operations of the system; terms which do not satisfy the symmetries must vanish. In fact, a multiband Hamiltonian $\mathcal{H}(\kappa)$ as a function of the tensor operators κ (e.g. components of $\mathbf{k}$, $\mathbf{B}$, $\mathbf{E}$, ε_{ij}) can be given by,

$$\mathcal{H}_{\alpha\beta}(\kappa) = \sum_{\mu,\nu} \mathcal{A}_{\mu\nu}^{\alpha\beta} \sum_l \chi_l^\nu \kappa^{\nu,\mu} \tag{1.57}$$

where blocks of $\mathcal{H}(\kappa)$ connecting α and β bands are signified as $\mathcal{H}_{\alpha\beta}(\kappa)$, which comprises of linearly independent matrices χ_l^ν and the μ-th irreducible tensor operator $\kappa^{\nu,\mu}$, which transform according to the irreducible representation $\Gamma_\nu \subset \left(\Gamma_\alpha \times \Gamma_\beta^*\right)$. The coefficients $\mathcal{A}_{\mu\nu}^{\alpha\beta}$ are material dependent. As an example, we can consider the 8×8 Kane model, which considers the lowest conduction band and the topmost valence band. In group

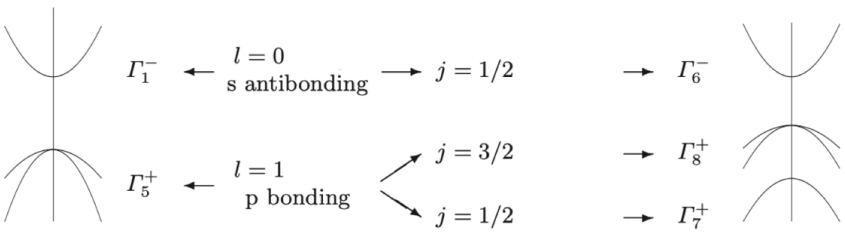

Figure 1.26: **The symmetry of the lowest conduction band and the topmost valence bands** from group theory. In presence of spin-orbit coupling, the degeneracy of the valence band is lifted. The Γ_6, Γ_7 and Γ_8 bands constitute the basis for the Kane model.[77]

theory, the s-type ($l = 0$) states (e.g. lowest conduction band) transform according to the irreducible representation Γ_1^- of O_h, whereas the p-type ($l = 1$) states (e.g. bonding p-type for topmost valence band, anti-bonding p-type for excited conduction band) transform as Γ_5^+ (fig. 1.26).[13] Electron or hole moving in the strong Coulomb potential of the atomic core regions results in spin-orbit coupling, and the electronic states become eigenstates

[13]The superscripts denote the bonding (even,+) or anti-bonding (odd,-) nature of the states.

of total angular momentum j. The electronic wavefunctions now must include the effect of symmetry on the spin wavefunction (e.g. rotation of 2π would change the sign of spin 1/2 particle's wavefunction). Hence, the $j = 1/2$ lowest conduction band transforms as the double group representation Γ_6^- of O_h. The p-type topmost valence band splits into $j = 3/2$ states transforming as Γ_8^+, and $j = 1/2$ split-off states (seperated by the bulk spin-orbit gap Δ_{SO}) which transform as Γ_7^+. The blocks connecting different bands in the 8×8 Kane model are as follows:

$$\mathcal{H}_{8\times 8} = \begin{pmatrix} \mathcal{H}_{6_-6_-} & \mathcal{H}_{6_-8_+} & \mathcal{H}_{6_-7_+} \\ \mathcal{H}_{8_+6_-} & \mathcal{H}_{8_+8_+} & \mathcal{H}_{8_+7_+} \\ \mathcal{H}_{7_+6_-} & \mathcal{H}_{7_+8_+} & \mathcal{H}_{7_+7_+} \end{pmatrix} \tag{1.58}$$

The diagonal blocks for the Γ_6^- conduction band and the Γ_8^+ valence band can be expanded as per Eqn. 1.57, with the knowledge of the irreducible representations of the blocks, and subsequently the symmetrized matrices (Tab. 1.3) and tensor operators (Tab. 1.4).

Block	Irreducible representations	Symmetrized matrices	Time reversal
$\mathcal{H}_{6_-6_-}$	$\Gamma_6 \times \Gamma_6^*$	$\Gamma_1 : \mathbb{I}_{2\times 2}$	+
	$= \Gamma_1 + \Gamma_4$	$\Gamma_4 : \sigma_x,\ \sigma_y,\ \sigma_z$	-
$\mathcal{H}_{8_+8_+}$	$\Gamma_8 \times \Gamma_8^*$	$\Gamma_1 : \mathbb{I}_{4\times 4};\ J^2$	+
	$= \Gamma_1 + \Gamma_2 + \Gamma_3$	$\Gamma_2 : J_xJ_yJ_z + J_zJ_yJ_x$	-
	$+2\Gamma_4 + 2\Gamma_5$	$\Gamma_3 : \frac{1}{\sqrt{3}}(2J_z^2 - J_x^2 - J_y^2),\ J_x^2 - J_y^2$	+
		$\Gamma_4 : J_x,\ J_y,\ J_z;\ J_x^3,\ J_y^3,\ J_z^3$	-
		$\Gamma_5 : \{J_y, J_z\},\ \{J_z, J_x\},\ \{J_x, J_y\};$	+
		$\{J_x, J_y^2 - J_z^2\}, \{J_y, J_z^2 - J_x^2\}, \{J_z, J_x^2 - J_y^2\}$	-

Table 1.3: **Symmetrized matrices for the $\mathcal{H}_{6_-6_-}$ and $\mathcal{H}_{8_+8_+}$ blocks**. Matrices for the other blocks of the 8×8 Kane model can be similarly written.[77] σ and $\mathbf{J}$ denote the Dirac matrices in spin 1/2 and spin 3/2 basis. The notation $\{A, B\}$ denotes symmetrized product of the operators A and B.

A few interesting properties could be pointed out: $\mathbf{k}, \mathbf{E}$ transform as Γ_5, while $\mathbf{B}$ belongs to Γ_4 ($\mathbf{B}$ and $\mathbf{J}$ are axial vectors). Also, $\mathbf{k}, \mathbf{B}$ break time reversal symmetry, while $\mathbf{E}$ is even under time reversal. In terms of parity, $\mathbf{k}, \mathbf{E}$ are even, while $\mathbf{B}$ is odd parity. In absence of magnetic field and SOC, the electronic dispersion is spin degenerate: $E_+(\mathbf{k}) = E_-(\mathbf{k})$ due to space and time invariance. Hence, the conduction band Hamiltonian can

Representations	Tensor operators
Γ_1	1; k^2; $\mathbf{k}\cdot\mathbf{E}$; -$B^2$
Γ_2	$\mathbf{B}\cdot\mathbf{k}$; $\mathbf{E}\cdot\mathbf{B}$
Γ_3	$\frac{1}{\sqrt{3}}(2k_z^2-k_x^2-k_y^2)$, $k_x^2-k_y^2$; $E_xB_x-E_yB_y$, $\frac{1}{\sqrt{2}}(-2E_zB_z+E_xB_x+E_yB_y)$
Γ_4	B_x, B_y, B_z; $\{k_x,k_y^2-k_z^2\}$, $\{k_y,k_z^2-k_x^2\}$, $\{k_z,k_x^2-k_y^2\}$ $(\mathbf{k}\times\mathbf{E})_x$, $(\mathbf{k}\times\mathbf{E})_y$, $(\mathbf{k}\times\mathbf{E})_z$; $B_yE_z+E_zB_y$, $B_zE_x+B_xE_z$, $B_xE_y+B_yE_x$; $B_yk_z+B_zk_y$, $B_zk_x+B_xk_z$, $B_xk_y+B_yk_x$
Γ_5	k_x, k_y, k_z; E_x, E_y, E_z; $\{k_y,k_z\}$, $\{k_z,k_x\}$, $\{k_x,k_y\}$; $(\mathbf{E}\times\mathbf{B})_x$, $(\mathbf{E}\times\mathbf{B})_y$, $(\mathbf{E}\times\mathbf{B})_z$; $(\mathbf{B}\times\mathbf{k})_x$, $(\mathbf{B}\times\mathbf{k})_y$, $(\mathbf{B}\times\mathbf{k})_z$; $E_yk_z+E_zk_y$, $E_zk_x+E_xk_z$, $E_xk_y+E_yk_x$

Table 1.4: **Irreducible tensor components for the Point group T_d.** Only the lowest order terms in k, B, E have been listed, and other irreducible tensor components in higher order can be derived by combining these terms.

be written by grouping the matrix of Γ_1 and the corresponding tensor operators in the lowest order of $\mathbf{k}$: $\mathcal{H}_{6\_6\_}(\mathbf{k})$=$E_0+\frac{\hbar^2}{2m'}k^2\mathbb{I}_{2\times2}$. Similarly for the valence band, the exact 4×4 Luttinger Hamiltonian is produced from the invariants with Γ_1, Γ_4 and Γ_5 irreducible representations:

$$\begin{aligned}\mathcal{H}_{8_+8_+}(\mathbf{k}) &= -\frac{\hbar^2}{2m_0}[\gamma_1\mathbb{I}_{4\times4}k^2-\gamma_2\left(\frac{1}{3}(2J_z^2-J_x^2-J_y^2)(2k_z^2-k_x^2-k_y^2)+(J_x^2-J_y^2)(k_x^2-k_y^2)\right)\\ &\quad -4\gamma_3\left(\{J_x,J_y\}\{k_x,k_y\}+\{J_y,J_z\}\{k_y,k_z\}+\{J_z,J_x\}\{k_z,k_x\}\right)] \qquad (1.59)\end{aligned}$$

hence, without carrying out any analytics, the symmetry arguments can predict the band dispersion in the 8×8 Kane model, which will be frequently applied in this study. Notably, the material dependent parameters such as the conduction band effective mass m' or the Luttinger parameters γ_1, γ_2, γ_3 have to be analytically/ numerically calculated. External magnetic field would break the time reversal symmetry and lift the spin degeneracy. It is easily shown that the magnetic interaction in the lowest order of $\mathbf{B}$ is due to Γ_4: $\mathcal{H}^Z_{6\_6\_}=\frac{1}{2}g\mu_B\sigma\cdot\mathbf{B}$, and $\mathcal{H}^Z_{8_+8_+}=-2\mu_B(\kappa\mathbf{J}\cdot\mathbf{B}+q\mathcal{J}\cdot\mathbf{B})$.

The bulk spin-orbit gap Δ_{SO} is the artifact of symmetry breaking due to the microscopic potential profile gradient. In general, the discussion of intrinsic and extrinsic spin-orbit coupling consists of two types of asymmetries: bulk inversion asymmetry (BIA) and struc-

tural inversion asymmetry (SIA). Bulk inversion asymmetric terms are odd in parity. For conduction band, the BIA term in the lowest order from Γ_4 representation is identified as, $\mathcal{H}^D_{6_-6_-} = \alpha^{41}_{6_-6_-}(\sigma_x\{k_x, k_y^2 - k_z^2\} + c.p.)$. Similar terms can be found for the topmost valence band, as listed in Tab. 1.5. On the other hand, SIA originates from the asymmetry in the microscopic and macroscopic confinement $V(r) = V_0 + e\mathbf{E}\cdot\mathbf{r}$, and therefore the invariant expansion consists of symmetrized and anti-symmetrized products of $\mathbf{k}$ and $\mathbf{E}$ combined with linear Dirac matrices. Alternatively, an SIA term originates from $\mathbf{E}$ combined with symmetrized products of Dirac matrices (Tab. 1.5). Note that the BIA terms are not

BIA	$\mathcal{H}^D_{6_-6_-} = \alpha^{41}_{D,6_-6_-}(\sigma_x\{k_x, k_y^2 - k_z^2\} + c.p.)$ $\mathcal{H}^D_{8_+8_+} = \alpha^{41}_{D,8_+8_+}(J_x\{k_x, k_y^2 - k_z^2\} + c.p.) + \alpha^{42}_{D,8_+8_+}(J_x^3\{k_x, k_y^2 - k_z^2\} + c.p.)$ $+\alpha^{51}_{D,8_+8_+}(\{J_x, J_y^2 - J_z^2\}\{k_x, k_y^2 + k_z^2\} + c.p.)$ $+\frac{2}{\sqrt{3}}C_k(\{J_x, J_y^2 - J_z^2\}k_x + c.p.)$ $+\alpha^{52}_{D,8_+8_+}(\{J_x, J_y^2 - J_z^2\}k_x^3 + c.p.)$
SIA	$\mathcal{H}^R_{6_-6_-} = \alpha^{41}_{R,6_-6_-}(\sigma_x(\mathbf{k}\times\mathbf{E})_x + c.p.)$ $\mathcal{H}^R_{8_+8_+} = \alpha^{41}_{R,8_+8_+}(J_x(\mathbf{k}\times\mathbf{E})_x + c.p.) + \alpha^{42}_{R,8_+8_+}(J_x^3(\mathbf{k}\times\mathbf{E})_x + c.p.)$ $+\alpha^{51}_{R,8_+8_+}(\{J_y, J_z\}E_x + c.p.)$ $+\alpha^{52}_{R,8_+8_+}(\{J_x, J_y^2 - J_z^2\}(k_yE_z + k_zE_y) + c.p.)$

Table 1.5: **The BIA and SIA invariants for for the $\mathcal{H}_{6_-6_-}$ and $\mathcal{H}_{8_+8_+}$ blocks of the 8×8 Kane model.** Notably, the irreducible tensor components are either time-reversal asymmetric, or odd parity,- lifting the spin degeneracy at finite $\mathbf{k}$. This is the $B = 0$ spin splitting.

inherent to the bulk dispersion of group-IV semiconductors such as Si and Ge. However, these terms are present for III-V semiconductors with tetrahedral symmetry, and are also present in Si or Ge quantum dots due to interface inversion asymmetry (IIA), or strain inhomogeneity.

1.4 Thesis motivation and outline

The above discussion on symmetry hints at important physics due to the non trivial interplay of the irreducible tensor components of $\mathbf{k}$, $\mathbf{E}$, $\mathbf{B}$, ε_{ij} etc. The resultant spin-orbit terms in the spin qubit Hamiltonian have important consequences in experiments. However, in obtaining the key results throughout this study, the symmetry arguments

will not be applied extensively. Instead, an effective mass approximation (EMA)-based theoretical modeling approach will be adopted.

In Chapter 2, a multidonor quantum dot spin qubit has been theorized with electron spin on phosphorus donors in Si. The design consisting of a $2P^+$ donor cluster and a 1P donor ~ 10 nm apart, features a large built-in dipole moment, making them ideal for electron dipole spin resonance (EDSR) using the donor hyperfine interaction. An ab initio calculation of such a $2P:1P$ donor qubit would be computationally expensive due to the multivalley nature of the ground state. In this study, by introducing a variational effective mass wavefunction, we examine the impact of qubit geometry and nearby charge defects on the electrical operation and coherence of a $2P:1P$ electron spin qubit, where the electron spin on $2P$ multi-donor quantum dot comprises the qubit in question. The existence of exchange oscillation and the possible suppression of it for donors raises another important probing the role of geometric orientation of the multidonor dot system. The main findings of Chapter 2 are as follows.

1. The difference in the hyperfine interaction between the $2P$ and $1P$ sites enables fast EDSR, with $T_\pi \sim 10 - 50$ ns and a Rabi ratio $(T_1/T_\pi) \sim 10^6$.

2. For the high symmetry crystallographic axes [100], [110] and [111], the fastest EDSR time T_π occurs when the $2P:1P$ axis is $\parallel$ [111], while the best Rabi ratio occurs when it is $\parallel$ [100]. This difference is attributed to the difference in the wavefunction overlap between $2P$ and $1P$ for different geometries. In contrast, the choice of orientation of the $2P$ axis has no visible impact on qubit operation.

3. For certain orientations of nearby charge defects, random telegraph noise has an appreciable effect on both detuning and $2P-1P$ tunneling, with the latter inducing gate errors.

4. The qubit is robust against $1/f$ noise provided it is operated away from the charge anticrossing.

5. Entanglement via exchange is several orders of magnitude faster than dipole-dipole

coupling.

From the point of view of all-electrical operation, spin qubits with electron often rely on extrinsic spin-orbit coupling, e.g. from a micromagnet or the hyperfine field of the nuclear spins. These conventional approaches to operating electron spin quantum computing have faced scaling problem, although providing long-lived qubits. Hole spin qubits in group-IV semiconductors, especially Ge and Si, are being actively investigated as platforms for ultrafast electrical spin manipulation, thanks to the strong intrinsic spin-orbit coupling for holes in the valence band. In chapter 3, a comprehensive theory of spin physics in planar germanium hole quantum dots in an in-plane magnetic field is presented. Comparison of the results from theory with experimental findings show that the orbital magnetic field terms[14] induce important spin-orbit coupling for the qubit. Morover, the quadrupolar gate controlled SIA Rashba spin-orbit coupling produces coherence sweet spots for hole qubits, where the qubit dephasing due to charge noise is minimized, yet the hole spin rotation is the fastest. A full 3D $\mathbf{k} \cdot \mathbf{p}$ analysis have been done in Chapter 3 for planar hole systems, capturing the variability in fundamental spin dynamics and coherence for hole spin qubit operation under different magnetic field orientation. The main findings of Chapter 3 are:

1. Hole qubit EDSR for in-plane magnetic fields varies non-linearly with the field strength and is weaker than for perpendicular magnetic fields.

2. The in-plane g-factor is strongly anisotropic for an elliptical dot, owing to the orbital magnetic field terms.

3. The effect of random telegraph noise in an in-plane magnetic field cannot be fully mitigated, as the orbital magnetic field terms expose the qubit to all components of the defect electric field.

In Chapter 4, the main focus is the numerical modeling of the gatestack-induced thermal strain and the atomistic random alloy disorder near interfaces in the hugely successful hole

[14]Orbital magnetic field terms refer to the vector potential $\mathbf{A}$ induced terms of the Peierls substitution: $\mathbf{k}'=\mathbf{k}+\frac{e\mathbf{A}}{\hbar}$.

qubit platform of $Ge/Si_{1-x}Ge_x$ heterostructures. Inclusion of these effects is motivated by the large variability of hole spin qubit properties over adjacent sites in a quantum dot array. The aggregated roughness leads to spin-orbit coupling $\propto k^1$ in the heavy hole qubit energy subspace via the strain gradient, in contrast to the $\propto k^3$ SIA Rashba spin-orbit coupling with the uniaxial strain assumption of the previous chapter. Within the framework of the 3D $\mathbf{k}\cdot\mathbf{p}$ formalism, the strain inhomogeneity due to random alloy disorder is calculated using the atomistic valence force field (VFF) method; while strain from a realistic gate-stack of planar hole quantum dot confinement is modeled in COMSOL Multiphysics via finite element method. The main findings of Chapter 4 are the following.

1. Roughness induces linear-k Dresselhaus spin-orbit coupling, which dominates the hole spin EDSR over the cubic Rashba SOC. The hybrid model presented in Section 4 accurately predicts the EDSR Rabi frequency to be $\sim$100 MHz for typical electric and magnetic fields in experiments, which represents at least an order of magnitude improvement over the phenomenological uniaxial strain assumption.

2. There exist specific in-plane orientations of the global magnetic field $\mathbf{B}$ and the microwave drive $\tilde{\mathbf{E}}_{\mathrm{ac}}$ for maximum EDSR Rabi frequency of the hole spin qubit.

3. The state-of-the-art atomistic tight-binding calculation via 3D nanoelectronic modeling (NEMO3D) calculation agrees with the quasi-2D limit of the $\mathbf{k}\cdot\mathbf{p}$ description of roughness-induced SOC.

1.5 Chapter summary

An overview of spin qubit architectures in group-IV semiconductors, especially in CMOS standard materials silicon and germanium, has been presented in this chapter. From condensed matter theory, a potential recipe is formulated for studying the underlying physics of self-defined and gate-defined quantum dot qubits. In the next chapters, two specific systems shall be studied: phosphorus multidonor dot in silicon and planar hole quantum dot in Ge/SiGe heterostructure. Coherent full-electrical control of spin qubits in these systems

exhibit significant variability owing to the contrast in confinement, design, and external electric and magnetic environments. The aim of this study is to build computationally inexpensive and effective theoretical models, while capturing the important underlying physics.

References

[1] Gordon E Moore. Cramming more components onto integrated circuits. *Proceedings of the IEEE*, 86(1):82–85, 1998.

[2] NW Hendrickx, WIL Lawrie, L Petit, A Sammak, G Scappucci, and M Veldhorst. A single-hole spin qubit. *Nature communications*, 11(1):3478, 2020.

[3] Ben Bartlett, Avik Dutt, and Shanhui Fan. Deterministic photonic quantum computation in a synthetic time dimension. *Optica*, 8(12):1515–1523, 2021.

[4] J Ignacio Cirac and H Jeff Kimble. Quantum optics, what next? *Nature Photonics*, 11(1):18–20, 2017.

[5] Samuel J Hile, Lukas Fricke, Matthew G House, Eldad Peretz, Chin Yi Chen, Yu Wang, Matthew Broome, Samuel K Gorman, Joris G Keizer, Rajib Rahman, et al. Addressable electron spin resonance using donors and donor molecules in silicon. *Science advances*, 4(7):eaaq1459, 2018.

[6] Michael A Nielsen and Isaac L Chuang. *Quantum computation and quantum information*. Cambridge university press, 2010.

[7] Andrea Morello, Jarryd J Pla, Floris A Zwanenburg, Kok W Chan, Kuan Y Tan, Hans Huebl, Mikko Möttönen, Christopher D Nugroho, Changyi Yang, Jessica A Van Donkelaar, et al. Single-shot readout of an electron spin in silicon. *Nature*, 467(7316):687–691, 2010.

[8] M Veldhorst, JCC Hwang, CH Yang, AW Leenstra, Bob de Ronde, JP Dehollain, JT Muhonen, FE Hudson, Kohei M Itoh, A t Morello, et al. An addressable quantum

dot qubit with fault-tolerant control-fidelity. *Nature nanotechnology*, 9(12):981–985, 2014.

[9] Daniel Loss and David P DiVincenzo. Quantum computation with quantum dots. *Physical Review A*, 57(1):120, 1998.

[10] Bruce E Kane. A silicon-based nuclear spin quantum computer. *nature*, 393(6681):133–137, 1998.

[11] JM Elzerman, R Hanson, LH Willems van Beveren, B Witkamp, LMK Vandersypen, and Leo P Kouwenhoven. Single-shot read-out of an individual electron spin in a quantum dot. *nature*, 430(6998):431–435, 2004.

[12] Jason R Petta, Alexander Comstock Johnson, Jacob M Taylor, Edward A Laird, Amir Yacoby, Mikhail D Lukin, Charles M Marcus, Micah P Hanson, and Arthur C Gossard. Coherent manipulation of coupled electron spins in semiconductor quantum dots. *Science*, 309(5744):2180–2184, 2005.

[13] Frank HL Koppens, Christo Buizert, Klaas-Jan Tielrooij, Ivo T Vink, Katja C Nowack, Tristan Meunier, LP Kouwenhoven, and LMK Vandersypen. Driven coherent oscillations of a single electron spin in a quantum dot. *Nature*, 442(7104):766–771, 2006.

[14] Katja C Nowack, FHL Koppens, Yu V Nazarov, and LMK Vandersypen. Coherent control of a single electron spin with electric fields. *Science*, 318(5855):1430–1433, 2007.

[15] KC Nowack, M Shafiei, M Laforest, GEDK Prawiroatmodjo, LR Schreiber, C Reichl, W Wegscheider, and LMK Vandersypen. Single-shot correlations and two-qubit gate of solid-state spins. *Science*, 333(6047):1269–1272, 2011.

[16] G Feher and EA Gere. Electron spin resonance experiments on donors in silicon. ii. electron spin relaxation effects. *Physical Review*, 114(5):1245, 1959.

[17] D. M. Zajac, A. J. Sigillito, M. Russ, F. Borjans, J. M. Taylor, G. Burkard, and J. R.

Petta. Resonantly driven cnot gate for electron spins. *Science*, 359(6374):439–442, 2018.

[18] Bernhard Klemt, Victor Elhomsy, Martin Nurizzo, Pierre Hamonic, Biel Martinez, Bruna Cardoso Paz, Cameron Spence, Matthieu C Dartiailh, Baptiste Jadot, Emmanuel Chanrion, et al. Electrical manipulation of a single electron spin in cmos using a micromagnet and spin-valley coupling. *npj Quantum Information*, 9(1):107, 2023.

[19] Menno Veldhorst, CH Yang, JCC Hwang, W Huang, JP Dehollain, JT Muhonen, S Simmons, A Laucht, FE Hudson, Kohei M Itoh, et al. A two-qubit logic gate in silicon. *Nature*, 526(7573):410–414, 2015.

[20] Adam R Mills, Charles R Guinn, Michael J Gullans, Anthony J Sigillito, Mayer M Feldman, Erik Nielsen, and Jason R Petta. Two-qubit silicon quantum processor with operation fidelity exceeding 99%. *Science Advances*, 8(14):eabn5130, 2022.

[21] Ensar Vahapoglu, JP Slack-Smith, Ross CC Leon, Wee Han Lim, FE Hudson, Tom Day, JD Cifuentes, Tuomo Tanttu, Chih-Hwan Yang, Andre Saraiva, et al. Coherent control of electron spin qubits in silicon using a global field. *npj Quantum Information*, 8(1):126, 2022.

[22] M Pioro-Ladriere, T Obata, Y Tokura, Y-S Shin, Toshihiro Kubo, K Yoshida, T Taniyama, and S Tarucha. Electrically driven single-electron spin resonance in a slanting zeeman field. *Nature Physics*, 4(10):776–779, 2008.

[23] Erika Kawakami, Pasquale Scarlino, Daniel R Ward, FR Braakman, DE Savage, MG Lagally, Mark Friesen, Susan N Coppersmith, Mark A Eriksson, and LMK Vandersypen. Electrical control of a long-lived spin qubit in a si/sige quantum dot. *Nature nanotechnology*, 9(9):666–670, 2014.

[24] Xanthe Croot, Xiao Mi, Stefan Putz, Mónica Benito, Felix Borjans, Guido Burkard, and Jason R Petta. Flopping-mode electric dipole spin resonance. *Physical Review Research*, 2(1):012006, 2020.

[25] Brett M Maune, Matthew G Borselli, Biqin Huang, Thaddeus D Ladd, Peter W Deelman, Kevin S Holabird, Andrey A Kiselev, Ivan Alvarado-Rodriguez, Richard S Ross, Adele E Schmitz, et al. Coherent singlet-triplet oscillations in a silicon-based double quantum dot. *Nature*, 481(7381):344–347, 2012.

[26] TF Watson, SGJ Philips, Erika Kawakami, DR Ward, Pasquale Scarlino, Menno Veldhorst, DE Savage, MG Lagally, Mark Friesen, SN Coppersmith, et al. A programmable two-qubit quantum processor in silicon. *nature*, 555(7698):633–637, 2018.

[27] L Petit, M Russ, HGJ Eenink, WIL Lawrie, JS Clarke, LMK Vandersypen, and M Veldhorst. High-fidelity two-qubit gates in silicon above one kelvin. *arXiv preprint arXiv:2007.09034*, 2020.

[28] Bent Weber, YH Matthias Tan, Suddhasatta Mahapatra, Thomas F Watson, Hoon Ryu, Rajib Rahman, Lloyd CL Hollenberg, Gerhard Klimeck, and Michelle Y Simmons. Spin blockade and exchange in coulomb-confined silicon double quantum dots. *Nature nanotechnology*, 9(6):430–435, 2014.

[29] Mateusz T Mądzik, Serwan Asaad, Akram Youssry, Benjamin Joecker, Kenneth M Rudinger, Erik Nielsen, Kevin C Young, Timothy J Proctor, Andrew D Baczewski, Arne Laucht, et al. Precision tomography of a three-qubit donor quantum processor in silicon. *Nature*, 601(7893):348–353, 2022.

[30] Juha T Muhonen, Juan P Dehollain, Arne Laucht, Fay E Hudson, Rachpon Kalra, Takeharu Sekiguchi, Kohei M Itoh, David N Jamieson, Jeffrey C McCallum, Andrew S Dzurak, et al. Storing quantum information for 30 seconds in a nanoelectronic device. *Nature nanotechnology*, 9(12):986–991, 2014.

[31] Irene Fernández de Fuentes, Tim Botzem, Mark AI Johnson, Arjen Vaartjes, Serwan Asaad, Vincent Mourik, Fay E Hudson, Kohei M Itoh, Brett C Johnson, Alexander M Jakob, et al. Navigating the 16-dimensional hilbert space of a high-spin donor qudit with electric and magnetic fields. *Nature communications*, 15(1):1380, 2024.

[32] Jarryd J Pla, Kuan Y Tan, Juan P Dehollain, Wee H Lim, John JL Morton, Floris A Zwanenburg, David N Jamieson, Andrew S Dzurak, and Andrea Morello. High-fidelity

readout and control of a nuclear spin qubit in silicon. *Nature*, 496(7445):334–338, 2013.

[33] Lisa A Tracy, Dwight R Luhman, Stephen M Carr, Nathaniel C Bishop, Gregory A Ten Eyck, Tammy Pluym, Joel R Wendt, Michael P Lilly, and Malcolm S Carroll. Single shot spin readout using a cryogenic high-electron-mobility transistor amplifier at sub-kelvin temperatures. *Applied Physics Letters*, 108(6), 2016.

[34] David N Jamieson, William IL Lawrie, Simon G Robson, Alexander M Jakob, Brett C Johnson, and Jeffrey C McCallum. Deterministic doping. *Materials Science in Semiconductor Processing*, 62:23–30, 2017.

[35] Matthias Koch, Joris G Keizer, Prasanna Pakkiam, Daniel Keith, Matthew G House, Eldad Peretz, and Michelle Y Simmons. Spin read-out in atomic qubits in an all-epitaxial three-dimensional transistor. *Nature nanotechnology*, 14(2):137–140, 2019.

[36] D Keith, MG House, MB Donnelly, TF Watson, Bent Weber, and MY Simmons. Single-shot spin readout in semiconductors near the shot-noise sensitivity limit. *Physical Review X*, 9(4):041003, 2019.

[37] Lukas Fricke, Samuel J Hile, Ludwik Kranz, Yousun Chung, Yu He, Prasanna Pakkiam, Matthew G House, Joris G Keizer, and Michelle Y Simmons. Coherent control of a donor-molecule electron spin qubit in silicon. *Nature communications*, 12(1):3323, 2021.

[38] Jarryd J Pla, Kuan Y Tan, Juan P Dehollain, Wee H Lim, John JL Morton, David N Jamieson, Andrew S Dzurak, and Andrea Morello. A single-atom electron spin qubit in silicon. *Nature*, 489(7417):541–545, 2012.

[39] Arne Laucht, Juha T Muhonen, Fahd A Mohiyaddin, Rachpon Kalra, Juan P Dehollain, Solomon Freer, Fay E Hudson, Menno Veldhorst, Rajib Rahman, Gerhard Klimeck, et al. Electrically controlling single-spin qubits in a continuous microwave field. *Science advances*, 1(3):e1500022, 2015.

[40] Arne Laucht, Rachpon Kalra, Stephanie Simmons, Juan P Dehollain, Juha T Muhonen, Fahd A Mohiyaddin, Solomon Freer, Fay E Hudson, Kohei M Itoh, David N Jamieson, et al. A dressed spin qubit in silicon. *Nature nanotechnology*, 12(1):61–66, 2017.

[41] FN Krauth, SK Gorman, Y He, MT Jones, P Macha, S Kocsis, C Chua, B Voisin, S Rogge, R Rahman, et al. Flopping-mode electric dipole spin resonance in phosphorus donor qubits in silicon. *Physical Review Applied*, 17(5):054006, 2022.

[42] Abhikbrata Sarkar, Joel Hochstetter, Allen Kha, Xuedong Hu, Michelle Y Simmons, Rajib Rahman, and Dimitrie Culcer. Optimisation of electron spin qubits in electrically driven multi-donor quantum dots. *npj Quantum Information*, 8(1):127, 2022.

[43] Gary Wolfowicz, Matias Urdampilleta, Mike LW Thewalt, Helge Riemann, Nikolai V Abrosimov, Peter Becker, Hans-Joachim Pohl, and John JL Morton. Conditional control of donor nuclear spins in silicon using stark shifts. *Physical Review Letters*, 113(15):157601, 2014.

[44] David P Franke, Moritz PD Pflüger, Pierre-André Mortemousque, Kohei M Itoh, and Martin S Brandt. Quadrupolar effects on nuclear spins of neutral arsenic donors in silicon. *Physical review B*, 93(16):161303, 2016.

[45] Serwan Asaad, Vincent Mourik, Benjamin Joecker, Mark AI Johnson, Andrew D Baczewski, Hannes R Firgau, Mateusz T Mądzik, Vivien Schmitt, Jarryd J Pla, Fay E Hudson, et al. Coherent electrical control of a single high-spin nucleus in silicon. *Nature*, 579(7798):205–209, 2020.

[46] MA Broome, SK Gorman, MG House, SJ Hile, JG Keizer, Daniel Keith, CD Hill, TF Watson, WJ Baker, LCL Hollenberg, et al. Two-electron spin correlations in precision placed donors in silicon. *Nature communications*, 9(1):980, 2018.

[47] Yu He, SK Gorman, Daniel Keith, Ludwik Kranz, JG Keizer, and MY Simmons. A two-qubit gate between phosphorus donor electrons in silicon. *Nature*, 571(7765):371–375, 2019.

[48] Mateusz T Mądzik, Arne Laucht, Fay E Hudson, Alexander M Jakob, Brett C Johnson, David N Jamieson, Kohei M Itoh, Andrew S Dzurak, and Andrea Morello. Conditional quantum operation of two exchange-coupled single-donor spin qubits in a mos-compatible silicon device. *Nature communications*, 12(1):181, 2021.

[49] Xuedong Hu and S Das Sarma. Spin-based quantum computation in multielectron quantum dots. *Physical Review A*, 64(4):042312, 2001.

[50] CJ Wellard, LCL Hollenberg, F Parisoli, LM Kettle, H-S Goan, JAL McIntosh, and DN Jamieson. Electron exchange coupling for single-donor solid-state spin qubits. *Physical Review B*, 68(19):195209, 2003.

[51] John King Gamble, N Tobias Jacobson, Erik Nielsen, Andrew D Baczewski, Jonathan E Moussa, Inès Montaño, and Richard P Muller. Multivalley effective mass theory simulation of donors in silicon. *Physical Review B*, 91(23):235318, 2015.

[52] Benjamin Joecker, Andrew D Baczewski, John K Gamble, Jarryd J Pla, André Saraiva, and Andrea Morello. Full configuration interaction simulations of exchange-coupled donors in silicon using multi-valley effective mass theory. *New Journal of Physics*, 23(7):073007, 2021.

[53] R Maurand, X Jehl, D Kotekar-Patil, Andrea Corna, Heorhii Bohuslavskyi, R Laviéville, L Hutin, S Barraud, M Vinet, M Sanquer, et al. A cmos silicon spin qubit. *Nature communications*, 7(1):13575, 2016.

[54] Leon C Camenzind, Simon Geyer, Andreas Fuhrer, Richard J Warburton, Dominik M Zumbühl, and Andreas V Kuhlmann. A hole spin qubit in a fin field-effect transistor above 4 kelvin. *Nature Electronics*, 5(3):178–183, 2022.

[55] NW Hendrickx, DP Franke, A Sammak, M Kouwenhoven, D Sabbagh, L Yeoh, Roy Li, MLV Tagliaferri, M Virgilio, G Capellini, et al. Gate-controlled quantum dots and superconductivity in planar germanium. *Nature communications*, 9(1):2835, 2018.

[56] Stefano Bosco, Bence Hetényi, and Daniel Loss. Hole spin qubits in si finfets with

fully tunable spin-orbit coupling and sweet spots for charge noise. *PRX Quantum*, 2(1):010348, 2021.

[57] Xian Wu, Daniel R Ward, JR Prance, Dohun Kim, John King Gamble, RT Mohr, Zhan Shi, DE Savage, MG Lagally, Mark Friesen, et al. Two-axis control of a singlet–triplet qubit with an integrated micromagnet. *Proceedings of the National Academy of Sciences*, 111(33):11938–11942, 2014.

[58] S Nadj-Perge, SM Frolov, EPAM Bakkers, and Leo P Kouwenhoven. Spin–orbit qubit in a semiconductor nanowire. *Nature*, 468(7327):1084–1087, 2010.

[59] Gang Xu, Fei Gao, Ke Wang, Ting Zhang, He Liu, Gang Cao, Ting Wang, Jian-Jun Zhang, Hong-Wen Jiang, Hai-Ou Li, et al. Hole spin in tunable ge hut wire double quantum dot. *Applied Physics Express*, 13(6):065002, 2020.

[60] SD Liles, DJ Halverson, Zhanning Wang, Aaquib Shamim, RS Eggli, Ik Kyeong Jin, Joe Hillier, Krittika Kumar, Isaac Vorreiter, Matthew Rendell, et al. A singlet-triplet hole-spin qubit in mos silicon. *arXiv preprint arXiv:2310.09722*, 2023.

[61] Juan P Dehollain, Juha T Muhonen, Kuan Y Tan, Andre Saraiva, David N Jamieson, Andrew S Dzurak, and Andrea Morello. Single-shot readout and relaxation of singlet and triplet states in exchange-coupled p 31 electron spins in silicon. *Physical review letters*, 112(23):236801, 2014.

[62] MA Broome, TF Watson, D Keith, SK Gorman, MG House, JG Keizer, SJ Hile, W Baker, and MY Simmons. High-fidelity single-shot singlet-triplet readout of precision-placed donors in silicon. *Physical review letters*, 119(4):046802, 2017.

[63] SA Studenikin, J Thorgrimson, GC Aers, A Kam, P Zawadzki, ZR Wasilewski, A Bogan, and AS Sachrajda. Enhanced charge detection of spin qubit readout via an intermediate state. *Applied Physics Letters*, 101(23), 2012.

[64] Patrick Harvey-Collard, Benjamin D'Anjou, Martin Rudolph, N Tobias Jacobson, Jason Dominguez, Gregory A Ten Eyck, Joel R Wendt, Tammy Pluym, Michael P

Lilly, William A Coish, et al. High-fidelity single-shot readout for a spin qubit via an enhanced latching mechanism. *Physical Review X*, 8(2):021046, 2018.

[65] Lucas A Orona, John M Nichol, Shannon P Harvey, Charlotte GL Bøttcher, Saeed Fallahi, Geoffrey C Gardner, Michael J Manfra, and Amir Yacoby. Readout of singlet-triplet qubits at large magnetic field gradients. *Physical Review B*, 98(12):125404, 2018.

[66] Jann H Ungerer, Alessia Pally, Artem Kononov, Sebastian Lehmann, Joost Ridderbos, Patrick P Potts, Claes Thelander, Kimberly A Dick, Ville F Maisi, Pasquale Scarlino, et al. Strong coupling between a microwave photon and a singlet-triplet qubit. *Nature Communications*, 15(1):1068, 2024.

[67] Cécile X Yu, Simon Zihlmann, José C Abadillo-Uriel, Vincent P Michal, Nils Rambal, Heimanu Niebojewski, Thomas Bedecarrats, Maud Vinet, Étienne Dumur, Michele Filippone, et al. Strong coupling between a photon and a hole spin in silicon. *Nature Nanotechnology*, 18(7):741–746, 2023.

[68] Xiao Mi, Mónica Benito, Stefan Putz, David M Zajac, Jacob M Taylor, Guido Burkard, and Jason R Petta. A coherent spin–photon interface in silicon. *Nature*, 555(7698):599–603, 2018.

[69] Andreas J Landig, Jonne V Koski, Pasquale Scarlino, UC Mendes, Alexandre Blais, Christian Reichl, Werner Wegscheider, Andreas Wallraff, Klaus Ensslin, and T Ihn. Coherent spin–photon coupling using a resonant exchange qubit. *Nature*, 560(7717):179–184, 2018.

[70] Eoin G Kelly, Alexei Orekhov, Nico W Hendrickx, Matthias Mergenthaler, Felix J Schupp, Stephan Paredes, Rafael S Eggli, Andreas V Kuhlmann, Patrick Harvey-Collard, Andreas Fuhrer, et al. Capacitive crosstalk in gate-based dispersive sensing of spin qubits. *Applied Physics Letters*, 123(26), 2023.

[71] Pasquale Scarlino, Jann H Ungerer, David J van Woerkom, Marco Mancini, Peter Stano, Clemens Müller, Andreas J Landig, Jonne V Koski, Christian Reichl, Werner

Wegscheider, et al. In situ tuning of the electric-dipole strength of a double-dot charge qubit: Charge-noise protection and ultrastrong coupling. *Physical Review X*, 12(3):031004, 2022.

[72] Melina Luethi, Katharina Laubscher, Stefano Bosco, Daniel Loss, and Jelena Klinovaja. Planar josephson junctions in germanium: Effect of cubic spin-orbit interaction. *Physical Review B*, 107(3):035435, 2023.

[73] Maria Spethmann, Xian-Peng Zhang, Jelena Klinovaja, and Daniel Loss. Coupled superconducting spin qubits with spin-orbit interaction. *Physical Review B*, 106(11):115411, 2022.

[74] Alberto Tosato, Vukan Levajac, Ji-Yin Wang, Casper J Boor, Francesco Borsoi, Marc Botifoll, Carla N Borja, Sara Martí-Sánchez, Jordi Arbiol, Amir Sammak, et al. Hard superconducting gap in germanium. *Communications Materials*, 4(1):23, 2023.

[75] Lin-Ding Yuan, Shu-Shen Li, and Jun-Wei Luo. Direct bandgap emission from strain-doped germanium. *Nature Communications*, 15(1):618, 2024.

[76] YU Peter and Manuel Cardona. *Fundamentals of semiconductors: physics and materials properties*. Springer Science & Business Media, 2010.

[77] R Winkler. *Spin-orbit coupling in two-dimensional electron and hole systems*, volume 41. Springer, 2003.

[78] Weng W Chow and Stephan W Koch. *Semiconductor-laser fundamentals: physics of the gain materials*. Springer Science & Business Media, 2013.

[79] Jeongwook Koh. *Low-Frequency-Noise Reduction Technique for Linear Analog CMOS IC's*. PhD thesis, Technische Universität München, 2005.

[80] Rogerio de Sousa. Electron spin as a spectrometer of nuclear-spin noise and other fluctuations. In *Electron spin resonance and related phenomena in low-dimensional structures*, pages 183–220. Springer, 2009.

Chapter 2

Optimisation of electron spin qubits in electrically driven multi-donor quantum dots

"An approximate answer to the right question is worth a great deal more than a precise answer to the wrong question."

- John Tukey

Building on our understanding of spin-orbit coupling in full-electrical qubit control mechanisms from Chapter 1, this chapter investigates a donor-atom-based electron spin qubit architecture, constituting the first publication of this thesis. Silicon-based quantum computing benefits from the precise implantation of phosphorus donor atoms, which naturally form self-defined quantum dots that host electron spins. These donor-based qubits exhibit long coherence times and allow for the implementation of fast single-qubit gates via a nearby electron spin resonance (ESR) channel. However, electrons inherently lack strong intrinsic spin-orbit coupling, which is essential for enabling full electrical control. As a result, electric dipole spin resonance (EDSR) is often introduced by placing a micromagnet in close proximity to the donor dots. In this study, we propose an alternative approach that circumvents the need for a micromagnet by leveraging hyperfine interaction-mediated

electrical control of donor spin qubits. Our proposed architecture is based on a multi-donor 2P:1P quantum dot system, where a double donor (2P) and a single donor (1P) are separated by ∼10 nanometers. The spatially varying magnetic field generated by the three nuclear spins (2P+1P) provides strong spin-orbit interaction, enabling electrical control of the electron spin residing on the 2P donor.

The multivalley effective mass theory utilized here accounts for the six-fold valley degeneracy in bulk silicon, which is lifted when the electron is confined in a quantum dot. Our analysis begins with the derivation of a variational model for the 2P system, followed by the construction of the 2P:1P qubit wavefunction within the Hund-Mulliken approach. The methodology outlined in this chapter also incorporates an optimization aspect, as it enables the modeling of critical parameters such as inter- and intra-dot distances and relative orientations with respect to the crystallographic axes. We identify that variations in these geometric parameters significantly impact qubit operation due to differences in valley composition, overlap integrals, and tunneling energies.

Finally, we discuss two possible entanglement mechanisms for multi-donor dot qubits: dipole-dipole interaction and two-qubit exchange coupling. This work advances our understanding of donor-based qubits by bridging the gap between fundamental effective mass theory and experimentally relevant qubit control strategies.

This chapter contains a verbatim copy of the following publication apart from minor changes to section/appendix numbering:

- **title:** Optimisation of electron spin qubits in electrically driven multi-donor quantum dots. (DOI: https://doi.org/10.1038/s41534-022-00646-9)
- **authors:** Abhikbrata Sarkar, Joel Hochstetter, Allen Kha, Xuedong Hu, Michelle Y. Simmons, Rajib Rahman & Dimitrie Culcer.
- **journal:** npj Quantum Information volume 8, Article number 127.
- **publication date:** 4 November 2022.

Chapter 3

Electrical operation of planar germanium hole spin qubits in an in-plane magnetic field

"The usefulness of a model is not whether it is 'true'
but whether it is predictive."
- Walter Kohn

"A theory that fits all the data is necessarily false. One that explains the essential facts while ignoring the details is more likely to be true"
- Lev Landau

In alignment with the central theme of this thesis, the previous chapter explored the spin-orbit coupling-mediated all-electrical control of multi-donor dot electron spin qubits. Our focus now transitions from spin-1/2 electrons to spin-3/2 holes, which have gained significant traction in recent years, particularly in planar and CMOS-compatible quantum dot architectures. Hole spins in the p-type valence band of silicon and germanium inherently exhibit strong spin-orbit interaction, which can be further modulated by extrinsic asymmetries. This tunability of spin-orbit coupling introduces substantial variability in qubit

properties, influenced by external electric and magnetic fields, quantum dot dimensions, strain, and other factors.

While chapter 2 was dedicated to engineering full-electrical control of electron spin qubits, this chapter delves into the comparative contributions of various spin-orbit interactions affecting hole spin qubits, with a particular emphasis on planar germanium heterostructures. This work constitutes the second publication of the thesis, where, using the $\mathbf{k} \cdot \mathbf{p}$ formalism within the effective mass approximation, a comprehensive three-dimensional model of a single hole spin qubit is developed. We highlight the growing prominence of planar germanium heterostructures as a platform for hole qubits, attributed to their type-I band alignment, low hole effective mass, and high hole mobility. The model systematically investigates key operational concepts, including the existence of operational sweet spots, successfully reproduces recent experimental qubit g-factor data, and elucidates the physical origins of various spin-orbit interactions and their intricate mixing mechanisms. To further enhance conceptual clarity, we also examine the quasi-2D limit of the hole qubit Hamiltonian, providing deeper insight into the underlying physics governing planar systems. Additionally, we discuss the implications of these findings for scalable hole spin qubit architectures, particularly in the context of quantum information processing.

This chapter contains a verbatim copy of the following publication apart from minor changes to section/appendix numbering:

- **title:** Electrical operation of planar Ge hole spin qubits in an in-plane magnetic field. (DOI: https://doi.org/10.1103/PhysRevB.108.245301)
- **authors:** Abhikbrata Sarkar, Zhanning Wang, Matthew Rendell, Nico W Hendrickx, Menno Veldhorst, Giordano Scappucci, Mohammad Khalifa, Joe Salfi, Andre Saraiva, A. S. Dzurak, A. R. Hamilton & Dimitrie Culcer.
- **journal:** Physical Review B volume 108, issue 24, pages 245301.
- **publication date:** 15 December 2023.

Chapter 4

Effect of disorder and strain on the operation of planar Ge hole spin qubits

"A good simulation tells you something you didn't already know;
a bad one just confirms what you assumed."
- Freeman Dyson

In the previous two chapters, we explored the all-electrical control of electron spin qubits in donor quantum dots and hole spin qubits in planar gate-defined quantum dots. Our approach, based on the effective mass approximation, remains computationally efficient while successfully capturing essential aspects of the underlying physics governing these architectures. However, the substantial variability observed in qubit properties in experiments often arises from device-specific factors, which demand a more detailed investigation beyond idealized models.

Building upon our previous theoretical study of hole qubits in planar germanium heterostructures, this chapter extends the analysis to incorporate the effects of random alloy disorder and gate-stack contraction-induced strain. In our third publication, these device-specific perturbations are modeled using the valence force field (VFF) method for alloy disorder and COMSOL Multiphysics for gate-induced strain calculations. The spatial

anisotropy is captured through an evaluation of the cumulative strain matrix elements of the 4×4 spin-3/2 Luttinger-Kohn-Bir-Pikus strain Hamiltonian. Fundamentally, these perturbations introduce additional spin-orbit coupling within the system, significantly impacting hole spin qubit operation. Independent calculations derived from both the three-dimensional $\mathbf{k} \cdot \mathbf{p}$ model and the tight-binding approximation (TBA) reveal that the hole qubit electric dipole spin resonance (EDSR) mechanism is predominantly influenced by the Dresselhaus spin-orbit interaction induced by disorder and strain. Furthermore, the interplay between Rashba spin-orbit coupling (SOC), driven by the structural inversion asymmetry (SIA) from the top-gate electric field, and roughness-induced Dresselhaus SOC leads to specific orientations of the external magnetic field and microwave electrical drive that maximize single-gate operation speeds.

In the broader context of this thesis, this chapter represents a significant step forward in the theoretical study of spin qubits in silicon and germanium platforms. By integrating hybrid analytical and numerical techniques, we establish a comprehensive framework that not only accounts for critical device-dependent effects but also deepens our understanding of the intricate physical mechanisms underlying planar Ge hole qubit systems. The insights gained from this approach provide a pathway toward more precise modeling of realistic quantum dot architectures, bridging the gap between idealized theory and experimental implementations.

This chapter contains a verbatim copy of the following publication apart from minor changes to section/appendix numbering:

- **title:** Effect of disorder and strain on the operation of planar Ge hole spin qubits. (DOI: https://doi.org/10.48550/arXiv.2502.06949)
- **authors:** Abhikbrata Sarkar, Pratik Chowdhury, Xuedong Hu, Andre Saraiva, A. S. Dzurak, A. R. Hamilton, Rajib Rahman, S. Das Sarma & Dimitrie Culcer.
- **journal:** arXiv preprint arXiv:2502.06949.
- **submission date:** 10 February 2025.

Chapter 5

Conclusion and Future Directions

"Everything should be made as simple as possible, but not simpler."

- Albert Einstein

5.1 Thesis summary

This thesis presented a detailed theoretical analysis of spin-orbit coupling mediated properties of spin qubits synthesized in group-IV semiconductors. While two separate material platforms were studied, namely donor-bound electron spin qubits in silicon and hole spin qubits in planar germanium heterostructures, the underlying theme of fast, full-electrical, coherent qubit control mechanism provided a unified motivation: identifying and analyzing the various sources of spin-orbit interaction in the system. Out of the numerous avenues of studying spin qubits theoretically, the one chosen in this study focused on addressing and modeling the large variability of the qubit properties observed experimentally. We adopted an effective mass approximation based approach, which not only simplified the computational task, but also produced a rather simple understanding of the effects stemming from external factors such as qubit geometry, electric and magnetic fields, and so on.

In chapter 2, we developed a multivalley envelope function approximation based model of 2P:1P multidonor dot qubit, a configuration involving two phosphorus donors adjacent to a single phosphorus donor where the electron spin residing on the 2P makes up the qubit. We examined the role of qubit geometry in optimizing donor electron spin qubit gate operation, as well as relaxation and dephasing. Our findings are extremely important in the context of donor qubit experiments. For example, exchange oscillation of multidonor dot electron spin qubits can be suppressed for specific geometrical orientations of the donor clusters.[1] Also, faster gate operation of donor bound electron spin qubits can also be achieved by enhancing the hyperfine stark shift by aligning the multidonor clusters along specific crystallographic directions.[2] This chapter in particular also focused on understanding the influence of charge noise and optimizing qubit coupling strategies, since they constitute crucial steps toward realizing scalable quantum computing architectures based on donor dot systems. Additionally, our proposed donor qubit architecture relied on the difference in the hyperfine interaction between the 2P and 1P dots generating spatially varying magnetic field. This circumvents the need for a micromagnet to be attached for fast EDSR, improving the chances of scaling up donor spin qubits purely via precise doping.

Chapter 3 focused on the spin-3/2 physics of holes in the topmost valence band of planar germanium systems. Using the effective mass $\mathbf{k} \cdot \mathbf{p}$ formalism, we investigated the non-trivial interplay of the intrinsic spin-orbit coupling of holes and the extrinsic spin-orbit coupling due to electric and magnetic fields. The findings of this chapter underscored the critical influence of magnetic field orientation on the performance of planar germanium hole spin qubits. The identified anisotropic behaviors and susceptibility to electric field noise provided valuable insights for optimizing qubit design and operation. We examined the possible enhancement of the speed and coherence of hole spin qubits enabled via the careful selection of magnetic field directions and the underlying orbital interactions.

As mentioned above, the large variability in experiments poses a significant challenge in developing an all-encompassing theoretical model of semiconductor spin qubits. In view of this chapter 4 examined the nonuniform strain present in realistic devices using the $\mathbf{k} \cdot \mathbf{p}$ formalism and tight-binding approach independently. We showed that for holes in planar

Ge heterostructures, strain inhomogeneity due to the random alloy disorder and gatestack contraction leads to important linear-k Dresselhaus spin-orbit interaction, which eventually dominates hole spin qubit operation. This chapter provided a theoretical framework that aligns more closely with experimental data for planar Ge hole qubits. Taking an important stride towards realistic device modelling, this chapter produces crucial insight into optimizing multi-qubit arrays, which is climacteric for scalable quantum computing.

5.2 Path forward

This work serves as inspiration for a few future directions, as listed below.

5.2.1 $1/f$ noise calculation for holes

As delineated in chapters 1 and 2, the common form of noise impacting semiconductor spin qubits is the low-frequency pink ($1/f$) noise, originating from the defects and impurities in the material causing slow, random variations over time. Spin-orbit coupling mediates fast electrical operation of spin qubits, but at the same time, can cause the qubit to tunnel in or out of a nearby two-level charge defect. While the other form of noise originating from the nuclear hyperfine interaction can be suppressed for specific magnetic field orientations, charge noise remains detrimental to spin qubits and requires a proper theoretical understanding for optimization. The cumulative effect of many independent two-level fluctuators with different time constants naturally leads to a $1/f$-like spectrum.

Chapter 2 of this thesis gave a convincing model of $1/f$ noise for electron spin qubits. The spin-3/2 nature of holes, however, gives rise to interesting physical understanding regarding the $1/f$ spectrum. The picture that emerges is that individual defects induces fluctuation in the confinement potential. In view of the theory of invariants, such a time dependent electric field $\mathbf{E}(t)$ changes the qubit Zeeman splitting via a term $\propto \sigma_z \langle k_z \rangle \mathbf{B} \cdot \mathbf{E}(t)$ in the heavy hole energy subspace. Therefore, in presence of external magnetic field, the interplay of the spin-orbit coupling effect (captured in $\langle k_z \rangle$) and the noise electric

field leads to decoherence. The full-3D formalism developed in chapter 3 is capable of capturing such non-trivial mixing, hence can be used to correctly model $1/f$ noise for hole qubits. Moreover, realistic effects from alloy disorder, interface roughness and gatestack contraction strain may play a significant role in understanding hole qubit decoherence in experiments. The formalism developed in chapter 4 can be scaled up for an non-uniform distribution of charge defects in the vicinity of the quantum dot to predict realistic dephasing rates. Furthermore, the theory of invariants can be further implemented to identify potential sweet spots and sweet lines of dephasing.

5.2.2 Strain engineering and variability analysis of spin qubits

Chapter 2 emphasized a couple of important factors in the context of semiconductor spin qubits' optimization, engineered environment and geometry. The constitution of individual donor clusters as well the arrangement of P donors in a cluster plays a crucial role. Similarly for hole qubits, large variations exist across experiments regarding dot sizes, magnetic field orientation, and so on. This thesis can be extended to carry out a variability analysis of electron and hole spin qubit operation, where the focus would be to identify the set of experimental parameters for the most efficient operation of the qubits. This would require modifying our simplistic effective mass approach to include realistic effects present in samples. For example, neighboring quantum dots would experience different local strain. Upon electrical manipulation, the dots would then be effectively 'shaken' in different ways, leading to site-dependent qubit properties. The metallic gatestack for coherent control can also be studied, since the relative distances of the gates and the quantum dots play an important role in determining the qubit principle g-tensor orientation as well as spin-orbit field orientation. In future, the calculations of chapter 4 can be carried out for several proposed gatestacks to identify the optimal design. Moreover, the types of spin-orbit coupling present in the discussed material platforms and quantum dot architectures are heavily influenced by the geometry and symmetry. For example, a systematic structural asymmetry in the quantum dot confining potential leads to Rashba SOC, while the existence of an asymmetric interface across the quantum well results in

Dresselhaus SOC. A potential future direction is studying the realistic strength of these asymmetries and the consequent effect on spin qubits in Si and Ge.

5.2.3 Hybrid semiconductor-superconductor applications

The results presented in this thesis can be used as a foundation for exploring the quantum dot-resonator coupling in hybrid semiconductor-superconductor systems. The strong capacitive coupling between superconductor and quantum dots makes such hybrid systems ideal for reaching strong spin–photon, or charge-photon coupling; paving the way to long-range quantum circuit and scaling up quantum devices. Experiments in past years have observed double quantum dot in Si[3] and resonant exchange qubit in GaAs [4] exhibiting strong coupling between the spin and charge degrees of freedom of electron and microwave photon. More recently, coupling of planar Ge and Si hole systems to superconducting resonators have gained a lot of attention. Experiments in these systems have been able to unlock new technological precedence, such as RF reflectometry via resonator response in gate-based dispersive sensing,[5] in-situ tunnel barrier instead of conventional gate electrodes which simplifies the integration with superconducting circuits.[6] But more importantly, there are fundamental advantages for hole systems due to their intrinsic spin-orbit interaction offering fine tuning of hybrid quantum circuit. Planar Ge hole QD with cubic Rashba favors Majorana bound states[7] and Andreev spin qubits[8, 9]. Ge hole singlet-triplet qubits can be operated at much lower fields, making on-chip integration with superconducting resonators more plausible.[10] In future works, theoretical models can be developed to optimize the coupling in these hybrid devices. For instance, meticulous engineering of the local strain profile could provide a *mechanical* control 'knob' in hybrid semiconductor QD- superconducting resonator high quality opto-electrical/ opto-mechanical qubits.

5.3 Concluding remarks

Semiconductor quantum computing has garnered significant interest over the past two decades, driven largely by its fabrication advantages and seamless integration with microelectronics. The effective mass approximation (EFA)-based theoretical modeling provides essential insights into the fundamental physics governing semiconductor spin qubits. The interaction between the host material's intrinsic properties and the external conditions affecting quantum dots is analyzed using principles of condensed matter physics, quantum mechanics, and quantum information theory. While this approach has been remarkably successful, as demonstrated in this thesis, its models have inherent limitations in fully capturing certain experimental complexities. The broad outlook of this work therefore is to advance theoretical modeling toward capturing device-specific variability in semiconductor spin qubits. The primary objective of this thesis, however, has been to develop a fundamental physical understanding of these qubit architectures.

```
"Essentially, all models are wrong, but some are useful"
- George E. P. Box
```

References

[1] Bent Weber, YH Matthias Tan, Suddhasatta Mahapatra, Thomas F Watson, Hoon Ryu, Rajib Rahman, Lloyd CL Hollenberg, Gerhard Klimeck, and Michelle Y Simmons. Spin blockade and exchange in coulomb-confined silicon double quantum dots. *Nature nanotechnology*, 9(6):430–435, 2014.

[2] Michael T Jones, Md Serajum Monir, Felix N Krauth, Pascal Macha, Yu-Ling Hsueh, Angus Worrall, Joris G Keizer, Ludwik Kranz, Samuel K Gorman, Yousun Chung, et al. Atomic engineering of molecular qubits for high-speed, high-fidelity single qubit gates. *ACS nano*, 17(22):22601–22610, 2023.

[3] Xiao Mi, JV Cady, DM Zajac, PW Deelman, and Jason R Petta. Strong coupling of a single electron in silicon to a microwave photon. *Science*, 355(6321):156–158, 2017.

[4] Andreas J Landig, Jonne V Koski, Pasquale Scarlino, UC Mendes, Alexandre Blais, Christian Reichl, Werner Wegscheider, Andreas Wallraff, Klaus Ensslin, and T Ihn. Coherent spin–photon coupling using a resonant exchange qubit. *Nature*, 560(7717):179–184, 2018.

[5] Eoin G Kelly, Alexei Orekhov, Nico W Hendrickx, Matthias Mergenthaler, Felix J Schupp, Stephan Paredes, Rafael S Eggli, Andreas V Kuhlmann, Patrick Harvey-Collard, Andreas Fuhrer, et al. Capacitive crosstalk in gate-based dispersive sensing of spin qubits. *Applied Physics Letters*, 123(26), 2023.

[6] Jann H Ungerer, Alessia Pally, Artem Kononov, Sebastian Lehmann, Joost Ridderbos, Patrick P Potts, Claes Thelander, Kimberly A Dick, Ville F Maisi, Pasquale Scarlino, et al. Strong coupling between a microwave photon and a singlet-triplet qubit. *Nature Communications*, 15(1):1068, 2024.

[7] Melina Luethi, Katharina Laubscher, Stefano Bosco, Daniel Loss, and Jelena Klinovaja. Planar josephson junctions in germanium: Effect of cubic spin-orbit interaction. *Physical Review B*, 107(3):035435, 2023.

[8] Maria Spethmann, Xian-Peng Zhang, Jelena Klinovaja, and Daniel Loss. Coupled superconducting spin qubits with spin-orbit interaction. *Physical Review B*, 106(11):115411, 2022.

[9] Alberto Tosato, Vukan Levajac, Ji-Yin Wang, Casper J Boor, Francesco Borsoi, Marc Botifoll, Carla N Borja, Sara Martí-Sánchez, Jordi Arbiol, Amir Sammak, et al. Hard superconducting gap in germanium. *Communications Materials*, 4(1):23, 2023.

[10] Daniel Jirovec, Andrea Hofmann, Andrea Ballabio, Philipp M Mutter, Giulio Tavani, Marc Botifoll, Alessandro Crippa, Josip Kukucka, Oliver Sagi, Frederico Martins, et al. A singlet-triplet hole spin qubit in planar ge. *Nature Materials*, 20(8):1106–1112, 2021.